WWU
MÜNSTER

institut für
theoretische physik

MASTER'S THESIS

From Instabilities to Coexistence in Active Mixtures

Submitted by

DANIEL GREVE

September 13, 2023

First examiner
Prof. Dr. Uwe THIELE

Second examiner
Priv. Doz. Dr. Svetlana V. GUREVICH

Universität Münster
Fachbereich Physik
Institut für Theoretische Physik

Abstract

In this thesis we study instabilities and phase coexistence in active mixtures, i.e. in systems described by conserved scalar order parameters that do not approach a thermodynamic equilibrium and can therefore show non-monotonic and especially time-periodic behaviour. We argue, that the nonreciprocal Cahn-Hilliard (NRCH) equation is a prototypical example for a system that contains a conserved large-scale oscillatory instability, i.e. a conserved Hopf instability. To investigate the universal behaviour at the onset of this instability, we derive an ansatz, that connects the oscillatory fast-timescale behaviour to the slow evolution of the amplitude through a linear-Schrödinger-type relation. Using multiscale analysis for a simplistic version of the NRCH equation, we derive an evolution equation for the amplitude that contains nonlocal nonlinearities. Combining analytic results with numerical bifurcation analysis and direct time simulations, we explain a universal mechanism of coarsening suppression in oscillatory phase separation, i.e. that in general a system at the onset of a conserved Hopf instability will adopt stable travelling wave states with a finite intrinsic wavelength which is not governed by the system size. Further, we investigate phase coexistence in "conserved spurious gradient dynamics", a class of systems that allow for a Maxwell construction, but that do not necessarily approach an equilibrium and hence allow for oscillatory behaviour. We introduce a formalism to derive the coexistence conditions and apply it for three specific examples. First, we investigate active model B and use our formalism to reproduce known results for the coexisting densities and the chemical potential. Second, we investigate the NRCH equation to derive phase diagrams for the active case and discuss special cases, where nonreciprocal coupling results in a coexistence between stable homogeneous states and states that have an oscillatory instability. Third, we extend the formlism to crystalline states and construct the phase diagram for two nonreciprocally coupled phase-field-crystal equations to show that nonreciprocity has an overall similar effect on the phase diagrams in the active case.

Kurzfassung

In dieser Masterarbeit werden Instabilitäten und Phasen-Koexistenz in aktiven Mischungen untersucht. Diese bezeichnen Systeme konservierter Ordnungsparameter, die keinem Gleichgewicht zustreben und deshalb nicht-monotones und im Besonderen oszillatorisches Verhalten zeigen können. Hierbei stellt die nichtreziproke Cahn-Hilliard (NRCH) Gleichung den Prototypen eines Systems dar, das eine konservierte, oszillatorische und langwellige Instabilität – in anderen Worten eine konservierte Hopf-Instabilität – enthält. Um das universelle Verhalten bei schwacher Instabilität zu beschreiben, wird ein Ansatz hergeleitet, der das oszillatorische Verhalten auf einer schnellen Zeitskale mit der langsamen Dynamik einer Amplitude auf einer langsamen Zeitskale über eine Zeitenwicklung verbindet, die sich analog zur linearen Schrödingergleichung verhält. Mithilfe schwach nichtlinearer Analyse wird für eine minimalistische version der NRCH Gleichung eine Amplitudengleichung hergeleitet, die nicht-lokale Nichtlinearitäten enthält. Durch die Kombination von analytischen Ergebnissen mit numerischer Bifurkationsanalyse und Zeitsimulationen wird ein Mechanismus zur Auswahl von Wellenlängen nah an der konservierten Hopf-Instabilität offengelegt. Dieser zeigt, dass laufende Wellen keine das System ausfüllende Wellenlänge annehmen und dass diese von den intrisischen Systemeigenschaften und nicht von der Systemgröße abhängt.
Des Weiteren wird Phasenkoexistenz in „konservierter uneigentlicher Gradientendynamik “untersucht. Damit wird eine Klasse von Systemen bezeichnet, die zwar einerseits eine Maxwell Konstruktion ermöglichen, aber andererseits keinem thermodynamischen Gleichgewicht zustreben müssen und deshalb oszillatorisches Verhalten ermöglichen. Für diese wird ein Formalismus zur Ableitung der Koexistenzbedingungen hergeleitet und für drei Beispiele benutzt. Erstens werden für “active model B” die bekannten Ergebnisse für die Dichten und das chemische Potenzial koexistierender Phasen reproduziert. Zweitens wird die NRCH Gleichung untersucht und Phasendiagramme für den aktiven Fall hergeleitet. In diesen wird besonders die Koexistenz von stabilen, homogenen Phasen mit Phasen mit oszillatorischer Instabilität hervorgehoben. Als drittes wird der Formalismus auf kristalline Phasen erweitert und ein nichtreziprok gekoppeltes Phasenfeldkristall-Modell untersucht. Damit wird bestätigt, dass nichtreziproke Kopplungen im Allgemeinen ähnliche Auswirkungen auf die Phasendiagramme aktiver Systeme haben.

Contents

1. Introduction

The development of physical theories often begins with a phenomenological, "ad-hoc" description of a single observed effect. Then afterwards, generalisations may be found, that reduce several observed effects to being consequences of a more general underlying principle. Historically, an important example is the discovery of the law of gravitation. With the two prominent examples being the discovery of Keplers laws of planetary motion and the first investigation of free fall dynamics by Galileo, several gravitational effects were first described seemingly independent from each other. Then, in his *principia mathematica*[1] Sir Isaac Newton formulated his laws of motion and the distance-squared law of the gravitational force, connecting these seemingly unrelated observations to an underlying theory that is nowadays referred to as "classical mechanics".

A similar sketch can be drawn of the discovery of thermodynamics. Important dependencies between pressure, volume and temperature were discovered by Boyle, Gay-Lussac and Charles and then later combined to the ideal gas law. The additional notion of concepts of reversibility and irreversibility then lead to the formulation of the laws of thermodynamics. Only relying on these principles, James Clerk-Maxwell was able to derive a necessary condition for phase coexistence in the gas model of Clausius using a graphical argument that is now referred to as the "Maxwell construction" or the "double-tangent construction"[2].

Despite being spread across several disciplines of natural science, the origins of the theory of pattern formation can be sketched in a similar way. With these origins being most prominently represented by Turings explanation of patterns occurring in reaction-diffusion systems [3], a more systematic view of pattern formation has been established later, when Cross and Hohenberg classified systems by their dispersion relation [4]. Also symmetries and symmetry breaking were increasingly brought into focus (see [5] for an introduction).

This simplified picture of disconnected theories is by no means accurate or complete. Cross-links, unifications and further reductions to deeper underlying theories lead to a complex structure of connected theories that – all combined – form our modern scientific image of the world. The three mentioned examples were not chosen arbitrarily, but because of their interesting relation, as many systems studied in pattern formation seemingly violate Newtons third law or the laws of thermodynamics [6]. Despite these contradictions being only on a superficial level as these apparent violations arise through effective interactions in nonequilibrium systems, it is an intriguing question, in which cases a "thermodynamic-like" description remains possible [7, 8].

The subject of this thesis is pattern formation in a class of such systems, that are here called "active mixtures", i.e. mixtures that do not approach thermodynamic equilibrium, and can therefore show rich complex behaviour like oscillations. In the spirit of the aforementioned process of revealing underlying principles, we develop a universal description of large scale oscillatory instabilities in active mixtures. Further we explore a subclass of active mixtures, that – despite being active – retain thermodynamic properties to an extend that allows for a Maxwell construction.

Before starting with the actual thesis, we briefly describe the connection between dynamical systems and classical thermodynamics through variational principles and motivate the usage of an important

ad-hoc example of an active mixture, that is used throughout the rest of the thesis whenever a specific reference system is needed, namely the nonreciprocal Cahn-Hilliard equation.

1.1. Variational principle and conservation laws

A central connection between thermodynamics and pattern formation can be drawn by discussing variational principles. Classic equilibrium thermodynamics can be deduced from the concept, that an isolated, closed or open system approaches an extremum of a thermodynamic potential, namely the entropy, Helmholtz or Gibbs free energy or grand potential. This (global) extremum is then called the thermodynamic equilibrium. Pattern formation is often described using the mathematical structure of spatially extended dynamical systems. The equivalent of a thermodynamic system that approaches equilibrium in terms of dynamical systems is often called a "variational system", with the equivalent of the thermodynamic potential being a Lyapunov-function. In the absence of conservation laws, thermodynamic systems close to equilibrium can also be directly translated into terms of a spatially extended dynamical system [9], i.e. they can then be written in the form

$$\partial_t \boldsymbol{u} = -\underline{Q}(\boldsymbol{u}) \frac{\delta \mathscr{F}[\boldsymbol{u}]}{\delta \boldsymbol{u}}. \tag{1.1}$$

Here $\boldsymbol{u} = (u_1(\vec{x},t),...,u_N(\vec{x},t))^T$ is a vector of N scalar order parameters, t is time and $\vec{x}$ is space[1]. $\underline{Q}(\boldsymbol{u})$ is a symmetric, positive definite mobility matrix that can depend on $\boldsymbol{u}$ and its spatial derivatives, where the symmetry is a consequence of the Onsager reciprocal relations. $\mathscr{F}[\boldsymbol{u}]$ is a functional that is bounded from below. Being a set of coupled partial differential equations Eqs. (1.1) have to be supplemented with appropriate initial and boundary conditions. For the free energy the boundary condition has to prevent fluxes across the boundary and preserve the mass in the system. In our case of a mixture, the fields $\boldsymbol{u} = (u_1,\dots,u_N)^T$ are the local concentrations of each constituent.

In this thesis though, we deal with mixtures, where the mass of each component is individually conserved, i.e. we exclude for example chemical reactions that convert components into each other. Each component then has to follow a local conservation law

$$\partial_t u_i = -\vec{\nabla} \cdot \vec{j}_i. \tag{1.2}$$

Changes in each concentration u_i can only arise through a redistribution of the component in terms of the divergence of a flux $\vec{j}_i$. For mixtures in local thermodynamic equilibrium, this flux is proportional to a mobility times a chemical potential gradient, i.e. to a generalised thermodynamic force, that arises as the functional variation of the free energy functional $\mathscr{F}[\boldsymbol{u}]$ with respect to the fields $\boldsymbol{u}$, that is

$$\vec{\boldsymbol{j}} = -\underline{Q}(\boldsymbol{u}) \vec{\nabla} \boldsymbol{\mu} \qquad \text{with} \qquad \boldsymbol{\mu} = \frac{\delta \mathscr{F}[\boldsymbol{u}]}{\delta \boldsymbol{u}}. \tag{1.3}$$

[1] Here and for the whole thesis we use bold symbols to display vectorial character in terms of the N field components and arrows to indicate vectorial character in space, i.e. in up to three relevant spatial dimensions. Further, scalar products in space are denoted by a "$\cdot$", while such products are not marked in $\boldsymbol{u}$-space.

Here, this kind of mixture will be called "passive", as it preserves the thermodynamic property of approaching an equilibrium. In these systems, phase coexistence has already been systematically investigated by Thiele et al. [10], showing that these systems approach a Maxwell construction in the limit of an infinite system. Further, a technique to numerically calculate the Maxwell construction in the infinite-system limit has been developed [11].
Here we introduce an "active mixture" as the negative of a passive one, i.e. any system that breaks the structure of Eq. (1.3) will be called active. Keeping all conservation laws intact, there arise two ways of breaking this structure. One can either introduce an additional flux, that is not driven by a chemical potential gradient, or one can omit the variational origin of the chemical potential, introducing "nonvariational" contributions to the chemical potential. The active mixtures dealt with in this thesis originate from the latter, with the most prominent example being the nonreciprocal Cahn-Hilliard model, that is introduced in the following.

1.2. The nonreciprocal Cahn-Hilliard model

A minimal version of the classical Cahn-Hilliard model [12, 13] without quadratic interaction reads

$$\partial_t u = \partial_{xx}\left[\sigma u + u^3 - \partial_{xx} u\right]. \tag{1.4}$$

Here σ is an effective temperature parameter, where $\sigma = 0$ indicates the critical point and u is an order parameter that describes e.g. the concentration of a component in a binary mixture. Given the overall mean concentration in the system is zero, there occurs a second-order demixing phase transition (a.k.a. a Cahn-Hilliard instability) at $\sigma = 0$, where for $\sigma < 0$ the homogeneous state becomes unstable and the system will phase separate into two regions, one of high and one of low concentration. As this equation is variational, it is the prototype of a passive mixture.
In contrast, our prototypical active mixture consists of two coupled Cahn-Hilliard equations, which we will denote in the form

$$\begin{aligned}\partial_t u_1 &= \partial_{xx}\left[\sigma_1 u_1 + u_1^3 - \partial_{xx} u_1 - (\rho+\alpha)u_2\right]\\ \partial_t u_2 &= \partial_{xx}\left[\sigma_2 u_2 + u_2^3 - \kappa\partial_{xx} u_2 - (\rho-\alpha)u_1\right].\end{aligned} \tag{1.5}$$

Here $u_1(x,t)$ and $u_2(x,t)$ describe the concentrations of two constituents of a ternary mixture. Both fields are already rescaled, such that the cubic nonlinearities occur without a prefactor. Further, κ represents a rigidity ratio and σ_1 and σ_2 the temperature parameters of each constituent with respect to their individual critical point[2]. The two equations are linearly coupled via a symmetric coupling of strength ρ and an antisymmetric coupling of strength α. The linear interaction can be seen as a first order approximation, that neglects nonlinear contributions, that are e.g. $\sim u_1 u_2^2$. The case $\alpha = 0$ resembles a thermodynamic system, where both constituents then attract each other with the same interaction strength ρ. As we will later see in the case $|\alpha| < |\rho|$ the system retains all important

[2]Our notation is based on [14, 15], but here we differ as there the linear self interactions are $\sigma_1 = a$ and $\sigma_2 = a + a_\Delta$. Doing this we establish a more symmetric formulation and avoid confusion with the later occuring amplitude variable a.

properties of a thermodynamic system, whereas at $|\alpha| > |\rho|$ it looses the property of approaching an equilibrium.

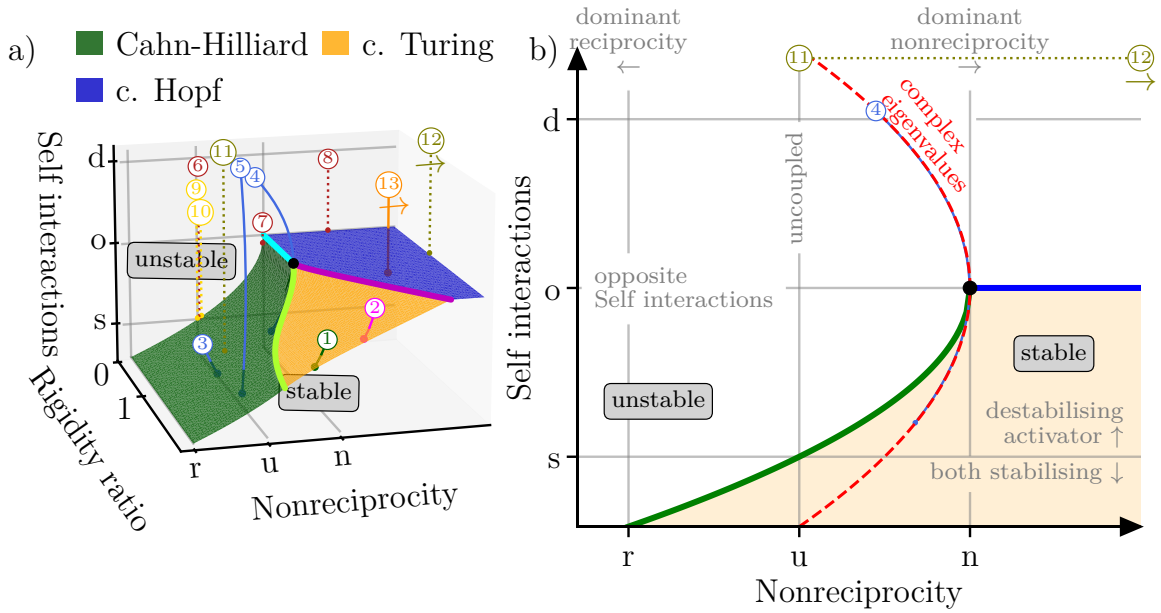

Figure 1.1: Panel (a) shows the linear stability landscape for NRCH-type models with possible Cahn-Hilliard, conserved Turing and conserved Hopf instabilities parametrised by self interaction (trace), rigidity ratio and nonreciprocity parameter (for the definitions see section 2.2). The region below [above] the instability surface indicates stable [unstable] homogeneous steady states. Panel (b) shows a cut through the plane with equal rigidities. The ticks on the vertical axis mark the values where both self interactions become **d**estabilising, **s**tabilising or have exactly the **o**pposite strength. The ticks on the horizontal axis mark the nonreciprocity parameter values, where the system starts to be dominated by **r**eciprocal coupling, **n**onreciprocal coupling or is **u**ncoupled. The circled numbers mark bifurcation analysis (thick lines) and time simulations (dotted vertical lines) from various publications with data corresponding to 1: [15, Fig. 2], 2: [16, Fig. 5a], 3-5: [14, Fig. 5b, 8d, 11c], 6-8: [17, Fig. 5b, 5c, 6a], 9,10: [18, Fig. 1a, 1b](circled numbers are lowered to avoid overlap with 6), 11,12: [19, Fig. 1b, 1e], 13: [20, Fig. 4]. The nonreciprocities used in 12 and 13 lie outside the displayed region.

This system and slight variations have recently gained attention, as it – being the conserved equivalent of a very general two-component-reaction diffusion system – can contain three different primary instabilities, namely a Cahn-Hilliard, conserved Turing and conserved Hopf instability. Further, many types of intricate nonlinear behaviour far from the primary linear instabilities are observed that we briefly summarise in the following. An overview of the parameter sets used by selected publications is given in Fig. 1.1.

Stationary periodic and localized states were first investigated by Frohoff-Hülsmann and Thiele [16], who showed that close to the primary conserved-Turing-bifurcation a snakes-and-ladders structure comparable to a phase-field-crystal model emerges. Further studies then focused on coarsening suppression and subcriticality, showing that both occur in the case of a nonreciprocal interaction combined with unequal rigidities, even if the primary instability is large-scale, i.e. a Cahn-Hilliard instability

[14].
Travelling waves were described by You et al. [18], who focused on the transition from stationary to time-periodic states in small systems. Further, using a reduced system, where one equation is purely linear, they derive a Maxwell-construction for coexisting states and show that the interface-mode governs the velocity and travelling-onset of moving structures [17]. They observe a narrow distribution of selected wavelengths close to a conserved Hopf instability and a broad distribution close to the Bogdanov-Takens instability, i.e. the codimension-two instability, where Cahn-Hilliard and conserved Hopf instability occur simultaneously. The codimension-two conserved Hopf-Turing instability was also systematically investigated and an amplitude equation for two simultaneously destabilising modes, one large scale oscillatory and one small scale stationary, has been derived [21]. Travelling waves in a highly nonreciprocal regime were also observed in two dimensions by Saha et al. [19], but close to the onset of the conserved Hopf instability they observe more complicated moving patterns.
Lately, the NRCH system has been placed in a more general context by Frohoff-Hülsmann and Thiele [20] and [15]. On the one-hand in Ref. [20] an effective equation for an arbitrary system close to the onset of a conserved Hopf instability is derived, which resembles the form of a generalised nonreciprocal Cahn-Hilliard model. Therefore, it is argued that this is the universal amplitude equation for the conserved Hopf instability. We will deal with this statement in more detail in sections 2 and 3.
On the other hand, it is demonstrated in Ref. [15], that the NRCH model as presented in Eq. (1.5) fits into a model structure, that we will generalise and call "spurious gradient dynamics". There, they proof that this class of models is nongeneric in a sense, that stationary broken parity states exist. These immediately start travelling, if the model structure is broken.

1.3. Structure of the thesis

The overall structure of this thesis is guided by the title: After some preparatory work in section 2 has been done, we first study instabilities and then coexistence in active mixtures in sections 3 and 4 respectively.
Section 2 first focuses on linear stability. After introducing the concept of linear stability analysis in spatially extended systems, we apply it to the simplest examples of general nonconserved and conserved two-component systems, namely two-component reaction-diffusion systems and NRCH-type systems. Having already found six different instabilities in these systems, we introduce a classification of eight different linear instabilities and the concepts of a minimal system and an amplitude equation. Pointing out that a conserved Hopf instability occurs primarily in active mixtures, that its amplitude equation is still unknown and that the amplitude equation can not be obtained by simple analogies, sets the stage for section 3.
There, we derive an amplitude equation for the conserved Hopf instability. Starting with the derivation of the ansatz and the time- and lengthscales, we discuss the consequences of time-translation symmetry for occuring terms in the amplitude equation. We then derive the amplitude equation in a minimalistic parameter set, verify it numerically and discuss the relation between the full dynamics and the dynamics of the amplitude equation regarding their bifurcation structure and their temporal dynamics. We end

the discussion of the conserved Hopf instability with the generalisation to the general NRCH equation and an outlook.

Then, in section 4, before turning towards coexistence in active mixtures, we review the classic Maxwell construction in the one-component Cahn-Hilliard system. We then deal with the active case and establish a Maxwell construction on a class of systems called "spurious gradient dynamics". After showing that two frequently used models of active mixtures fit in this class, namely active matter models from motility induced phase separation and systems with linear coupling, we choose these two specific examples to analyse the consequences of the Maxwell construction. Afterwards we show an outlook towards the inclusion of crystalline states. We end with a conclusion of our findings in section 5.

2. Linear and weakly nonlinear analysis

This chapter sets the stage for chapters 3 and 4. We review the concept of Linear stability analysis and specifically perform it for spatially extended two-component systems with only lowest order derivatives, noting that the "ad-hoc" NRCH system is a prototype of this system in the conserved case. Further, we introduce a classification of linear instabilities in spatially extended systems used by e.g. Frohoff-Hülsmann and Thiele [20] and the concept of multiscale/weakly nonlinear analysis. Based on this classification, we then discuss the concepts of a "minimal system" and an "amplitude equation" with special focus on the conserved Hopf instability, arguing that here the NRCH equation serves as the former whereas we derive the latter in section 3.

2.1. Linear stability of dynamical systems

We start by considering a general dynamical system of the form

$$\partial_t \boldsymbol{u} = \boldsymbol{F}(\boldsymbol{u}, \boldsymbol{\mu}), \tag{2.1}$$

where the dynamics of N real variables $\boldsymbol{u} = (u_1(t), ..., u_N(t))^T$ is described by a general right-hand-side function $\boldsymbol{F}(\boldsymbol{u}, \boldsymbol{\mu}) = (f_1(\boldsymbol{u}, \boldsymbol{\mu}), f_2(\boldsymbol{u}, \boldsymbol{\mu}))^T$ depending on a set of control parameters $\boldsymbol{\mu}$, that we keep fixed for the moment. A steady solution $\boldsymbol{u}_\mathrm{F}$ of $\boldsymbol{F}(\boldsymbol{u}_\mathrm{F}, \boldsymbol{\mu}) = 0$ imposes $\partial_t \boldsymbol{u} = 0$ and is therefore called a fixed point of the dynamical system.

We now consider the effect of a small perturbation around the fixed point, i.e. we set $\boldsymbol{u}(t) = \boldsymbol{u}_\mathrm{F} + \delta\boldsymbol{u}(t)$ with $\delta\boldsymbol{u}(t) \ll 1$ and linearise Eq. (2.1)

$$\partial_t \boldsymbol{u} = \partial_t \delta\boldsymbol{u} = \underbrace{\boldsymbol{F}(\boldsymbol{u}, \boldsymbol{\mu})\big|_{\boldsymbol{u}=\boldsymbol{u}_\mathrm{F}}}_{=0} + \underbrace{\left.\frac{\partial \boldsymbol{F}(\partial\boldsymbol{u}, \boldsymbol{\mu})}{\mathrm{d}\boldsymbol{u}}\right|_{\boldsymbol{u}=\boldsymbol{u}_\mathrm{F}}}_{:=\underline{L}=\underline{L}(\boldsymbol{u}_\mathrm{F}(\boldsymbol{\mu}),\boldsymbol{\mu})} \delta\boldsymbol{u} + \mathscr{O}(\delta\boldsymbol{u}^2). \tag{2.2}$$

Hence, we obtain a homogeneous system of first-order linear differential equations $\partial_t \delta\boldsymbol{u} = \underline{L}\,\delta\boldsymbol{u}$, where $\underline{L}$ corresponds to the Jacobian of $\boldsymbol{F}$ evaluated at the fixed point. Solving it with the typical ansatz $\delta\boldsymbol{u} \sim \boldsymbol{u}_0 e^{\lambda t}$ yields the linear eigenvalue problem $\underline{L}\boldsymbol{u}_0 = \lambda\boldsymbol{u}_0$. Therefore the eigenvalues λ of $\underline{L}$ characterise the behaviour around the fixed point: If an eigenvalue has positive [negative] real part, a perturbation along its eigenmode will grow [decay] exponentially. Therefore, the real part of an eigenvalue is often called the "growth rate". A fixed point is called linearly stable if all eigenvalues have negative real part, i.e. if any small perturbation decays exponentially. One further distinguishes real and complex eigenvalues. Since $\underline{L}$ has real coefficients the latter can only occur in complex conjugate pairs and make the system show oscillatory behaviour in the subspace spanned by the two involved eigenmodes. As it corresponds to the (angular) frequency of the oscillation, the imaginary part of an eigenvalue is often called frequency in this context.

At this point, we can already investigate the consequences of an existing potential. If $\boldsymbol{F}$ can be written as the (negative) gradient of a potential $V(\boldsymbol{u}, \boldsymbol{\mu})$, i.e. $\boldsymbol{F} = -\frac{\mathrm{d}V}{\mathrm{d}\boldsymbol{u}}$, we can identify the Jacobian of

the dynamical system as the negative Hessian of the potential: $\underline{L} = -\text{Hess}(V)\big|_{\boldsymbol{u}=\boldsymbol{u}_F}$. Since the latter is a symmetric matrix, in this special case the eigenvalue spectrum is restricted to real values. We further note that at stable fixed points the gradient of the potential becomes zero and its Hessian is positive definite. Hence, we conclude that stable fixed points correspond to local Minima in the potential landscape.

We now additionally allow the dynamic variables $\boldsymbol{u}$ to depend on continuos spatial coordinates $\vec{r}$, promoting them to fields with infinitely many degrees of freedom $\boldsymbol{u}(\vec{r},t)$. In principle a general right hand side can now arbitrarily depend on $\boldsymbol{u}$ and its spatial derivatives. Here though, we focus on time-, parity-, rotation- and translation-invariant systems of the form

$$\partial_t \boldsymbol{u} = \boldsymbol{D}(\vec{\nabla}, \boldsymbol{\mu})[\boldsymbol{u}], \tag{2.3}$$

where $\boldsymbol{D}$ is a set of nonlinear differential operators depending on the control parameters $\boldsymbol{\mu}$ that act on the fields $\boldsymbol{u}$. Note that the imposed symmetries rule out an explicit temporal and spatial dependence of $\boldsymbol{D}$ and also restrict it to special combinations of derivatives, most notably they can only occur in an even number. The most basic solution to Eq. (2.3) inherits all its symmetries and is therefore a homogeneous steady state $\boldsymbol{u}(\vec{r},t) = \boldsymbol{u}_0 = \text{const.}$. As in the previous discussion, we investigate its stability by adding a small perturbation $\delta\boldsymbol{u}(\vec{r},t)$ and linearising Eq. (2.3), which yields

$$\partial_t \delta\boldsymbol{u} = \underline{L}(\vec{\nabla}, \boldsymbol{\mu})\, \delta\boldsymbol{u}, \tag{2.4}$$

where $\underline{L}(\nabla, \boldsymbol{\mu})$ is now a linear differential operator obtained from linearizing $\boldsymbol{D}$ around $\boldsymbol{u} = \boldsymbol{u}_0$. As Eq. (2.4) is a system of linear partial differential equations it is solved by a superposition of Fourier modes of the form $\delta\boldsymbol{u} \sim \boldsymbol{u}_F e^{\mathrm{i}\vec{q}\cdot\vec{r} + \lambda(q^2)t}$. In finite systems the allowed wavenumbers $\vec{q}$ are discretized by the boundary conditions, but become continuous in the limit of an infinite system.

Inserting this ansatz yields a dispersion relation, i.e. a set of functions $\lambda(q^2)$ (technically only depending on $q^2 = |\vec{q}^2|$ because of the rotation invariance) describing the dependence of the eigenvalues of the matrix $\tilde{\underline{L}}(q^2)$ on the perturbation wavenumber q. Hence, the homogeneous state is linearly stable if $\Re(\lambda(q^2)) < 0$ for all q. The previous discussion of a potential can be generalised to the spatially extended case: If the differential operator applied to the field $\boldsymbol{u}$ on the right hand side can be written as a functional variation, the eigenvalue spectrum is real for all q and therefore forbids oscillatory instabilities.

A special case of Eq. (2.3) is the case introduced in section 1.1 where all fields obey a local conservation law. As there the right hand side has to be written as the divergence of a flux, every occurring term contains at least two spatial derivatives. Therefore, any homogeneous state is a steady state. Further, as any right hand side term contains at least two derivatives, the eigenvalue problem factorises like $\lambda_c(q^2) = q^2\tilde{\lambda}(q^2)$. This especially results in the homogeneous perturbation mode at $q^2 = 0$ always having a zero eigenvalue, which is a direct consequence of the conservation laws, that forbid perturbations of the total mass in the system.

2.2. Normal form of the linear two-component system

To give an example we first look at a two-component system without conservation laws, and assume that the highest occurring derivatives are of second order. In real space the linearised equation then reads

$$\partial_t \boldsymbol{u} = \underline{J} + \underline{D}\Delta\boldsymbol{u}. \tag{2.5}$$

Eq. (2.5) corresponds to the linearised problem for a two-component-reaction-diffusion system. Assuming that the diffusion matrix $\underline{D}$ can be diagonalised, we use redefined (internally rotated) fields $\tilde{\boldsymbol{u}}$ to diagonalise $\underline{D}$, such that the equation reads

$$\partial_t \tilde{\boldsymbol{u}} = \begin{pmatrix} J_{11} + D_{11}\Delta & J_{12} \\ J_{21} & J_{22} + D_{22}\Delta \end{pmatrix} \tilde{\boldsymbol{u}}. \tag{2.6}$$

Further, we assume that $J_{11} \geq J_{22}$ (we can exchange the fields to ensure this), i.e. in terms of a Turing system, we call $\tilde{u}_1$ the "activator" and $\tilde{u}_2$ the "inhibitor". We can further reduce the number of relevant parameters by introducing a time- and a lengthscale. We choose the scalings

$$\begin{aligned} t &= t_{0,\mathrm{nc}}\tilde{t} \qquad \text{with} \qquad t_{0,\mathrm{nc}} = \sqrt{\frac{2}{(J_{11}^2 + J_{22}^2)}} \\ \text{and} \qquad x &= x_{0,\mathrm{nc}}\tilde{x} \qquad \text{with} \qquad x_{0,\mathrm{nc}} = \sqrt{D_{11}t_0}. \end{aligned} \tag{2.7}$$

Here, the timescale $t_{0,\mathrm{nc}}$ is chosen with special care as it has to be positive. We could simply have chosen the absolute value of one component for the scaling, but then a distinction between positive and negative values is needed and the case where it vanishes is not included. Here, only the case is excluded, where both diagonal elements vanish, i.e. where both components are without coupling neutrally stable. Further, we have assumed positive diffusion as otherwise we would obtain an unphysical UV-divergent system. We then obtain the system

$$\partial_{\tilde{t}}\tilde{\boldsymbol{u}} = \begin{pmatrix} \vartheta + \sqrt{1-\vartheta^2} + \tilde{\Delta} & \rho_{12} \\ \rho_{21} & \vartheta - \sqrt{1-\vartheta^2} + \kappa\tilde{\Delta} \end{pmatrix} \tilde{\boldsymbol{u}} =: \tilde{\underline{L}}\tilde{u}, \tag{2.8}$$

with the dimensionless groups

$$\vartheta = \frac{J_{11} + J_{22}}{\sqrt{2(J_{11}^2 + J_{22}^2)}}, \qquad \rho_{12} = J_{12}t_0, \qquad \rho_{21} = J_{21}t_0 \qquad \text{and} \qquad \kappa = \frac{D_{22}}{D_{11}}. \tag{2.9}$$

Here $\vartheta \in [-1,1]$ is a dimensionless measure of (twice) the trace, and describes the self-interactions of the system. For $\vartheta \in (\sqrt{1/2}, 1]$ both activator and inhibitor are destabilising, for $\vartheta \in (-\sqrt{1/2}, \sqrt{1/2})$ the activator is destabilising and the inhibitor is stabilising and for $\vartheta \in [-1, -\sqrt{1/2})$ both are stabilising. Next, dropping the tildes, we analyse the linear stability properties of the rescaled system in

Eq. (2.8). Inserting the ansatz $\boldsymbol{u} \propto e^{\mathrm{i}\vec{q}\cdot\vec{x}+\lambda(\vec{q})}$, we obtain the dispersion relation

$$\begin{aligned} \lambda_{1,2,\mathrm{nc}}(q^2) &= \frac{1}{2}\left(\mathrm{tr}(q^2) \pm \sqrt{\mathrm{tr}(q^2)^2 - 4\det(q^2)}\right) \\ \text{with} \qquad \mathrm{tr}(q^2) &= 2\vartheta - (1+\kappa)q^2 \\ \text{and} \qquad \det(q^2) &= 2\vartheta^2 - 1 - \Xi - q^2\left[\vartheta(1+\kappa) + \sqrt{1-\vartheta^2}(\kappa-1)\right] + \kappa q^4, \end{aligned} \tag{2.10}$$

where we introduced the nonreciprocity parameter $\Xi = \rho_{12}\rho_{21}$. When $\Xi > 0$ the system is dominated by symmetric coupling, whereas for $\Xi < 0$ it is dominated by antisymmetric coupling. In the marginal case $\Xi = 0$ the systems decouple, i.e. one of the coupling strengths is zero. We now discuss three different instabilities, i.e. exceptional manifolds in the parameter space spanned by $\{\vartheta, \Xi, \kappa\}$[3] where the real part of one or both eigenvalues transitions zero. We start with the instabilities where the critical mode is $q_c = 0$. Here the eigenvalues $\lambda_{12,\mathrm{nc}}(q^2 = 0)$ are stable, whenever $\mathrm{tr}(q^2 = 0) < 0$ and $\det(q^2 = 0) > 0$. Hence, we obtain two different instabilities

- (i) The **Hopf** instability: It occurs where $\mathrm{tr}(q^2 = 0) = 2\vartheta = 0$ and two complex conjugated eigenvalues cross the imaginary axis.
- (ii) The **Allen-Cahn** instability: It occurs where $\det(q^2 = 0) = 2\vartheta^2 - 1 - \Xi = 0$ and one real eigenvalue crosses the imaginary axis.

Finally, there occurs an additional instability if $\max(\det(q^2)) = 0$ at $q = q_c > 0$. After some analytical considerations (finding a local extremum of $\det(q^2)$) we obtain

- (iii) The **Turing** instability: It occurs when

$$\det_{\min} = -\Xi - \frac{[\vartheta(\kappa-1) + \sqrt{1-\vartheta^2}(\kappa+1)]^2}{4\kappa} = 0 \qquad \text{if} \qquad \frac{\vartheta}{\sqrt{1-\vartheta^2}} > \frac{1-\kappa}{1+\kappa}$$

  and one real eigenvalue crosses the imaginary axis.

The second condition is necessary for the local extremum to exist. We can read off two further necessary conditions for the occurrence of the Turing instability. Firstly we need that $\Xi < 0$, i.e. the system has to be nonreciprocal. Secondly as it can only occur if the system is Hopf-stable, i.e. $\vartheta < 0$, we obtain from the necessary condition that $\kappa > 1$. This is the well known property of a Turing system, that the inhibitor needs to be more diffusive than the activator for the occurrence of the finite wavelength instability. Note that a Hopf instability at finite wavenumber $q_c > 0$ (a.k.a. a wave instability) cannot occur in this system, as $\mathrm{tr}(q^2)$ decreases monotonically with q^2 and does not have a local extremum.
Next, we turn to the conserved case. As discussed before, terms that cannot be written as a divergence are forbidden, and therefore, now including possible derivatives up to fourth order, a linearised

[3] We intentionally differ from the usual parametrisation with trace and determinant, that is used for two-component ODE systems by many textbooks like e.g. Strogatz [22] and could be extended with the rigidity ratio in a similar way. In our context of active mixtures though, we believe that the nonreciprocity parameter Ξ allows for a more intuitive physical interpretation than the determinant.

conserved two-component system can be written as

$$\partial_t \boldsymbol{u} = -\Delta\left[\underline{J} + \underline{D}\Delta\boldsymbol{u}\right], \tag{2.11}$$

where we put the minus to simplify the following discussion. Again note, that the only occurring terms have an even number of derivatives due to the underlying parity symmetry. Here, we use slightly different scalings

$$t_{0,\mathrm{c}} = \frac{2D_{11}}{J_{11}^2 + J_{22}^2} \qquad \text{and} \qquad x_{0,\mathrm{c}} = \sqrt[4]{t_0 D_{11}} \tag{2.12}$$

and the same dimensionless groups as in Eq. (2.9). We then arrive at the rescaled system $\partial_t \tilde{u} = -\Delta\tilde{\underline{L}}\tilde{u}$, where importantly $\tilde{\underline{L}}$ is precisely the operator on the r.h.s in Eq. (2.8). Then, again introducing the ansatz $\boldsymbol{u} \propto e^{\mathrm{i}\vec{q}\cdot\vec{x}+\lambda(q^2)}$ one obtains the dispersion relation, that is related to the previously discussed dispersion relation via

$$\lambda_{1,2,\mathrm{c}}(q^2) = q^2\lambda_{1,2\mathrm{nc}}(q^2). \tag{2.13}$$

Therefore, since q^2 is always positive, the instability thresholds precisely coincide with the nonconserved case and any instability in the nonconserved case has a conserved counterpart, namely the **Cahn-Hilliard** instability for the Allen-Cahn instability and the **conserved Turing** and **conserved Hopf** instability for the Turing and Hopf instability.

As the focus of this thesis is on the conserved case, we discuss the occurring dispersion relations in more detail. Fig. 2.1 gives an overview of possible scenarios of destabilisation, where panel (a) displays the parameter landscape spanned by $\{\vartheta, \Xi, \kappa\}$ and panels (b)-(j) show dispersion relations corresponding to selected paths that cross an instability threshold. Note that, as previously discussed, the nonconserved counterpart of panel (a) would look exactly the same, whereas the shown dispersion relations differ by a factor q^2. The surfaces in panel (a) are obtained by the conditions (i)-(iii) for the individual instabilities, i.e. each condition defines a two-dimensional submanifold in the three dimensional parameter space. The landscape is not symmetric under the transformation $\kappa \to \frac{1}{\kappa}$ as we introduced the diffusion ratio κ, such that it is always the relative diffusivity of the inhibitor with respect to the activator and therefore (conserved) Turing-instabilities occur only for $\kappa > 1$.

The lines where the surfaces of two codimension-one instabilities intersect, i.e. where two of the conditions are fulfilled at the same time, are called codimension-two instabilities. They all meet in the codimension-three point $\{\vartheta, \Xi, \kappa\} = \{0, -1, 1\}$.

All shown dispersion relations have a zero eigenvalue of multiplicity two at zero wavenumber as a consequence of the underlying conservation law. The codimension-one instabilities are shown in panels (b)-(d) of Fig. 2.1. At the Cahn-Hilliard bifurcation one real eigenvalue crosses zero and creates a band of unstable wavenumbers ranging from $q = 0$ to a finite largest unstable wavenumber. The dispersion relation of the conserved Hopf instability in panel (c) looks similar with the difference that now both eigenvalues become unstable, as their real parts have to coincide due to them being complex conjugates. The imaginary parts are opposite and in the relevant parameter region are approximately proportional to q^2. The dispersion relation of the conserved Turing instability in panel (d) starts with complex

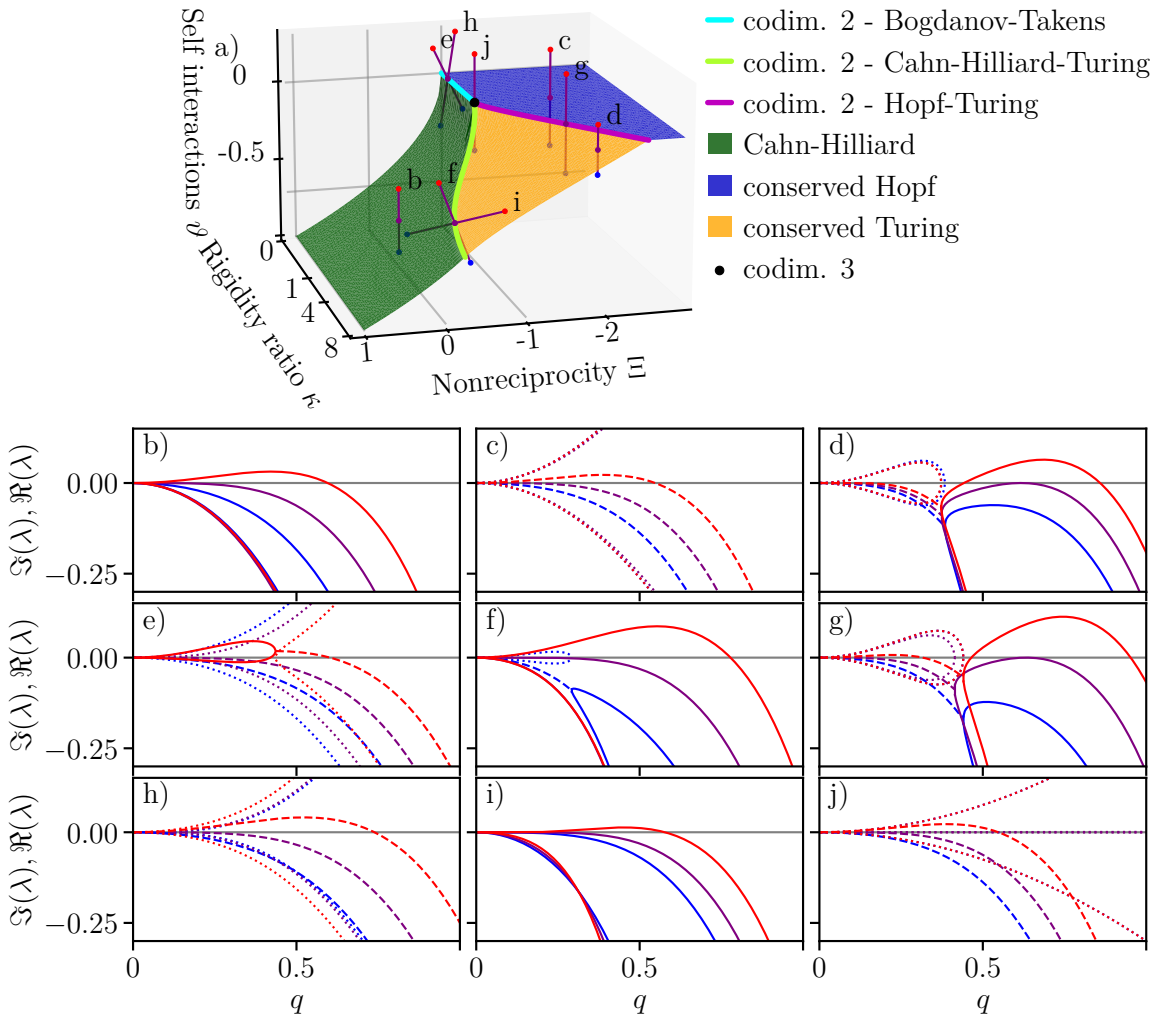

Figure 2.1: Panel (a) shows the instability landscape of the NRCH system. The κ-axis is four times scaled where $\kappa < 1$. Panels (b)-(j) show dispersion relations for chosen paths through the landscape, where panels (b)-(d) cross the planes defined by the codimension-one instabilities and panels (e)-(i) cross the lines defined by the codimension-two instabilities and (j) crosses the codimension-three point. Solid lines represent real eigenvalues and dashed lines the real part of complex eigenvalues. Dotted lines indicate the imaginary part of complex eigenvalues. The dispersion relations in the stable [unstable] regime are indicated in blue [red], and the dispersion relations at the onset in purple.

eigenvalues at small q that then become real for larger q. Beyond the instability threshold one of the real eigenvalues forms a band of unstable wavenumbers at finite wavelengths.

Fig. 2.1 (e)-(i) show exemplary dispersion relations along paths in the $\{\vartheta, \Xi, \kappa\}$-landscape that cross a codimension-two line. The codimension-two instability defined by a simultaneous Cahn-Hilliard and conserved Hopf instability is here called the "Bogdanov-Takens" instability. There, the linear problem has a zero eigenvalue of multiplicity two, but only one corresponding eigenvector as both trace and

determinant of the Jacobian at $q^2 = 0$ vanish simultaneously. The qualitative shape of the dispersion relation within and beyond the stable region differs depending on the specific path in the parameter space. E.g. the two paths f and i in Fig. 2.1 (a) cross the codimension-two Cahn-Hiliard-Turing line, but the red dispersion relation in panel (f) shows a Cahn-Hilliard instability, whereas the red dispersion relation in panel (i) shows a band of finite wavenumbers, i.e. a conserved Turing instability. Similar holds for the codimension-three point with an exemplary dispersion relation shown in panel (j). A complete discussion of all possible scenarios of destabilisation by passing a codimension-two line lies beyond the scope of this thesis[4].
To conclude this discussion, we observe that the linear problem of the "ad-hoc" NRCH model introduced in Eq. (1.5) coincides with the general conserved two-component system (in the form used, the spatial rescaling and diagonalization of the rigidity matrix is already applied), further justifying its usage as the "prototype" of an active mixture.

2.3. Classification of codimension-one instabilities

The six qualitatively different codimension-one instabilities observed in the two-component system (three for the nonconserved and three for the conserved case) raise the question of underlying systematics. More specifically we want to know

- How many qualitatively different codimension-one-instabilities exist?
- In which systems can they occur?
- What are minimal examples for their occurence?

These questions were prominently answered by Cross and Hohenberg [4], who established a classification with six categories. Later, as the role of conservation laws was better understood, two additional categories were added. Here, we will use this extended version that is used by e.g. Frohoff-Hülsmann and Thiele [20]. The classification is based on the three distinctions

- (i) large scale (L) vs. small scale (S)
- (ii) nonconserved (N) vs. conserved (C)
- (iii) stationary ($_\mathrm{s}$) vs. oscillatory ($_\mathrm{o}$).

These become visible in the dispersion relation. For a large scale instability (L) the critical mode is system filling, i.e. $q_c = 0$ in the nonconserved or $q_c = q_{\min}$ in the conserved case, where homogeneous perturbations are forbidden. A small scale instability (S) on the other hand comes with a finite critical wavelength. As already discussed, conservation laws restrict all occurring terms in the dispersion relation to contain at least a factor of q^2. Finally, at a stationary instability one real eigenvector crosses

[4] For a discussion of the Hopf-Turing case see Frohoff-Hülsmann et al. [21] and for the Bogdanov-Takens case see Brauns and Marchetti [17] and Pototsky et al. [23].

the imaginary axis, whereas at an oscillatory instability two complex conjugate eigenvalues cross the imaginary axis. Combining each of these distinctions yields a classification of eight different categories. Next, we partly answer the last question for each individual instability. Therefore, we inspect the overall structure of the linearised equation in terms of the number of fields needed and the order of the highest occurring derivative. We define, that they are minimal if

1. the number of fields equals the number of eigenvalues that simultaneously cross the imaginary axis.

2. the highest order of occurring derivatives is as low as possible and the dispersion is UV-convergent.

This is meant in the sense that the first demand is always secured before the second is considered. The consequences of the first claim are easy to analyse. For all stationary instabilities one real eigenvalue crosses the imaginary axis and we therefore only need one field, whereas for all oscillatory instabilities we need two fields, one for each of the complex conjugate eigenvalues. We then analyse the second condition looking at possible polynomials that fulfil the necessary properties of $\Re(\lambda(q^2))$, keeping in mind that in the process of perturbing the homogeneous steady state with a single mode we replace $\Delta \to -q^2$ in the linear operator $\underline{L}$. For one field this consideration is simple as we can directly convert a dispersion relation into a linear operator, as the eigenvalue of a 1x1-matrix is trivially the only entry. Note that often rescaling allows for a reduction of the occurring parameters as demonstrated in section 2.2. As this has to be considered individually for each case, we do not go into more detail here and instead only give sufficient examples, i.e. examples that do not necessarily arise from rescaling of the general case. Here, μ serves as the control parameter, such that the instability occurs at $\mu = 0$ and the system is unstable for $\mu > 0$.
The Allen-Cahn instability (LN_s) can be realised with a derivative of order two, i.e.

$$\lambda(q^2) = \mu - q^2 \qquad \Leftrightarrow \qquad L = \mu + \Delta. \tag{2.14}$$

For $\mu > 0$, this creates a band of unstable wavenumbers at the origin and the critical mode is $q_c = 0$.
For the Turing instability (SN_s), the dispersion needs to have a local maximum and therefore is a polynomial of at least order four. An example is

$$\lambda(q^2) = \mu - (1 - q^2)^2 \qquad \Leftrightarrow \qquad L = 1 - (1 + \Delta)^2, \tag{2.15}$$

where the dispersion relation has a local maximum at $q_c = 1$, that has a positive growth rate for $\mu > 0$. Equations with this kind of linearised operator are called Swift-Hohenberg-type equations. The dispersion relation of a Cahn-Hilliard instability (LC_s) has to start at $\lambda(q^2 = 0) = 0$ because of the conservation law, then has to increase and later decrease because of the UV-convergence. This again needs at least derivatives of fourth order, an example for the dispersion and the linearised operator are given by

$$\lambda(q^2) = q^2(\mu - q^2) \qquad \Leftrightarrow \qquad L = \Delta(-\mu - \Delta). \tag{2.16}$$

Table 2.1: Shown are all eight codimension-one instabilities, the minimal systems and the name of their amplitude equations. The center column shows schematic examples of exemplary dispersion relations, where solid [dashed] lines give the growth rate of real [complex] eigenvalues and dotted lines the frequencies of complex eigenvalues (see Fig. 2.1), The thick grey line corresponds to zero. The fifth column summarises the relevant lengthscales ("x") and timescales ("t"), where 1 is a shorthand notation for $\mathscr{O}(1)$, ε for $\mathscr{O}(\varepsilon)$ etc..

Instability		Minimal system	Dispersion	Scales	Amplitude equation
LN_s	Allen-Cahn	Allen-Cahn	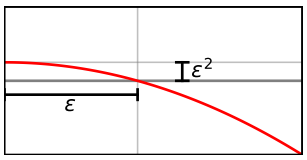	$x:\varepsilon$ $t:\varepsilon^2$	*Allen-Cahn*
SN_s	Turing	Swift-Hohenberg	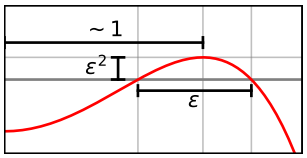	x: $1,\varepsilon$ $t:\varepsilon^2$	real Ginzburg-Landau
LC_s	Cahn-Hilliard	Cahn-Hilliard	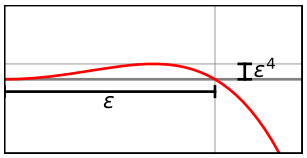	$x:\varepsilon$ $t:\varepsilon^4$	*Cahn-Hilliard*
SC_s	conserved Turing	Phase-field-crystal	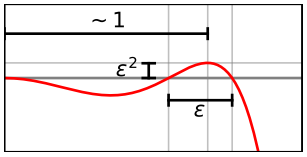	$x:1,\varepsilon$ $t:\varepsilon^2$	real Ginzburg-Landau + nonlin. diffusion
LN_o	Hopf	two-component reaction-diffusion	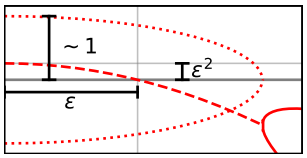	$x:\varepsilon$ $t:1,\varepsilon^2$	complex Ginzburg-Landau
SN_o	wave	*nonreciprocal Swift-Hohenberg*	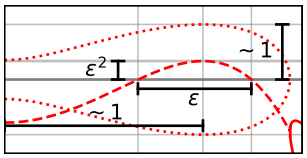	$x:1,\varepsilon$ $t:1,\varepsilon^2$	coupled complex Ginzburg-Landau
LC_o	conserved Hopf	nonreciprocal Cahn-Hilliard	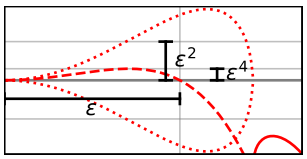	$x:\varepsilon$ $t:\varepsilon^2,\varepsilon^4$	*unknown* → section 3
SC_o	conserved wave	*nonreciprocal Phase-field-crystal*	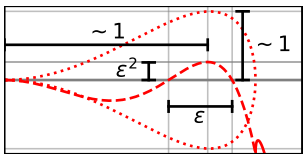	$x:1,\varepsilon$ $t:1,\varepsilon^2$	coupled complex Ginzburg-Landau + nonlin. diffusion

A conserved Turing instability (SC_s) cannot be realised with forth order derivatives, as the dispersion relation has to start at $\lambda(q^2=0)=0$, then first decrease as small wavenumbers are stable and also has to have a local maximum. Hence, we need a sixth order derivative. An example is given by

$$\lambda(q^2) = q^2[\mu-(1-q^2)^2] \qquad \Leftrightarrow \qquad L = \Delta[-\mu-(1+\Delta)^2] \tag{2.17}$$

At criticality, i.e. when $\mu=0$, the dispersion relation has a local maximum at $q_c=1$. In contrast to the nonconserved Turing instability the wavenumber with the largest growth rate depends on μ. Equations with this type of linearised operator are called Phase-field-crystal equation or conserved Swift-Hohenberg equation.

The consideration for the oscillatory instabilities is more intricate as there the dispersion relation and the linear operator are connected via the eigenvalue problem of a 2x2-matrix. Nonetheless, we can always create dispersion relations where the real part of the two complex conjugate eigenvalues coincides with the dispersion relation of the corresponding stationary instability by adding a copy of the one-component system and using antisymmetric coupling[5]. To show that these examples have the minimal order of derivatives needed, we need to use further exclusion arguments for each individual case.

For the Hopf instability (LN_o), second derivatives are sufficient, a minimal example is then

$$\lambda(q^2) = \mu - q^2 \pm i\omega \qquad \Rightarrow \qquad \underline{L} = \begin{pmatrix} \mu+\Delta & \omega \\ -\omega & \mu+\Delta \end{pmatrix}, \tag{2.18}$$

where at criticality, the critical mode is the homogeneous mode q_c with frequency (imaginary part) $\pm\omega$. Systems with this type of linearised operator (i.e. two components and up to second order derivatives) are often called two-component reaction-diffusion systems or also sometimes Turing systems or nonreciprocally coupled Allen-Cahn equations. As shown in section 2.2, a system with second order derivatives cannot have a wave instability (SN_o). A realisation of such an instability needs at least a fourth order derivative, our example is then

$$\lambda(q^2) = \mu-(1-q^2)^2 \pm \mathrm{i}\omega \qquad \Rightarrow \qquad \underline{L} = \begin{pmatrix} \mu-(1+\Delta)^2 & -\omega \\ \omega & \mu-(1+\Delta)^2 \end{pmatrix}, \tag{2.19}$$

which are nonreciprocally coupled Swift-Hohenberg equations. As seen in section 2.2 the conserved Hopf instability (LC_o) occurs in the system with second and fourth order derivatives with an example being

$$\lambda(q^2) = q^2(\mu-q^2) \pm \mathrm{i}q^2\omega \qquad \Rightarrow \qquad \underline{L} = \Delta\begin{pmatrix} -\mu-\Delta & \omega \\ -\omega & -\mu-\Delta \end{pmatrix}. \tag{2.20}$$

[5]The reason is that for a matrix with equal diagonal entries, i.e. $\underline{L} = \begin{pmatrix} a(q^2) & \omega \\ -\omega & a(q^2) \end{pmatrix}$, the eigenvalue problem reads

$$\lambda_{1,2} = \frac{1}{2}\left(\mathrm{tr}(\underline{L}) \pm \sqrt{\mathrm{tr}(\underline{L})^2 - 4\mathrm{det}(\underline{L})}\right)) = \frac{1}{2}\left(2a(q^2) \pm \sqrt{(2a(q^2))^2 - 4(a(q^2)^2+\omega^2)}\right) = a(q^2) \pm \mathrm{i}\omega\,.$$

As previously discussed, this type of linear operator occurs in a NRCH equation. Finally, we have already seen in section 2.2 that this system cannot have a conserved wave instability (SC_o). Therefore we need at least a sixth order derivative, hence the linear operator

$$\lambda(q^2) = q^2(\mu - (1-q^2)^2) \pm \mathrm{i}q^2\omega \qquad \Rightarrow \qquad \underline{L} = \Delta \begin{pmatrix} -\mu - (1+\Delta)^2 & -\omega \\ \omega & -\mu - (1+\Delta)^2 \end{pmatrix}, \quad (2.21)$$

is an example for the minimal linearised operator. In analogy to the previous discussion, these types of models could be called nonreciprocal phase-field-crystal model.

2.4. Multiscale analysis and amplitude equations

So far all of our considerations are purely linear, i.e. we investigated only a linear approximation of the r.h.s. of a partial differential equation. This will, with the exception of the case where an eigenvalue is precisely zero, always result in exponential growth [decay] in the direction of the eigenmode(s) corresponding to eigenvalues with a positive [negative] real part.

Next, we want to include the nonlinearities. Doing this, we cannot deduce any further general statements about the system behaviour without looking at a specific system. Even then, the dynamics can rarely be fully described analytically. Nonetheless, this changes dramatically when the system is close to the onset of an instability, where analytical treatment becomes possible. A prominent method used is "multiscale analysis" or "weakly nonlinear analysis". Here, we briefly sketch the procedure that is then applied to the specific example of the conserved Hopf instability in section 3.

Weakly nonlinear analysis relies on two key observations that become apparent, when inspecting the dispersion relation of a system that is close to the onset of an instability: On the one hand, the dispersion relation only has a positive growth rate in a small band of wavenumbers of $\mathscr{O}(\varepsilon)$ surrounding the critical mode, whereas every other wavenumber retains a negative growth rate of $\mathscr{O}(1)$[6]. We can therefore approximate the full dynamics with the dynamics of the modes in the unstable band. In terms of multiscale analysis this is equivalent to the introduction of a lengthscale $X = \varepsilon x$ (see Misbah [24, Ch. 10]).

On the other hand, as the largest growth rate is zero at the critical point, the growth rates of the modes in the unstable band are small. Therefore, the growth occurs only on a slow timescale, whereas e.g. the oscillation of oscillatory modes and the relaxation of stable modes happens on the fast timescale. The latter is often referred to as the "slaving principle", because the fast relaxationed modes relax to the state controlled by the slow modes. The scalings can be "read off" from the dispersion relation, see table 2.1 and section 3.1, where we analytically derive them for a specific example. Applying these scalings, the whole equation is then expanded in orders of the smallness parameter ε and solved order by order.

The classic way of applying the weakly nonlinear analysis leads to a "scale separation". There, the linearised equation, that arises at the lowest nontrivial order in the expansion, leads to a scale-separating

[6] An exception are the conserved Turing and conserved wave instability where in the vicinity of $q = 0$ the growth rates are negative but of $\mathscr{O}(\varepsilon)$ due to the conservation laws despite being separated from the critical mode $q = q_c$.

ansatz. A simple example can be given for the Turing instability occurring for the the Swift-Hohenberg equation, where the procedure at $\mathcal{O}(\varepsilon)$ yields a linear equation for the first order deviation $u^{(1)}$ from a homogeneous steady state

$$(1+\Delta)^2 u^{(1)} = 0 \quad \Rightarrow \quad u^{(1)} = A(X,T)e^{\mathrm{i}x} + A^*(X,T)e^{-\mathrm{i}x}, \tag{2.22}$$

i.e. we find that the behaviour on the scale x is a harmonic function, that is modulated by an amplitude $A(X,T)$ that varies on the much larger lengthscale X and the slow timescale T. The result of the expansion is then obtained as a solvability condition that arises from the Fredholm alternative at higher order. This yields a dynamical equation, that describes the spatiotemporal evolution of the amplitude on the scales X and T, i.e. the behaviour on the lengthscale x has been fully separated.

Recently, a slightly different way of applying a weakly nonlinear analysis has gained popularity, that we will here call "timescale recombination". There, no scale-separating amplitude ansatz is used at lowest order but instead the fields themselves are expanded into contributions on different timescales. The key procedure is that after applying the expansion in ε, dynamics from different orders up to a certain order are recombined. This has been used for the onset of a Cahn-Hilliard instability by Bergmann et al. [25] and Rapp et al. [26] to deduce a Cahn-Hilliard-type equation from a two-component reaction-diffusion system with one conservation law and for a system of motility-induced phase separation, i.e. for a conserved one-field model with nonlinear derivative terms. Further, Frohoff-Hülsmann and Thiele [20] have used this procedure for an arbitrary system close to the onset of a conserved Hopf instability to obtain a generalised NRCH equation.

Applying this method close to the onset of a Hopf instability yields a general two-component reaction-diffusion system, which is shown in appendix A. This demonstrates, that "timescale recombination" does not allow to incorporate a scale separation via a Fredholm alternative, i.e. one does not obtain the complex Ginzburg-Landau equation, that is considered as the universal amplitude equation in that case.

A comparison to our previous discussion of minimal examples for each instability leads to the hypothesis that the timescale recombination procedure results in an effective minimal system for any system at the onset of one of the eight codimension-one instabilities, i.e. any system is projected onto a reduced set of variables that describe the values of the fields projected onto the marginally stable eigenmodes. The obtained approximate system will then consist of as many fields as unstable eigenvalues, where derivatives and nonlinearities occur only up to the highest expansion order (e.g. if the expansion goes up to $\mathcal{O}(\varepsilon^3)$, the highest occurring nonlinearties are cubic and the derivative terms can contain a maximum of two derivatives).

Next, we consider the amplitude equation for each instability. Here, we only give a brief summary of a recent review in Ref. [20] and refer to it for an extended discussion. Remarkably, the Allen-Cahn and Cahn-Hilliard equation can – to some extend – be seen as their own amplitude equations, as there is only one time- and one lengthscale apparent in the dispersion relation. Therefore, there are no scales to be separated, or equivalently one could say that the behaviour on the fast time- and large lengthscale is trivial. For the other known amplitude equations, we briefly introduce the amplitude equation and the connection to the dynamics of the underlying system, i.e. to the lowest-order perturbation $u^{(1)}$ of a

homogeneous steady state. Again, we give rescaled versions where possible without further discussion, i.e. the occurring real parameters ν, σ, α, β, γ and κ are determined by the underlying system. For the Turing instability we have the real Ginzburg-Landau equation

$$\partial_T A = \mu A - A|A|^2 + \partial_{xx} A \qquad \text{with} \qquad u^{(1)}(x,X,T) = A(X,T)e^{\mathrm{i}kx} + A^*(X,T)e^{-\mathrm{i}kx}, \tag{2.23}$$

i.e. as shown before, the amplitude captures the modulation on a large lengthscale X as separated from a harmonic spatial oscillation with wavenumber k on the lenghtscale x. For the conserved Turing instability we have the system

$$\begin{aligned} \partial_T A = \mu A - A|A|^2 + \partial_{XX} A - AB \qquad &\text{and} \qquad \partial_T B = \partial_{XX}(\nu B + \sigma |A|^2), \\ \text{where} \qquad u^{(1)}(x,X,T) = A(X,T)e^{\mathrm{i}kx} + A^*(X,T)e^{-\mathrm{i}kx} &+ B(X,T), \end{aligned} \tag{2.24}$$

Similar to the standard Turing-case, the amplitude $A(X,T)$ describes the modulation of a spatial harmonic function, but here this is superposed and coupled with an additional field $B(X,T)$ that describes the small wavenumbers close to zero, that have growth rates of $\mathscr{O}(\varepsilon)$ due to the conservation law.

For the Hopf instability, we have the complex Ginzburg-Landau equation

$$\begin{aligned} \partial_T A &= \mu A - (1+\mathrm{i}\beta)A|A|^2 + (1+\mathrm{i}\alpha)\partial_{xx} A, \\ \text{where} \qquad u^{(1)}(x,X,T) &= A(X,T)e^{\mathrm{i}\omega t} + A^*(X,T)e^{-\mathrm{i}\omega t}. \end{aligned} \tag{2.25}$$

Here, the amplitude describes the modulation of a temporal oscillation with frequency ω, that is modulated on large length- and timescales.

The amplitude equation for the wave instability consists of two coupled equations. In the case of small group velocity c (see [27, 28, 29] for a discussion on this restriction), one obtains the coupled complex Ginzburg-Landau equations

$$\begin{aligned} \partial_T A_1 &= \mathrm{sgn}(\varepsilon)A_1 - c\partial_X A_1 + (1+\mathrm{i}\kappa_i)\partial_{XX} A_1 - (1+\mathrm{i}\alpha_i)|A_1|^2 A_1 - (\beta_r + \mathrm{i}\beta_i)|A_2|^2 A_1 \\ \partial_T A_2 &= \mathrm{sgn}(\varepsilon)A_2 + c\partial_X A_2 + (1+\mathrm{i}\kappa_i)\partial_{XX} A_2 - (1+\mathrm{i}\alpha_i)|A_2|^2 A_2 - (\beta_r + \mathrm{i}\beta_i)|A_1|^2 A_2 \\ \text{where} \qquad u^{(1)}(x,X,T) &= A_1(X,T)e^{\mathrm{i}(kx-\omega t)} + c.c. + A_2(X,T)e^{\mathrm{i}(kx+\omega t)} + c.c., \end{aligned} \tag{2.26}$$

i.e. $A_1(X,T)$ and $A_2(X,T)$ describe the amplitudes of a right- and a left-travelling wave with frequency ω and wavenumber k.

Similarly, one obtains for the conserved wave instability

$$\begin{aligned} \partial_T A_1 &= \mathrm{sgn}(\varepsilon)A_1 - c\partial_X A_1 + (1+\mathrm{i}\kappa_i)\partial_{XX} A_1 - (1+\mathrm{i}\alpha_i)|A_1|^2 A_1 - (\beta_r + \mathrm{i}\beta_i)|A_2|^2 A_1 - (1+\mathrm{i}\gamma_i)A_1 B \\ \partial_T A_2 &= \mathrm{sgn}(\varepsilon)A_2 + c\partial_X A_2 + (1+\mathrm{i}\kappa_i)\partial_{XX} A_2 - (1+\mathrm{i}\alpha_i)|A_2|^2 A_2 - (\beta_r + \mathrm{i}\beta_i)|A_1|^2 A_2 - (1+\mathrm{i}\gamma_i)A_2 B \\ \partial_T B &= \partial_{XX}\left(\nu B + \mu(|A_1|^2 - |A_2|^2)\right), \qquad \text{where} \\ u^{(1)}(x,X,T) &= A_1(X,T)e^{\mathrm{i}(kx-\omega t)} + c.c. + A_2(X,T)e^{\mathrm{i}(kx+\omega t)} + c.c. + B(X,T), \end{aligned} \tag{2.27}$$

i.e. a combination of the previous cases with $A_1(X,T)$ and $A_2(X,T)$ describing right- and left-travelling waves and $B(X,T)$ describing large-scale modes.

Last but not least, we arrive at the conserved Hopf instability, where the amplitude equation is still unknown. Here, using the method of timescale recombination, Frohoff-Hülsmann and Thiele [20] propose that the resulting equation corresponds to the NRCH equation. Analogously to Allen-Cahn and Cahn-Hilliard equation, it describes a "trivial amplitude" of the original equation, i.e. the value of the conserved fields. However, there are strong arguments against this. On the one hand, in contrast to the stationary cases, here the dispersion implies that the dynamics take place on two different timescales, because the frequencies of the unstable modes are up to $\mathcal{O}(\varepsilon^2)$ whereas the growth rates are only of order $\mathcal{O}(\varepsilon^4)$, see table 2.1. The main challenge for timescale separation is though, that there is no constant frequency at lowest order, i.e. unlike in all other dispersion relations of oscillatory instabilities, the lowest order approximation of the frequency is not $\omega = \text{const.}$, but $\omega \sim q^2$. On the other hand, as derived in section 2.2, the NRCH equation can have three different codimension-one instabilities, namely Cahn-Hilliard, conserved Turing and conserved Hopf instabilities. Hence, one could argue, that the NRCH equation arises, when a system containing these three instabilities is expanded around the codimension-three point, where they coincide, but not for a singular codimension-one instability.

To summarise this section, we have seen that the occurrence of conserved Hopf instabilities is a key distinction between passive and active mixtures, since it requires nonreciprocity, i.e. antisymmetric coupling. We have further seen, that the NRCH equation has the role of the prototypical system for this instability, comparable to e.g. the role of the Swift-Hohenberg equation for the Turing instability. It is therefore of great interest for our understanding of active mixtures to find the specific amplitude equation of the conserved Hopf instability and to discuss the dynamics on the different timescales. We will devote section 3 to this topic.

3. The conserved Hopf instability

We will now derive a leading order envelope equation for the conserved Hopf instability. Before starting the weakly nonlinear analysis, general considerations are made, that justify the scalings and show how our ansatz arises solely from the dispersion relation. Then, symmetry arguments are used to discuss possible terms occurring in the envelope equation. Subsequently, we provide a full derivation for a minimalistic version of the NRCH equation. This shall guide the reader through the most important steps of the derivation avoiding distractions arising from lengthy algebraic expressions. We then numerically illustrate the consistency of the derived envelope equation with the full dynamics. We also investigate how its predictions start to deviate further away from onset. Finally we then extend the theory to a more general case lifting the restrictions we had.

3.1. Scaling and ansatz for the conserved Hopf instability

In an analogous way to Misbah [24, Ch. 10, 12], we derive an ansatz for the weakly nonlinear analysis and justify the time- and lenghtscales based on linear considerations, here only using the properties of the dispersion relation. In the conserved Hopf-case, the Taylor-expanded dispersion relation reads:

$$\begin{aligned} \lambda_{\pm}(k) &= \Delta(k) \pm i\Omega(k) \\ \Delta(k) &= \mu k^2 - \delta' k^4 + \mathscr{O}(k^6) \\ \Omega(k) &= \omega k^2 + \omega' k^4 + \mathscr{O}(k^6), \end{aligned} \tag{3.1}$$

where the control parameter $|\mu| = |\tilde{\mu}|\varepsilon^2 \ll 1$ indicates the onset of the instability. When μ becomes positive, all modes where $\Delta(k) > 0$, i.e. all modes with $k < k_{\max} = \varepsilon\sqrt{\tilde{\mu}/\delta'}$ will grow whereas others will decay exponentially. In Fourier space, we can therefore approximate the full dynamics as

$$\boldsymbol{u}(x,t) = \sum_k \tilde{\boldsymbol{u}}(k,t) e^{-\mathrm{i}kx} \approx \sum_{|k|<k_{\max}} \tilde{\boldsymbol{u}}(k,t) e^{-\mathrm{i}kx}, \tag{3.2}$$

where $\tilde{\boldsymbol{u}}(k,t)$ is the Fourier-transform of $\boldsymbol{u}(x,t)$, corresponding to the time-dependent amplitude of the mode e^{ikx}. This demonstrates that the only relevant occurring k are of $\mathscr{O}(\varepsilon)$. We can make this dependence explicit by introducing a rescaled wavenumber $K = k/\varepsilon$ and a lengthscale $X = \varepsilon x$.
Further, we know that in the linear regime the modes will behave as $\tilde{u}(k,t) \sim e^{\lambda_{\pm}(k^2)t}\boldsymbol{v}_{\pm}(k^2)$, where $\boldsymbol{v}_{\pm}(k^2)$ are the eigenvectors corresponding to $\lambda_{\pm}(k^2)$. Introducing the rescaled wavenumber K yields

$$\begin{aligned} \tilde{\boldsymbol{u}}(k,t) \sim \exp(\lambda_+ t)\boldsymbol{v}_+ + c.c. &= \exp\left([-\mu k^2 - \delta' k^4 \pm i(\omega k^2 + \omega' k^4)]t\right)\boldsymbol{v}_+(k^2) + c.c. \\ &= \exp\left(i\omega K^2\varepsilon^2 t + [-\tilde{\mu}K^2 - \delta' K^4 + i\omega' K^4]\varepsilon^4 t\right)\boldsymbol{v}_+(\varepsilon^2 K^2) + c.c. \end{aligned} \tag{3.3}$$

This demonstrates that for each individual mode k the dynamics separate onto two different scales. An oscillation occurs on a scale $\tau = \varepsilon^2 t$, whereas exponential growth of the Amplitude first occurs on the timescale $T = \varepsilon^4 t$. We therefore introduce the amplitude $\tilde{A}(K,T)$ of a Fourier mode that only depends on the slow timescale. Then we rewrite Eq. (3.2) in terms of the rescaled variables τ, T, X

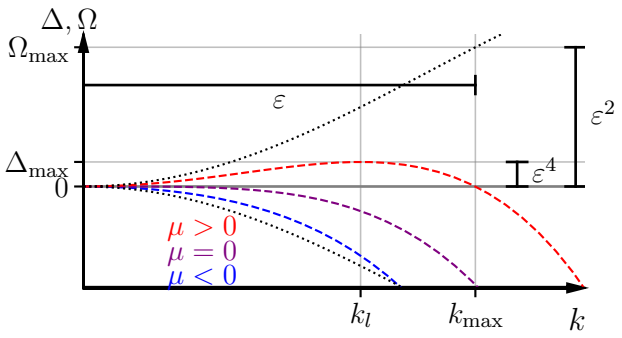

Figure 3.1: Dispersion relation of the conserved Hopf bifurcation . The growth rate is shown in blue, purple and red for $\mu > 0, \mu = 0$ and $\mu < 0$ respectively. The dotted lines indicate the frequencies $\pm\Omega$.

and K, taking only the first order contributions into account, i.e. $\boldsymbol{v}_+ := \boldsymbol{v}_+(K^2)|_{K^2=0}$ and therefore $\boldsymbol{v}(\varepsilon^2 K^2) = \boldsymbol{v}_+ + \text{h.o.t.}$. Finally we obtain the ansatz

$$\begin{aligned}\tilde{\boldsymbol{u}}(x,t) &= \varepsilon \sum_K \left(e^{\mathrm{i}\omega K^2 \tau} \tilde{A}(K,T) \boldsymbol{v}_+ + c.c. \right) e^{-\mathrm{i}KX} + \text{h.o.t.} \\ &= \varepsilon \left(e^{-\mathrm{i}\omega\tau\partial_{XX}} \sum_K \tilde{A}(K,T) e^{-\mathrm{i}KX} \boldsymbol{v}_+ + c.c. \right) + \text{h.o.t.} = \varepsilon e^{-\mathrm{i}\hat{\omega}\tau} A(X,T)\boldsymbol{v}_+ + c.c. + \text{h.o.t.},\end{aligned} \tag{3.4}$$

where we introduced the operator $\hat{\omega} = \omega\partial_{XX}$. Note that since $\partial_{XX}\tau$ is of $\mathscr{O}(1)$ the exponential $e^{-\mathrm{i}\hat{\omega}\tau}$ cannot be approximated by leading order terms. Further we emphasise that despite that we could mathematically equivalently write $\tau\partial_{XX} = t\partial_{xx}$ via shifting an ε^2 between the terms, the first form correctly implements the nature of the occurring oscillations, which is large scale modes oscillating on a slow timescale. Also note that we would have arrived at similar scalings if we "graphically" extracted the scalings from the dispersion relation, see Fig. 3.1.

3.2. Symmetry considerations

Before we formally derive the amplitude equation for a concrete system, we can already exclude a number of terms based on symmetry considerations. To do so, we start with a comparison with a simpler case, namely the nonconserved pendant of the conserved Hopf bifurcation: The complex Ginzburg-Landau equation. There, due to the frequency having a constant contribution at $\mathscr{O}(1)$, one obtains a fast timescale t and a slow timescale $\tau = \varepsilon^2 t$ and the ansatz:

$$\boldsymbol{u}(x,t) = \varepsilon e^{\mathrm{i}\omega_0 t} A(X,\tau)\boldsymbol{v}_+ + c.c.. \tag{3.5}$$

In contrast to the conserved Hopf bifurcation , here ω_0 has a constant real value. The relevant symmetry to consider is translation invariance in time, which means that the system does not change if we shift the time zero by a constant t_0, i.e. $t \to t + t_0$. Inserting this shift into Eq. (3.5) shows that the amplitude transforms like $A(X,\tau) \to e^{\mathrm{i}\omega_0 t_0} A(X,\tau)$. Since the amplitude equation has to be invariant under the

applied time shift, all occurring terms have to show the same transformation behaviour as A. From this we can conclude that the simplest occurring nonlinearity is $\sim A|A|^2$ as it transforms like the linear term, i.e. $A|A|^2 \to e^{\mathrm{i}\omega_0 t_0} A|A|^2$, whereas quadratic or other cubic terms are forbidden, because e.g. $A^2 \to e^{2i\omega_0 t_0} A^2$ shows a different transformation behaviour.

We now transfer this argument to the more involved relation between the amplitude and the original field given in Eq. (3.4) that we derived for the conserved Hopf dispersion relation. Applying a shift $\tau \to \tau + \tau_0$ transforms the amplitude as $A(X,T) \to e^{-\mathrm{i}\hat{\omega}\tau_0} A(X,T)$. Despite this transformation being a linear operator instead of a simple multiplicative factor, all linear terms will show the same transformation behaviour, as temporal and spatial derivatives commute with the spatial derivatives contained in $e^{-\mathrm{i}\hat{\omega}\tau_0}$, for example $\partial_{XX} A \to \partial_{XX} e^{-\mathrm{i}\hat{\omega}\tau_0} A = e^{-\mathrm{i}\hat{\omega}\tau_0} \partial_{XX} A$.

Now consider possible nonlinearities in Eq. (3.4). Remarkably, here we note, that the term $A|A|^2$ transforms like

$$A|A|^2 \to (e^{-\mathrm{i}\hat{\omega}\tau_0} A)(e^{-\mathrm{i}\hat{\omega}\tau_0} A)(e^{\mathrm{i}\hat{\omega}\tau_0} A^*) \neq^{7} e^{-\mathrm{i}\hat{\omega}\tau_0} A|A|^2, \tag{3.6}$$

and therefore cannot occur in the amplitude equation. Similar arguments hold for all other local nonlinear combinations of A and A^*.

Therefore, the time translation invariance combined with the ansatz forbids all local nonlinear terms in the amplitude equation. Nonetheless possible nonlinear terms exist, if we also take nonlocal contributions into account: For example for a domain of length L with periodic boundary conditions consider a term containing a spatial average, i.e.

$$A\overline{|A|^2} = A\frac{1}{L}\int_{-L/2}^{L/2} |A|^2 \mathrm{d}X. \tag{3.7}$$

The second part will transform as

$$\overline{|A|^2} \to \frac{1}{L}\int_{-L/2}^{L/2} (e^{\mathrm{i}\hat{\omega}\tau_0} A^*)(e^{-\mathrm{i}\hat{\omega}\tau_0} A)\mathrm{d}X = \frac{1}{L}\int_{-L/2}^{L/2} A^* A \mathrm{d}X = \overline{|A|^2}, \tag{3.8}$$

[7] To illustrate that these are unequal in the general case consider the counterexample of $A(X,T)$ being a linear combination of two single modes, i.e. $A(X,T) = e^{\mathrm{i}Q_1 X} + e^{\mathrm{i}Q_2 X}$. E.g. evaluating the prefactor of the terms proportional to $e^{\mathrm{i}(2Q_1 - Q_2)X}$ we obtain $e^{\mathrm{i}\omega(2Q_1^2 - Q_2^2)\tau_0}$ on the left side, whereas on the right side the prefactor reads $e^{\mathrm{i}\omega(2Q_1 - Q_2)^2\tau_0}$ which is unequal if $Q_1 \neq Q_2$.

where we made use of infinitely many partial integrations[8], or in a more abstract sense, used that $e^{\mathrm{i}\hat{\omega}\tau_0}$ is a unitary transformation leaving the (spatial) scalar product invariant because $\hat{\omega}$ is a Hermitian operator. As this expression is invariant under the transformation and clearly independent on X, the term $A\overline{|A|^2}$ transforms as $A\overline{|A|^2} \to (e^{-\mathrm{i}\hat{\omega}\tau_0}A)\overline{|A|^2} = e^{-\mathrm{i}\hat{\omega}\tau_0}A\overline{|A|^2}$ and is therefore compatible with the time translation symmetry of the underlying system.

3.3. Derivation for a minimalistic parameter configuration

We show the main part of the weakly nonlinear analysis in the specific example of a parameter set that simplifies occurring terms, that (with few exceptions that will be discussed later) captures all terms that occur in the general case, but frees the derivation from some linear algebra and complicated prefactors to make it easier for the reader to follow important steps. To do so, we consider the linear nonreciprocal Cahn-Hilliard equation, i.e. Eq. (1.5), assume the mean concentrations to be zero, and set $\sigma_1 = \sigma_2 = -\mu, \rho = 0$ and $\kappa = 1$. It then reads

$$\begin{aligned} \partial_t u_1 &= \partial_{xx}(-\mu u_1 + u_1^3 - \partial_{xx}u_1 - \alpha u_2) \\ \partial_t u_2 &= \partial_{xx}(-\mu u_2 + u_2^3 - \partial_{xx}u_2 + \alpha u_1). \end{aligned} \tag{3.9}$$

Here the linear self-interactions have to be small. Hence, we have renamed the trace of the linear system, as it is the relevant control parameter for the expansion, i.e. $|\mu| = \varepsilon^2|\tilde{\mu}| \ll 1$, since we know from our linear considerations in section 2.2, that the onset of the conserved Hopf instability is marked by a vanishing trace combined with a positive determinant of the linearised system. Here we set μ, such that the homogeneous steady state becomes unstable for $\mu > 0$. Now we apply the weakly nonlinear analysis specifically to this reduced nonreciprocal-Cahn-Hilliard model. Introducing the scalings i.e. setting $\partial_t = \varepsilon^2\partial_\tau + \varepsilon^4\partial_T$ and $\partial_x = \varepsilon\partial_X$, we start solving Eq. (3.56) order by order introducing

$$\boldsymbol{u} = \varepsilon\boldsymbol{u}^{(1)}(X,\tau,T) + \varepsilon^2\boldsymbol{u}^{(2)}(X,\tau,T) + \varepsilon^3\boldsymbol{u}^{(3)}(X,\tau,T) + \mathscr{O}(\varepsilon^4). \tag{3.10}$$

[8] To briefly demonstrate this, we expand the exponentials and reorder the equation in orders of $(\omega\tau)$

$$\begin{aligned} &\frac{1}{L}\int_{-L/2}^{L/2}(e^{\mathrm{i}\hat{\omega}\tau_0}A^*)(e^{-\mathrm{i}\hat{\omega}\tau_0}A)\mathrm{d}X \\ &= \frac{1}{L}\int_{-L/2}^{L/2}\left[A^* + i\omega\tau_0\partial_X A^* + \frac{1}{2}(i\omega\tau_0\partial_X)^2A^* + ...\right]\left[A - i\omega\tau_0\partial_X A + \frac{1}{2}(-i\omega\tau_0\partial_X)^2A + ...\right]\mathrm{d}X \\ &= \frac{1}{L}\int_{-L/2}^{L/2}\left\{A^*A + i\omega\tau_0[(\partial_X A^*)A - A^*(\partial_X A)] + \frac{\omega^2\tau_0^2}{2}[-(\partial_{XXX}A^*)A - A^*(\partial_{XXX}A) + 2(\partial_X A^*)(\partial_X A)] + ...\right\}\mathrm{d}X \\ &\overset{p.I.}{=} \frac{1}{L}\int_{-L/2}^{L/2}(A^*A + 0 + 0 + ...)\,\mathrm{d}X = \frac{1}{L}\int_{-L/2}^{L/2}A^*A\mathrm{d}X \end{aligned}$$

Higher order terms cancel in the same way. A rigouros proof works analogously to the proof of the identity $\exp(x)\exp(y) = \exp(x+y)$ for $x, y \in \mathbb{R}$ using the series expansion of the exponential function and the binomial theorem.

The first nonvanishing contribution occurs at $\mathcal{O}(\varepsilon^3)$ and reads

$$\partial_\tau \begin{pmatrix} u_1^{(1)} \\ u_2^{(1)} \end{pmatrix} = \partial_{XX} \begin{pmatrix} 0 & -\alpha \\ \alpha & 0 \end{pmatrix} \begin{pmatrix} u_1^{(1)} \\ u_2^{(1)} \end{pmatrix}. \tag{3.11}$$

This set of coupled linear partial differential equations is solved by the ansatz $\boldsymbol{u}^{(1)} \sim e^{\mathrm{i}(QX+\omega(Q)\tau)}\boldsymbol{v}$. The resulting eigenvalue problem yields $\omega(Q) = \pm\omega Q^2$ with $\omega = \alpha$ and corresponding eigenvectors $\boldsymbol{v}_\pm = (\mp i, 1)^T/\sqrt{2}$. Note that here they form an orthonormal system, i.e. both are normalised and $\langle \boldsymbol{v}_+; \boldsymbol{v}_- \rangle = \sum_j (\boldsymbol{v}_+)_j^* (\boldsymbol{v}_-)_j = 0$.

We can now write the general solution as a superposition of harmonic modes with amplitudes $\tilde{A}(Q,T)$ depending on the slow timescale T:

$$\begin{aligned} \boldsymbol{u}^{(1)} &= \sum_Q \left[\tilde{A}(Q,T) e^{\mathrm{i}(QX+\omega Q^2\tau)} \boldsymbol{v}_+ + \tilde{A}^*(Q,T) e^{-\mathrm{i}(QX+\omega Q^2\tau)} \boldsymbol{v}_- \right] \\ &= e^{-\mathrm{i}\omega\tau\partial_{XX}} \sum_Q \tilde{A}(Q,T) e^{\mathrm{i}QX}\, \boldsymbol{v}_+ + e^{\mathrm{i}\omega\tau\partial_{XX}} \sum_Q \tilde{A}^*(-Q,T) e^{\mathrm{i}QX}\, \boldsymbol{v}_- \\ &= e^{-\mathrm{i}\hat{\omega}\tau} A(X,T) \boldsymbol{v}_+ + c.c., \end{aligned} \tag{3.12}$$

where we introduced the operator $\hat{\omega} = \omega\partial_{XX}$, and the Amplitude $A(X,T) = \sum_Q \tilde{A}(Q,T) e^{\mathrm{i}QX}$. As expected, this precisely resembles the previous discussion of the general case, i.e. the linear problem obtained at first nonvanishing order recreates the ansatz.

At this point we also note that Eq. (3.11) is, up to prefactors, the well known linear Schrödinger equation for a free particle[9]. Similarly, the operator $e^{-\mathrm{i}\hat{\omega}\tau}$ resembles the time evolution operator in the Schrödinger picture with $\hat{\omega}$ serving as the Hamiltonian. Therefore on the fast timescale τ the amplitude $A(X,T)$ resembles an "initial wave packet", that freely propagates in space. If it is a single-mode it will therefore just be translated in space, i.e. a single-mode solution of the amplitude corresponds to a travelling wave in the original equation. A more intricate $A(X,T)$ corresponds to more intricate behaviour of the solutions of the original equation, e.g. to the spreading of a wave package of a Gaussian amplitude distribution.

Here we do not need to deal with $\mathcal{O}(\varepsilon^4)$ as the equations determine $\boldsymbol{u}^{(2)}$ up to linear order and do not

[9]The fields correspond to the real and imaginary part of the wave function ψ, i.e. the Schrödinger equation in its most common form can be brought into this form via adding and subtracting its complex conjugate:

$$\begin{aligned} i\partial_t\psi = -\partial_{xx}\psi \quad &\Leftrightarrow \quad \partial_t \mathrm{Im}(\psi) = -\partial_{xx}\mathrm{Re}\psi \\ -i\partial_t\psi^* = -\partial_{xx}\psi^* \quad &\qquad\quad \partial_t \mathrm{Re}(\psi) = \partial_{xx}\mathrm{Im}\psi \end{aligned}$$

enter at $\mathcal{O}(\varepsilon^5)$. At $\mathcal{O}(\varepsilon^5)$ we obtain an inhomogeneous equation that has the form

$$\begin{aligned} &\underline{L}u^{(3)} = \boldsymbol{q}_5 \\ \text{with} \qquad &\underline{L} = \underline{1}\partial_\tau - \begin{pmatrix} 0 & -\alpha \\ \alpha & 0 \end{pmatrix} \partial_{XX} \\ \text{and} \qquad &\boldsymbol{q}_5 = \partial_{XX} \begin{pmatrix} -\mu u_1^{(1)} + {u_1^{(1)}}^3 - \partial_{XX} u_1^{(1)} \\ -\mu u_2^{(1)} + {u_2^{(1)}}^3 - \partial_{XX} u_2^{(1)} \end{pmatrix} - \begin{pmatrix} \partial_T u_1^{(1)} \\ \partial_T u_2^{(1)} \end{pmatrix}. \end{aligned} \tag{3.13}$$

For a finite domain of length l with periodic boundary conditions, we define a spatial and temporal scalar product. As the smallest possible wavenumber is $k_{\min} = \frac{2\pi}{l}$, for a domain $L = \varepsilon l$ it follows that $K_{\min} = 2\pi/L$ is the smallest possible spatial mode. Therefore the slowest possible temporal mode on the fast timescale has the frequency $\Omega_{\min} = \omega K_{\min}^2/(2\pi) = 2\pi\omega/L^2$. Therefore we can define a scalar product as

$$\langle \boldsymbol{F}(X,\tau); \boldsymbol{G}(X,\tau) \rangle = \frac{\Omega_{\min}}{L} \int_{-L/2}^{L/2} \mathrm{d}X \int_0^{1/\Omega_{\min}} \mathrm{d}\tau \boldsymbol{F}^\dagger(X,\tau) \boldsymbol{G}(X,\tau). \tag{3.14}$$

As we approach the limit of an infinite system $L \to \infty$, both spatial and temporal domain size will diverge. From here on we no longer state the limits and normalization and note that the integral of a harmonic function is only nonzero if both spatial and temporal frequencies vanish, i.e. $\int \mathrm{d}X \int \mathrm{d}\tau e^{\mathrm{i}KX} e^{\mathrm{i}\Omega\tau} = 1$ if $K = \Omega = 0$ and zero otherwise.

By the Fredholm alternative Eq. (3.13) has a solution if $\boldsymbol{q}_5$ is orthogonal to the kernel of the adjoint linear operator $\underline{L}^\dagger$, given by

$$\underline{L}^\dagger = -\underline{1}\partial_\tau - \begin{pmatrix} 0 & \alpha \\ -\alpha & 0 \end{pmatrix} \partial_{XX} = -\underline{L}. \tag{3.15}$$

In line with Eqs. (3.11) and (3.12), the kernel of this linear operator is given by

$$\boldsymbol{k} = e^{-\mathrm{i}\hat{\omega}\tau} B(X) \boldsymbol{v}_+ + e^{\mathrm{i}\hat{\omega}\tau} C(X) \boldsymbol{v}_-, \tag{3.16}$$

where $B(X)$ and $C(X)$ are arbitrary functions. To obtain an equation for the Amplitude $A(X',T)$ we choose $B(X) = \delta(X - X')$ and $C(X) = 0$[10]. Here, we briefly demonstrate the use of the Fredholm alternative, i.e. we calculate $\langle \boldsymbol{k}, \boldsymbol{q}_5 \rangle$. The linear terms in $\boldsymbol{u}^{(1)}$ within $\boldsymbol{q}_5$ contribute as

$$\begin{aligned} &\langle e^{-\mathrm{i}\hat{\omega}\tau} \delta(X - X') \boldsymbol{v}_+; (-\tilde{\mu}\partial_{XX} - \partial_{XXXX} - \partial_T) \boldsymbol{u}^{(1)} \rangle \\ &= \langle e^{-\mathrm{i}\hat{\omega}\tau} \delta(X - X') \boldsymbol{v}_+; (-\tilde{\mu}\partial_{XX} - \partial_{XXXX} - \partial_T)(e^{-\mathrm{i}\hat{\omega}\tau} A(X,T) \boldsymbol{v}_+ + e^{\mathrm{i}\hat{\omega}\tau} A(X,T) \boldsymbol{v}_-) \rangle \\ &= \int \mathrm{d}X \int \mathrm{d}\tau \left(e^{\mathrm{i}\hat{\omega}\tau} \delta(X - X') \right) (-\tilde{\mu}\partial_{XX} - \partial_{XXXX} - \partial_T) e^{-\mathrm{i}\hat{\omega}\tau} A(X,T) \\ &= (-\tilde{\mu}\partial_{X'X'} - \partial_{X'X'X'X'} - \partial_T) A(X',T), \end{aligned} \tag{3.17}$$

[10] This is meant in a sense that X' is a free parameter, i.e. we choose a specific point in space, where we want to evaluate the amplitude keeping in mind, that the Fredholm alternative can be applied for any other X' and therefore the derived Amplitude equation holds everywhere in space.

where in the final step we have used multiple partial integrations, or again in a more abstract sense, the unitarity of the operator $e^{\mathrm{i}\hat{\omega}\tau}$. Expressing $((u_1^{(1)})^3, u_2^{(1)})^3)^T$ by the amplitude, i.e. inserting Eq. (3.12) into the nonlinear part of q_5, it reads

$$\begin{aligned}
&\partial_{XX}\begin{pmatrix} u_1^{(1)^3} \\ u_2^{(1)^3} \end{pmatrix} \\
&= \partial_{XX}\Bigg[\left(e^{-\mathrm{i}\hat{\omega}\tau}A(X,T)\right)^3\begin{pmatrix}(\boldsymbol{v}_+)_1^3\\(\boldsymbol{v}_+)_2^3\end{pmatrix} + 3\left(e^{\mathrm{i}\hat{\omega}\tau}A^*(X,T)\right)\left(e^{-\mathrm{i}\hat{\omega}\tau}A(X,T)\right)^2\begin{pmatrix}(\boldsymbol{v}_+)_1^2(\boldsymbol{v}_-)_1\\(\boldsymbol{v}_+)_2^2(\boldsymbol{v}_-)_2\end{pmatrix} \\
&\qquad + 3\left(e^{\mathrm{i}\hat{\omega}\tau}A^*(X,T)\right)^2\left(e^{-\mathrm{i}\hat{\omega}\tau}A(X,T)\right)\begin{pmatrix}(\boldsymbol{v}_+)_1(\boldsymbol{v}_-)_1^2\\(\boldsymbol{v}_+)_2(\boldsymbol{v}_-)_2^2\end{pmatrix} + \left(e^{\mathrm{i}\hat{\omega}\tau}A^*(X,T)\right)^3\begin{pmatrix}(\boldsymbol{v}_-)_1^3\\(\boldsymbol{v}_-)_2^3\end{pmatrix}\Bigg] \\
&= \partial_{XX}\Bigg[\frac{1}{2}\left(e^{-\mathrm{i}\hat{\omega}\tau}A(X,T)\right)^3\boldsymbol{v}_- + \frac{3}{2}\left(e^{\mathrm{i}\hat{\omega}\tau}A^*(X,T)\right)\left(e^{-\mathrm{i}\hat{\omega}\tau}A(X,T)\right)^2\boldsymbol{v}_+ \\
&\qquad + \frac{3}{2}\left(e^{\mathrm{i}\hat{\omega}\tau}A^*(X,T)\right)^2\left(e^{-\mathrm{i}\hat{\omega}\tau}A(X,T)\right)\boldsymbol{v}_- + \frac{1}{2}\left(e^{\mathrm{i}\hat{\omega}\tau}A^*(X,T)\right)^3\boldsymbol{v}_+\Bigg].
\end{aligned} \tag{3.18}$$

Here we notice that the first and third term vanish upon applying the Fredholm alternative as $\langle \boldsymbol{v}_+; \boldsymbol{v}_- \rangle = 0$. We then deal with the second term first. Here, we use the identity $\delta(X-X') = \sum_Q e^{\mathrm{i}Q(X-X')}$ and express $A(X,T)$ through its Fourier transform $A(X,T) = \sum_K \tilde{A}(K,T)e^{\mathrm{i}QX}$ to evaluate the scalar product

$$\begin{aligned}
&\left\langle e^{-\mathrm{i}\hat{\omega}\tau}\delta(X-X')\boldsymbol{v}_+; \partial_{XX}\left(e^{\mathrm{i}\hat{\omega}\tau}A^*(X,T)\right)\left(e^{-\mathrm{i}\hat{\omega}\tau}A(X,T)\right)^2\boldsymbol{v}_+\right\rangle \\
&= \left\langle e^{-\mathrm{i}\hat{\omega}\tau}\sum_Q e^{\mathrm{i}Q(X-X')}\boldsymbol{v}_+; \partial_{XX}\left(e^{\mathrm{i}\hat{\omega}\tau}\sum_K \tilde{A}^*(K,T)e^{-\mathrm{i}KX}\right)\left(e^{-\mathrm{i}\hat{\omega}\tau}\sum_K \tilde{A}(K,T)e^{\mathrm{i}KX}\right)^2\boldsymbol{v}_+\right\rangle \\
&= \sum_{Q,K,K',K''} e^{\mathrm{i}QX'}\tilde{A}^*(K,T)\tilde{A}(K',T)\tilde{A}(K'',T)\left(-(-K+K'+K'')^2\right)\times \\
&\qquad \times \int e^{\mathrm{i}\omega\tau(-Q^2-K^2+K'^2+K''^2)}\mathrm{d}\tau\int e^{\mathrm{i}X(-Q-K+K'+K'')}\mathrm{d}X.
\end{aligned} \tag{3.19}$$

The two integrals in the last line vanish whenever one of the integrands has a nonzero phase. Therefore only terms with

$$-Q^2-K^2+K'^2+K''^2 = 0 \quad \text{and} \quad -Q-K+K'+K'' = 0 \tag{3.20}$$

contribute. This can only hold if the wavenumbers occur in equal pairs, i.e. if $Q = K'$ and $K = K''$ or if $Q = K''$ and $K = K'$[11]. As both solutions yield the same contribution, the scalar product Eq. (3.19)

[11] This can be proven as follows: the second equation yields $K'-Q = -(K''-K)$. Factorising the first equation using the 3rd binomial theorem and plugging this in yields

$$(K'-Q)(K'+Q)+(K''-K)(K''+K) = 0 \quad \Longrightarrow \quad (K'-Q)(K'+Q-K''-K) = 0$$

So either $K' = Q$ or $K'+Q-K''-K = 0$. In the latter case we can add the second equation to obtain $K' = K$. One can also think of this as an elastic scattering of two particles with equal energy and opposite momenta, where both particles can either pass each other unhindered or exchange their momenta.

becomes

$$\begin{aligned} &2\sum_Q e^{\mathrm{i}QX'}(-Q^2)\tilde{A}(Q,T)\sum_K \tilde{A}^*(K,T)\tilde{A}(K,T) - \sum e^{\mathrm{i}QX'}(-Q^2)\tilde{A}(Q,T)\tilde{A}(Q,T)\tilde{A}^*(Q,T) \\ &= \partial_{X'X'}\left(2A(X',T)\overline{|A|^2} - \mathscr{F}^{-1}[\tilde{A}|\tilde{A}|^2]\right) \end{aligned} \tag{3.21}$$

where in the last step we used Parsevals theorem (see Eq. (B.6) in appendix B). The second term accounts for double-counting the solution with $Q = K = K' = K''$ that is counted twice in the left expression but occurs only once in Eq. (3.19). Although possible, it is tedious to express the second term with the real space field $A(X,T)$, as it becomes a double-convolution, i.e. $\mathscr{F}^{-1}[\tilde{A}|\tilde{A}|^2](X) = [A(\tilde{X})\star A(\tilde{X})\star A^*(-\tilde{X})](X)$ (see Eq. B.8 for the transformation). We therefore stick to using the notation $\mathscr{F}^{-1}[\tilde{A}|\tilde{A}|^2]$. Going back to the fourth term in Eq. (3.18) that has not been dealt with yet, and after performing similar steps, there nonvanishing contributions have to fulfill

$$-Q^2 - K^2 - K'^2 - K''^2 = 0 \quad \text{and} \quad -Q - K - K' - K'' = 0. \tag{3.22}$$

The only solution is $Q = K = K' = K'' = 0$, which does not contribute since for the homogeneous modes we have $\tilde{A}(0,T) = 0$ because of the conservation law.

Collecting all contributions and dropping the dashes, we arrive at the amplitude equation

$$\partial_T A = \partial_{XX}(-\tilde{\mu}A + \frac{3}{2}(2A\overline{|A|^2} - \mathscr{F}^{-1}[\tilde{A}|\tilde{A}|^2]) - \partial_{XX}A). \tag{3.23}$$

Rescaling to the original variables and introducing $a = \varepsilon A$, it reads

$$\boxed{\partial_t a = \partial_{xx}\left(-\mu a + \frac{3}{2}(2a\overline{|a|^2} - \mathscr{F}^{-1}[\tilde{a}|\tilde{a}|^2]) - \partial_{xx}a\right)}, \tag{3.24}$$

which is related to the original fields via

$$\boldsymbol{u}(x,t) = e^{-\mathrm{i}\omega t\partial_{xx}}a(x,t)\boldsymbol{v}_+ + e^{\mathrm{i}\omega t\partial_{xx}}a^*(x,t)\boldsymbol{v}_- \tag{3.25}$$

Linearising the amplitude equation around the trivial steady state $a = 0$ yields a dispersion relation

$$\lambda(k^2) = k^2(\mu - k^2), \tag{3.26}$$

which resembles precisely the real part of the original dispersion relation, showing that - as intended - we achieved a separation of oscillatory behaviour on the fast timescale τ from the linear growth of the Fourier modes on the slow timescale T. Each pair of complex conjugate eigenvalues of the full dynamics now corresponds to a twice degenerate real eigenvalue (if one still counts real degrees of freedom despite this equation being complex). The easiest and most intuitive form of the amplitude equation is obtained in Fourier space, as the equation for the amplitude $\tilde{a}(k,t)$, i.e. the Fourier transform

of $a(x,t)$ in Eq. (3.24) reads

$$\partial_t \tilde{a} = -k^2 \left[-\mu \tilde{a} + \frac{3}{2} \left(\tilde{a} \sum_{k'} |\tilde{a}(k',t)|^2 - \tilde{a}|\tilde{a}|^2 \right) + k^2 \tilde{a} \right]. \tag{3.27}$$

There the Fourier modes almost uncouple, with the only exception being the contribution of their total sum $\sum_{k'} |\tilde{a}(k',t)|^2$. On the one hand, Eq. (3.27) clarifies, that despite the nonlocal contributions in Eq. (3.24), it can be numerically solved with affordable computational effort using spectral methods. On the other hand, Eq. (3.27) indicates that in search of an interpretation of the onset behaviour of the conserved Hopf bifurcation it is instructive to interpret Fourier modes as the central objects that interact with each other and not the original, real-space fields. We also observe remarkable parallels to a derivation by Knobloch and De Luca [29](see also [27, 30]) for the nonconserved wave instability, where comparable mean-field couplings occur. There they state that in the generic case where the group velocities (i.e. the derivatives of the imaginary part of the eigenvalues at the critical wavenumber) are of $\mathcal{O}(1)$, a right- and left- travelling "wavetrain" only interact via their means values.

Summarising these findings more figuratively, one might argue that on the fast timescale τ, each mode q freely propagates with a distinct phase velocity $v = 2\omega q$. After an infinitesimal time interval $\mathrm{d}T$ has passed on the slow timescale, several (and in the asymptotic limit infinitely many) maxima and minima of every other mode will have passed each other due to their propagation on the fast timescale. Therefore, the only property that a mode "witnesses" and interacts with, is the frequency-independent mean square of the other modes that are present[12].

3.4. Variational character of the amplitude equation

Remarkably Eq. (3.24) has a gradient dynamics form, i.e. $a_t = \partial_{xx} \frac{\delta \mathscr{F}[a]}{\delta a^*}$, where the functional is given by

$$\begin{aligned} \mathscr{F}[a] = &\int_{-l/2}^{l/2} \left(-\mu |a|^2 + |\partial_x a|^2 \right) \mathrm{d}x + \frac{3l}{2} \left(\frac{1}{l} \int_{-l/2}^{l/2} |a|^2 \mathrm{d}x \right)^2 \\ &- \frac{3}{4l^2} \iiint_{[-\frac{l}{2},\frac{l}{2}]^3} a^*(x) a^*(-x') a(x'') a(x - x' - x'') \mathrm{d}x \, \mathrm{d}x' \mathrm{d}x'' . \end{aligned} \tag{3.28}$$

For the calculation of the functional variations see Eqs. (B.10) and (B.12) in appendix B. This functional is bounded from below, although this is not directly apparent as the last term enters with negative sign. To prove this we express the final two terms in Fourier-space. Again using Parsevals theorem, we have

[12] An illustration of this is a light bulb: Despite being supplied by an alternating current, we only witness its reaction to the mean (square), since the timescale of the oscillating current is much faster compared to the heating and cooling of the incandescent filament

on the one hand

$$\frac{3l}{2}\left(\frac{1}{l}\int_{-l/2}^{l/2}|a|^2\mathrm{d}x\right)^2=\frac{3l}{2}\left(\sum_k|\tilde{a}(k)|^2\right)^2. \tag{3.29}$$

On the other hand, expressed by the Fourier transformed amplitude $\tilde{a}$, the last term reads (see Eq. (B.13) for the calculation)

$$\frac{3}{4l^2}\iiint_{[-\frac{l}{2},\frac{l}{2}]^3}a^*(x)a^*(-x')a(x'')a(x-x'-x'')\mathrm{d}x\mathrm{d}x'\mathrm{d}x''=\frac{3l}{4}\sum_k|\tilde{a}(k)|^4. \tag{3.30}$$

As $(\sum_k|\tilde{a}(k)|^2)^2\geq\sum_k|\tilde{a}(k)|^4$ the first term will always be at least twice as large as the second one, which shows that $\mathscr{F}[a(x)]$ is bounded from below.
The variational character has important implications for the behaviour of the amplitude equation. As usual the evaluation of the total time derivative of $\mathscr{F}[a]$, i.e.

$$\begin{aligned}\frac{\mathrm{d}}{\mathrm{d}t}\mathscr{F}[a(x,t)]&=\int_{-l/2}^{l/2}\left(\frac{\delta\mathscr{F}}{\delta a^*}\frac{\mathrm{d}a^*}{\mathrm{d}t}+\frac{\delta\mathscr{F}}{\delta a}\frac{\mathrm{d}a}{\mathrm{d}t}\right)\mathrm{d}x\\&=\int_{-l/2}^{l/2}\left[\frac{\delta\mathscr{F}}{\delta a^*}\left(\partial_{xx}\frac{\delta\mathscr{F}}{\delta a}\right)+\frac{\delta\mathscr{F}}{\delta a}\left(\partial_{xx}\frac{\delta\mathscr{F}}{\delta a^*}\right)\right]\mathrm{d}x\overset{\text{p.I.}}{=}-2\int_{-l/2}^{l/2}\left|\partial_x\frac{\delta\mathscr{F}}{\delta a}\right|^2\mathrm{d}x\leq 0,\end{aligned} \tag{3.31}$$

demonstrates, that $\mathscr{F}[a]$ is a Lyapunov functional of the amplitude equation. Therefore, the amplitude will eventually approach a stable steady state. Transferring this back to the original equation, we see that the whole temporal behaviour then has to happen on the timescale τ, resembling the free propagation of the amplitude steady state analogously to the time evolution of a free propagating wave packet in the Schrödinger equation.

3.5. Steady states of the amplitude equation

Before going into more detail, we discuss the simple solution to Eq. (3.25) given by

$$a(x,t)=a_0e^{\mathrm{i}qx}\quad\text{with}\quad\frac{3}{2}|a_0|^2=\mu-q^2, \tag{3.32}$$

where $|q|\in(0,\sqrt{\mu})$ for $\mu>0$. These solutions are – up to prefactors – identical to the "phase-winding solutions", that occur in the real Ginzburg-Landau equation. There, going back to the original fields, they correspond to a large scale modulation of a small scale pattern. In contrast here we find

$$\boldsymbol{u}=e^{-\mathrm{i}\omega\tau}a(x,t)\boldsymbol{v}_++c.c.=a_0e^{\mathrm{i}(qx+\omega q^2t)}\boldsymbol{v}_++c.c.=\sqrt{2}|a_0|\begin{pmatrix}\sin(qx+\omega q^2t+\phi)\\\cos(qx+\omega q^2t+\phi)\end{pmatrix}. \tag{3.33}$$

Therefore a single-mode solution of the amplitude equation becomes a travelling wave with velocity $-\omega q$, where the fields u_1 and u_2 are phase shifted by $\pi/2$. Left-travelling [right-travelling] waves are

hence given by $q > 0$ [$q < 0$] and have equal amplitudes. The global phase ϕ is determined by the initial condition.

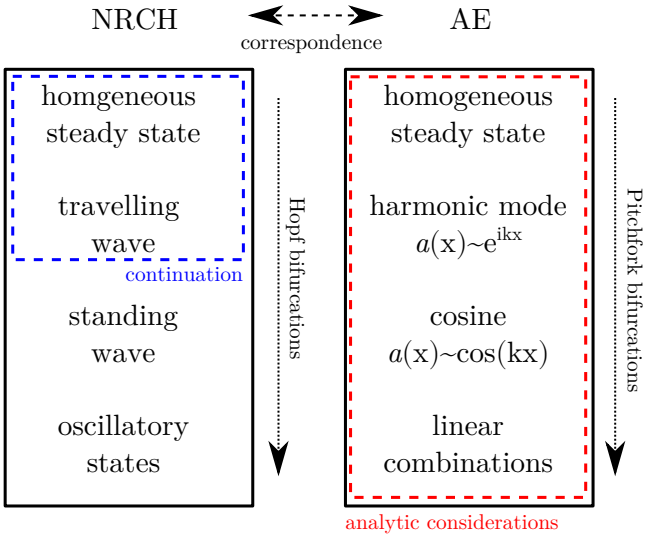

Figure 3.2: Sketch of the correspondence between the two levels of description obtained from the full NRCH dynamics and the amplitude equation (AE). The blue and red boxes mark the states that will be further investigated in a bifurcation analysis in section 3.6.1.

To find the general solution of the steady state equation, i.e. Eq. (3.24) with $\partial_t a = 0$, we integrate twice. The first integration constant vanishes as we request the net flux to be zero. Remarkably, here we can also eliminate the second integration constant as we have to demand $\overline{a} = 0$, because the amplitude a was introduced as the perturbation from the mean value of the original field. As a result we have

$$-\mu a + 3a\overline{|a|^2} - \frac{3}{2}\mathscr{F}^{-1}[\tilde{a}|\tilde{a}|^2] - \partial_{xx} a = 0\,. \tag{3.34}$$

To solve it, we reintroduce the Fourier-transform, i.e. we substitute $a(x,t) = \sum_q \tilde{a}(q)e^{\mathrm{i}qx}$, or equivalently we set $\partial_t \tilde{a} = 0$ in Eq. (3.27)

$$\sum_q \left(-\mu + 3\sum_k |\tilde{a}(k)|^2 - \frac{3}{2}|\tilde{a}(q)|^2 + q^2 \right) \tilde{a}(q) e^{\mathrm{i}qx} = 0. \tag{3.35}$$

Since the $e^{\mathrm{i}qx}$ are linear independent, all contributing modes, i.e. all modes where $\tilde{a}(q) \neq 0$ satisfy $-\mu + 3\sum_k |\tilde{a}(k)|^2 - \frac{3}{2}|\tilde{a}(q)|^2 + q^2 = 0$. We can therefore construct solutions as follows: We pick an arbitrary set of N pairwise disjoint contributing modes $q_1, \ldots, q_N$. Then the mean squares of their amplitudes $\tilde{a}_1, \ldots, \tilde{a}_N$ are determined by the linear system

$$\begin{pmatrix} \frac{1}{2} & 1 & \ldots & 1 \\ 1 & \frac{1}{2} & \ldots & 1 \\ \ldots & \ldots & \ldots & \ldots \\ 1 & 1 & \ldots & \frac{1}{2} \end{pmatrix} \begin{pmatrix} |\tilde{a}_1|^2 \\ |\tilde{a}_2|^2 \\ \ldots \\ |\tilde{a}_N|^2 \end{pmatrix} = \frac{1}{3} \begin{pmatrix} \mu - q_1^2 \\ \mu - q_2^2 \\ \ldots \\ \mu - q_N^2 \end{pmatrix}, \tag{3.36}$$

and the phases are left arbitrary. As the solutions have to fulfill $|\tilde{a}_i|^2 > 0$ for all i, for each configuration there exists a threshold value μ_t, such that the solution exists if $\mu > \mu_t$. Note that the single-mode solution arises as the special case for $N = 1$. To illustrate the procedure and its result, we also discuss the case $N = 2$ in more detail. In this case Eq. (3.36) reduces to

$$\begin{pmatrix} \frac{1}{2} & 1 \\ 1 & \frac{1}{2} \end{pmatrix} \begin{pmatrix} |\tilde{a}_1|^2 \\ |\tilde{a}_2|^2 \end{pmatrix} = \frac{1}{3} \begin{pmatrix} \mu - q_1^2 \\ \mu - q_2^2 \end{pmatrix}, \tag{3.37}$$

and is solved by

$$\begin{pmatrix} |\tilde{a}_1|^2 \\ |\tilde{a}_2|^2 \end{pmatrix} = \frac{2}{9} \begin{pmatrix} \mu + q_1^2 - 2q_2^2 \\ \mu - 2q_1^2 + q_2^2 \end{pmatrix}. \tag{3.38}$$

For $q_1 = -q_2 =: q_s$ both equations are similar and reduce to

$$|\tilde{a}_{1,2}|^2 = \frac{2}{9}(\mu - q_s^2). \tag{3.39}$$

Notably the condition for the existence of the solution is $\mu - q_s^2 > 0$ and is therefore precisely the same as for the single harmonic mode with the same wavelength. Specifically if $\tilde{a}_1 = \tilde{a}_2$ the solution then reads:

$$a(x,t) = \tilde{a}_s \cos(kx) \quad \text{with} \quad |\tilde{a}_s|^2 = \frac{8}{9}(\mu - q_s^2) \tag{3.40}$$

For this solution the original fields become

$$\boldsymbol{u}(x,t) = \sqrt{2}|a_s| \cos(kx) \begin{pmatrix} \sin(\omega q_s^2 t + \phi) \\ \cos(\omega q_s^2 t + \phi) \end{pmatrix}, \tag{3.41}$$

which is a standing wave, where independently of space and time, the two fields are phase-shifted in time by $\frac{\pi}{2}$. Note that this solution can be viewed as a superposition of the left and right travelling waves, that have already been discussed. For the case $q_2 > q_1$, Eq. (3.38) has a solution, when $\mu - 2q_2^2 + q_1^2 > 0$, i.e. it exists only for μ-values that are strictly larger than the critical ones for each individual mode with wavenumbers q_1 and q_2. Further we note, that going back to the full dynamics, we see that any steady state of the amplitude equation corresponds to a superposition of travelling waves in the dynamics of the original equation, that we will here simply denote as "oscillatory states". An overview of the discussed solution types on the two levels of description, i.e. for the NRCH equation and the amplitude equation, is given in Fig. 3.2.

3.5.1. Linear stability of single-mode solutions

To analyse the stability of the single-mode solutions described above, we introduce a small complex perturbation $\varepsilon a_p(x,t)$ with $\varepsilon \ll 1$

$$a(x,t) = \left(\sqrt{\frac{2}{3}(\mu - q^2)} + \varepsilon a_p(x,t) \right) e^{\mathrm{i}qx} \quad \text{with} \quad a_p(x,t) \sim e^{\mathrm{i}kx + \lambda t}. \tag{3.42}$$

At $\mathscr{O}(\varepsilon)$ the terms in Eq. (3.24) contribute as

$$\partial_{xx}\mu a = -\mu(q+k)^2 e^{\mathrm{i}(q+k)x} \tag{3.43}$$

$$3\partial_{xx}a\overline{|a|^2} = -2(1+2\delta_{k,0})\,(q+k)^2\,(\mu-q^2)e^{\mathrm{i}(q+k)x} \tag{3.44}$$

$$\frac{3}{2}\partial_{xx}\mathscr{F}^{-1}[\tilde{a}|\tilde{a}|^2] = -3\delta_{k,0}(q+k^2)(\mu-q^2)e^{\mathrm{i}(q+k)x} \tag{3.45}$$

$$\partial_{xxxx}a = (q+k)^4\, e^{\mathrm{i}(q+k)x} \tag{3.46}$$

Note that the discontinuities, i.e. the terms $\sim \delta_{k,0}$ arise from the evaluation of integrals $\sim \int_{-l/2}^{l/2} e^{\mathrm{i}kx}\mathrm{d}x$. In other words, homogeneous perturbations of the amplitude are treated separately. Collecting all terms and multiplying with $e^{-\mathrm{i}(q+k)x}$ yields the dispersion relation

$$\lambda(k) = (q+k)^2\left[-\delta_{k,0}(\mu-q^2) - \mu + q^2 - 2qk - k^2\right]. \tag{3.47}$$

At $k=-q$ the dispersion relation always has a zero eigenvalue of multiplicity two, which originates from the mass-conserving character of the amplitude equation, i.e. multiplying out Eq. (3.42), we see that $k=-q$ corresponds to a homogeneous, zero-wavenumber perturbation that is forbidden due to the conservation law. Exemplary dispersion relations are sketched in Fig. 3.3.

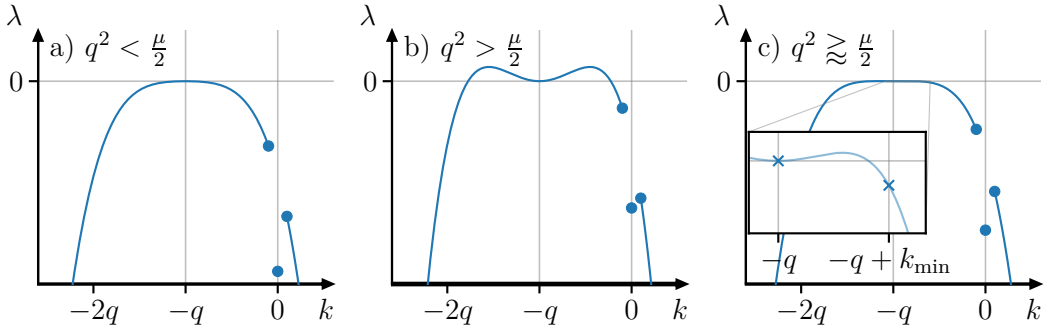

Figure 3.3: Shown are exemplary dispersion relations of the single mode-solution according to Eq. (3.47). Panels (a) and (b) show the stable and unstable case respectively. Panel (c) illustrates the effect of the discretised wavenumbers on the linear stability, i.e. in the displayed dispersion relation the wavenumber q is unstable in the infinite-system limit but stable for a finite domain of length $2\pi/k_{\min}$.

For a specific q the single-mode solution is stable if the right square bracket in Eq. (3.47) is negative for all k. The bifurcation parameter μ was introduced such that the instability occurs, when $\mu > \mu_c = 0$. Therefore $\mu - q^2 > 0$ is necessary for the existence of the single-mode solution with wavelength q and it is always stable with respect to homogeneous perturbations of the amplitude ($k=0$) despite the occurring discontinuity in the dispersion relation. For all other k the remaining terms in the square bracket, i.e. $-\mu + q^2 - 2qk - k^2$, describe a parabola with a (global) maximum at $k=-q$. In a finite system the wavenumbers are discretised, s.t. the first allowed perturbation occurs at $k=-q+k_{\min}$, see

Fig. 3.3 (c), which yields

$$q \text{ stable} \quad \Leftrightarrow \quad q^2 \leq \frac{1}{2}\left(\mu + k_{\min}^2\right). \tag{3.48}$$

In the limit of an infinite system, we have that $k_{\min} \to 0$ and therefore this then reduces to

$$\boxed{q \text{ stable} \quad \Leftrightarrow \quad q^2 \leq \frac{\mu}{2}}. \tag{3.49}$$

This is a remarkable result, since the spatial periodicity of the amplitude equation transfers to the full dynamics. Therefore, as it is independent of the system size, we have shown that in general there exist stable states with a higher periodicity than one, i.e. we have analytically shown, that oscillatory phase separation has a natural mechanism of coarsening suppression. Further note that this is completely different to the Turing instability since it does not rely on any notion of distinct rigidities as we deal with the case $\kappa = 1$.

The derived multistability naturally raises the question of wavelength selection, i.e. as there are multiple stable single-mode solutions with different wavenumbers, we want to know which one is realised in a system in dependence of the initial condition. For comparable systems like e.g. the real Ginzburg-Landau equation, this question is highly nontrivial and several different approaches can be chosen depending on the type of initial and boundary condition (see e.g. Misbah [24, Ch. 14]). Using Eq. (3.29) to calculate the free energy of a single-mode solution with wavenumber q yields

$$\frac{1}{l}\mathscr{F}[a] = -\frac{1}{3}(\mu - q^2)^2. \tag{3.50}$$

As single-mode solutions only exist for $\mu > q^2$, the minimal free energy is always attained at $q = k_{\min}$, implying that the system-filling wavelength is globally stable. In contrast though, one can also argue from the dispersion relation, that the mode with $q^2 = \mu/2$ has the largest growth rate, which makes this wavennumber seem to be more likely realised if the initial condition is a noisy homogeneous state.

To further validate our findings and investigate the raised question of wavelength selection, we continue with a numerical comparison between the amplitude equation and the full NRCH dynamics.

3.6. Numerical treatment

For the numerical analysis we employ two common methods, namely a bifuraction analysis and direct time simulations, where both are applied to the full dynamics and the amplitude equation, i.e. Eq. (3.9) and Eq. (3.24).

Remarkably, the steady states of the amplitude equation are fully determined by the analytic discussion in section 3.5, such that a numerical analysis does not provide further insights. As the NRCH dynamics contain various oscillatory states that are not easily tracked numerically, we restrict to the continuation of two simple types of solutions, namely steady states and travelling waves. We further employ the

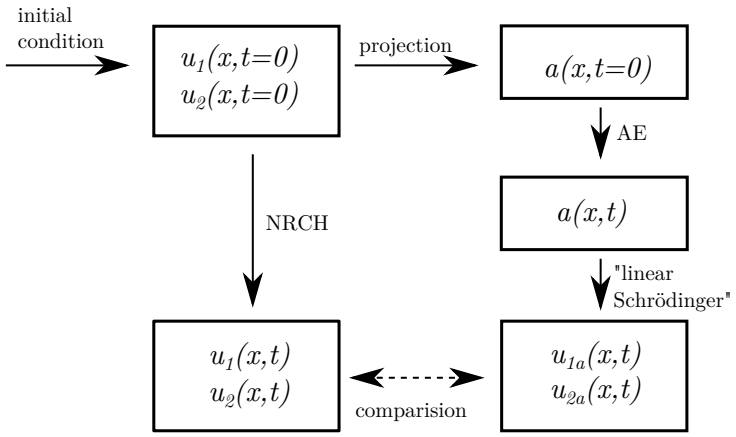

Figure 3.4: Sketch of the time-simulation scheme to compare the Nonreciprocal-Cahn-Hilliard-model (NRCH) with the derived amplitude equation (AE) at the onset of the conserved Hopf instability.

L^2-norm of the amplitude and the original field, i.e.

$$||a(x)||_{L^2} = \frac{1}{l}\sqrt{2\int_{-l/2}^{l/2}|a|^2\mathrm{d}x} \qquad \text{and} \qquad ||\boldsymbol{u}(x)||_{L^2} = \frac{1}{l}\sqrt{\int_{-l/2}^{l/2}(u_1^2+u_2^2)\mathrm{d}x}, \tag{3.51}$$

respectively as solution measures. The latter is evaluated in the comoving frame in the case of a travelling wave. Note that due to the relation between amplitude and real field derived in Sec. 3.5 the amplitude norm was scaled by a factor $\sqrt{2}$, such that the single mode solution in the amplitude equation and the corresponding travelling wave in the full dynamics have the same norm. The numerical continuation of the full NRCH dynamics is performed employing the finite element library *pde2path* [31].

For the time simulations, we use a semi-implicit Euler method for both the amplitude equation and the full dynamics. To match the initial condition, we set $t = 0$ in Eq. (3.25) and apply a scalar product with $\boldsymbol{v}_-$ to obtain

$$a(x,t=0) = \frac{1}{\sqrt{2}}\left[\mathrm{i}u_1(x,t=0)+u_2(x,t=0)\right], \tag{3.52}$$

i.e. the initial fields (u_1,u_2) correspond to the imaginary and real part of the initial amplitude. To compare the two levels of description we calculate the original fields from the solution of the amplitude equation, i.e. we evaluate

$$\begin{aligned}
\boldsymbol{u}_a(x,t) =& e^{-\mathrm{i}\omega t\partial_{xx}}a(x,t)\boldsymbol{v}_+ + e^{\mathrm{i}\omega t\partial_{xx}}a^*(x,t)\boldsymbol{v}_- \\
=& e^{-\mathrm{i}\omega t\partial_{xx}}\sum_k \tilde{a}(k,t)e^{\mathrm{i}kx}\boldsymbol{v}_+ + e^{\mathrm{i}\omega t\partial_{xx}}\sum_k \tilde{a}^*(k,t)e^{-\mathrm{i}kx}\boldsymbol{v}_- \\
=& \sum_k e^{\mathrm{i}kx}\left(e^{\mathrm{i}\omega tk^2}\tilde{a}(k,t)\boldsymbol{v}_+ + e^{-\mathrm{i}\omega tk^2}\tilde{a}^*(-k,t)\boldsymbol{v}_-\right) \\
=& \mathscr{F}^{-1}\left[e^{\mathrm{i}\omega tk^2}\mathscr{F}[a]\boldsymbol{v}_+ + e^{-\mathrm{i}\omega tk^2}\mathscr{F}[a^*]\boldsymbol{v}_-\right].
\end{aligned} \tag{3.53}$$

Here the inner Fourier-transformations do not result in any additional computational expense since they are already known as we solve the amplitude equation with a spectral method. A sketch of the scheme is shown in Fig. 3.4. Note that despite the circumstance that this backtransformation looks more complicated than for comparable cases (e.g. for the nonconserved pendant we would just multiply the amplitude with $e^{\mathrm{i}\omega t}$), it is still a completely linear procedure, analogous to solving a linear Schrödinger equation with a spectral method, i.e. the nonlinear behaviour arises solely from the amplitude equation.

3.6.1. Bifurcation structure

We start with a discussion of the bifurcation structure. Fig. 3.5 (a) collects the analytical considerations from section 3.5 in a bifurcation diagram whereas (b) shows the homogeneous steady state and travelling waves states in the NRCH model as obtained by path continuation. We start with a discussion of (a). At $\mu = 0.01$ the homogeneous branch becomes unstable in a pitchfork bifurcation as the state becomes unstable with respect to perturbations of the system filling mode $k_{\min} = \frac{2\pi}{l}$. After the bifurcation the homogeneous state has a fourfold degenerate positive eigenvalue[13], corresponding to real and imaginary perturbations with $\pm k_{\min}$. There three branches emerge, corresponding to the stable harmonic functions $a \sim e^{\pm \mathrm{i} k_{\min} x}$ and their unstable superposition $a \sim \cos(k_{\min} x)$. Note that the former have the same norm as they are related by symmetry.

Similar bifurcations happen on the homogeneous steady state branch for the modes with $k_n = n k_{\min}$, here up to $n = 6$, each further destabilising it (with fourfold degeneracy). Next, following the primary $(n = 2)$-branch, we observe a secondary bifurcation. At $\mu \approx 0.06$ three secondary branches emerge from the primary branch, corresponding to the linear combinations of $a(x) = a_1 e^{\pm \mathrm{i} k_1 x} + a_2 e^{\mathrm{i} k_2 x}$ and $a(x) = a_{1,s} \cos(k_1 x) + a_{2,s} e^{\pm \mathrm{i} k_2 x}$. There, the fourfold degenerate eigenvalue changes its sign from positive to negative and the primary branch is stabilised. Something similar occurs for the primary $(n = 3)$-branch, that emerges from the homogeneous branch with two fourfold degenerate positive eigenvalues. Following its path, we see that first the two mode-solutions with $n = \{1, 3\}$ emerge to stabilize the first eigenvalue and afterwards the two-mode-solutions with $n = \{2, 3\}$ emerge, such that also this primary branch becomes linearly stable. Something similar happens for every primary branch, e.g. the $(n = 4)$-branch is stabilised via three consecutive pitchfork bifurcations.

The analytic consideration allows us to find further branches – in fact all branches –, for example those with three contributing modes, that emerge from the ones with two contributing modes in tertiary bifurcations, indicated by the small circles in Fig. 3.5 (a).

Next, turning to the bifurcation diagram of the corresponding NRCH system displayed in Fig. 3.5 (b), we see that each pitchfork bifurcation of the trivial branch in (a) corresponds to a Hopf bifurcation in (b). At each bifurcation four complex eigenvalues cross the imaginary axis, corresponding to two equal pairs of complex conjugate eigenvalues, one for the left- and one for a right-travelling wave. Despite our technical restriction to the continuation of travelling wave states, it is obvious that another branch

[13] Note that for a clearer comparison with the real fields of the NRCH equation we count real degrees of freedom. Therefore, every eigenvalue of the complex equation is twice degenerate as any complex perturbation corresponds to an arbitrary linear combination of real and imaginary perturbations.

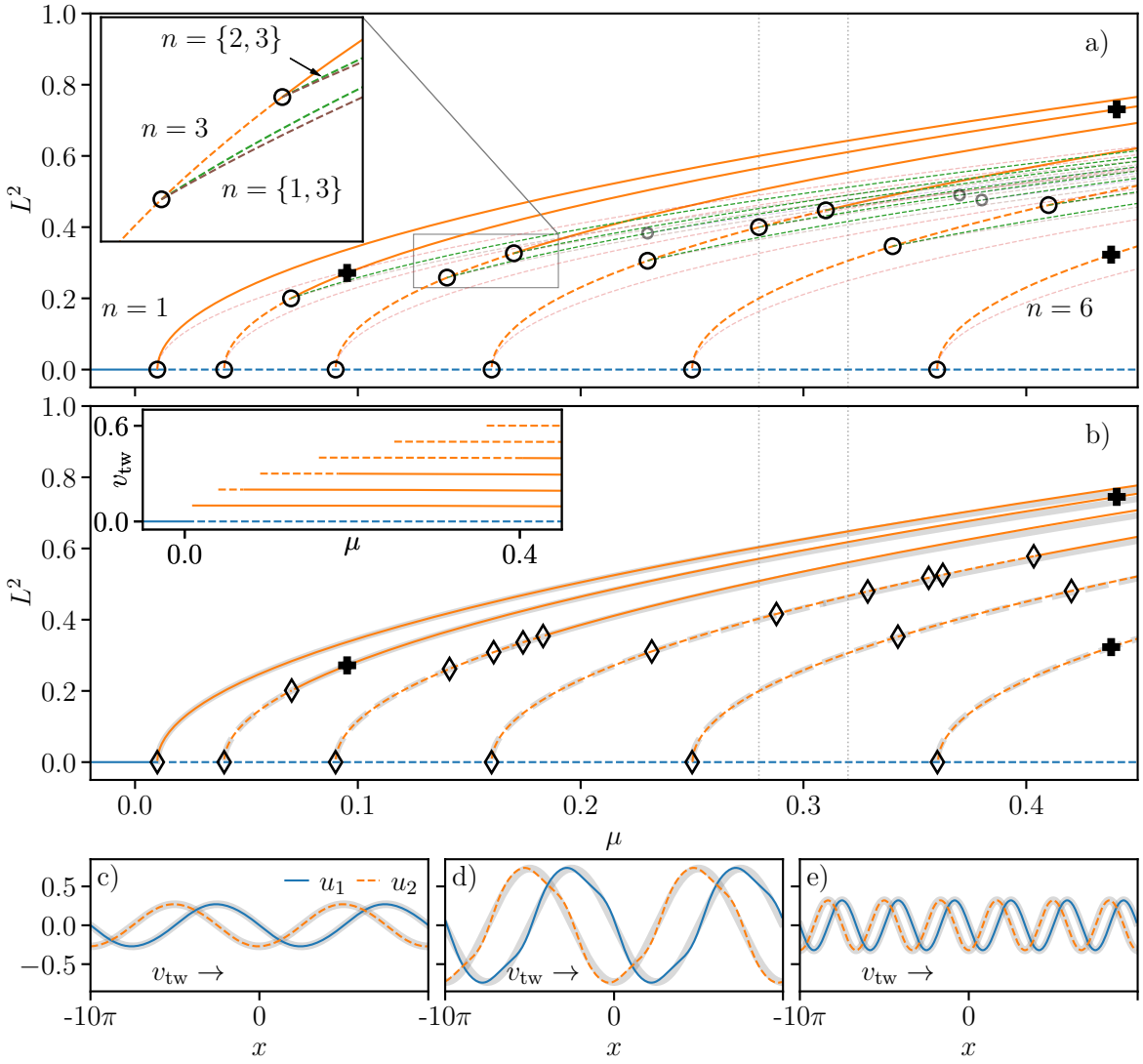

Figure 3.5: Bifurcation diagrams obtained for (a) the amplitude equation Eq. (3.24) and (b) the NRCH model Eq. (3.9). Solid [dashed] lines represent stable [unstable] states. The light gray lines in (b) reproduce the single-mode branches from (a) to allow for a comparison. The inset in panel (b) shows the velocity v_{tw} of travelling waves. Circles mark pitchfork bifurcations and diamonds mark Hopf bifurcations, the small circles indicate tertiary bifurcations of two-mode branches. Panels (c), (d) and (e) show the travelling wave states at loci marked by the crosses in (b), the light gray curves reflect the real and imaginary part of the corresponding steady states in the amplitude equation (rescaled by a factor $\sqrt{2}$). The dotted vertical lines in (a) and (b) indicate the parameter values where the time simulations in Fig. 3.7 are performed. The remaining parameters are $l = 20\pi$, $\alpha = 1$, $\kappa = 1$ and $\rho = 0$.

will emerge as the superposition of a right- and left-travelling wave, which is a standing wave. In fact this degeneracy is a general consequence of the translation- and parity invariance, i.e. it is guaranteed by the underlying O(2)-symmetry and can be rigorously proven as the *equivariant Hopf-theorem* [28, 32].

Following the emerging travelling wave branches, we see that analogously to the amplitude equation, the $(n = 1)$-branch is unconditionally stable, whereas branches for higher n stabilize in a sequence of secondary Hopf bifurcations. With the exception of the $(n = 2)$-branch, where the numerical precision is not sufficient to unambiguously tell, the degeneracy is partly lost, i.e. the $(n = 3)$-branch stabilises in four consecutive Hopf bifurcations, where at each time only one complex conjugate pair of eigenvalues crosses the imaginary axis. In terms of the amplitude amplitude equation the degeneracy is due to the relative sign of the superposed harmonic mode having no impact, i.e. the superpositions of the contributing modes $\{k_2, k_1\}$ and $\{k_2, -k_1\}$ behave equivalently. In terms of the full dynamics this would mean, that the superposition of a right-travelling wave with a left-travelling wave behaves analogously to the superposition of a right-travelling wave with a right-travelling wave. As this degeneracy is not seen in the full dynamics one might speculate that it is also resolved in a higher-order expansion of the weakly nonlinear analysis.

Fig. 3.5 (c)-(e) show various examples of travelling wave states from the numerical continuation. The underlying grey lines show the steady state solutions for imaginary and real part of the corresponding solution of the amplitude equation, demonstrating that they also quantitatively match. Note that further away from the primary instability, the travelling waves are deformed, i.e. they do not have the exact shape of the harmonic function predicted by the amplitude equation. The inset in panel (b) shows the velocity of travelling wave states, that is independent on the control parameter and scales linearly with the periodicity n. This quantitatively agrees with the dispersion relation that yields the phase velocity $v_{\mathrm{tw}} = 2\omega k_n$.

3.6.2. Time simulations

For the time simulations we start close to the critical point, here at $\mu = 1/16$, to verify that the amplitude equation reflects the dynamics correctly. We chose the domain size $l = 50\pi$, such that the previous analytical discussion predicts the largest stable wavenumber to be four-periodic. Fig. 3.6 shows spacetime plots for various initial conditions, namely white noise, an unstable $(n = 6)$-travelling wave solution and an $(n = 4)$-standing wave solution. The latter two are superposed with white noise of small amplitude ($\sim 10^{-3}$). Panels (b1), (d1) and (f1) show the field u_{1a} predicted from the amplitude equation (see Fig. 3.4), whereas panels (b2), (d2) and (f2) show the full dynamics of u_1. As we cannot visually resolve all oscillations over the whole simulation time, we show intermediate time intervals at critical times, i.e. when a transition happens. With the exception of (e) we restrict to showing $\Im(a)$ and u_1 as $\Re(a)$ and u_2 look qualitatively similar due to the underlying symmetries.

As u_1 and u_{1a} are visually indistinguishable in all panels, we conclude that the fields are well described by the amplitude equation, even after long simulation times. The absolute deviation between u_{1a} and u_1 is around 1 % of the maximal attained values.

All the considered initial conditions settle to the $(n = 4)$-travelling wave solution. For white noise the simulation is repeatedly done (10 times, not shown), always yielding the same final state, with left- and right-travelling waves appearing approximately equally often. This indicates that the basin of attraction of the $(n = 4)$-solution is large compared to that of the stable travelling wave states with

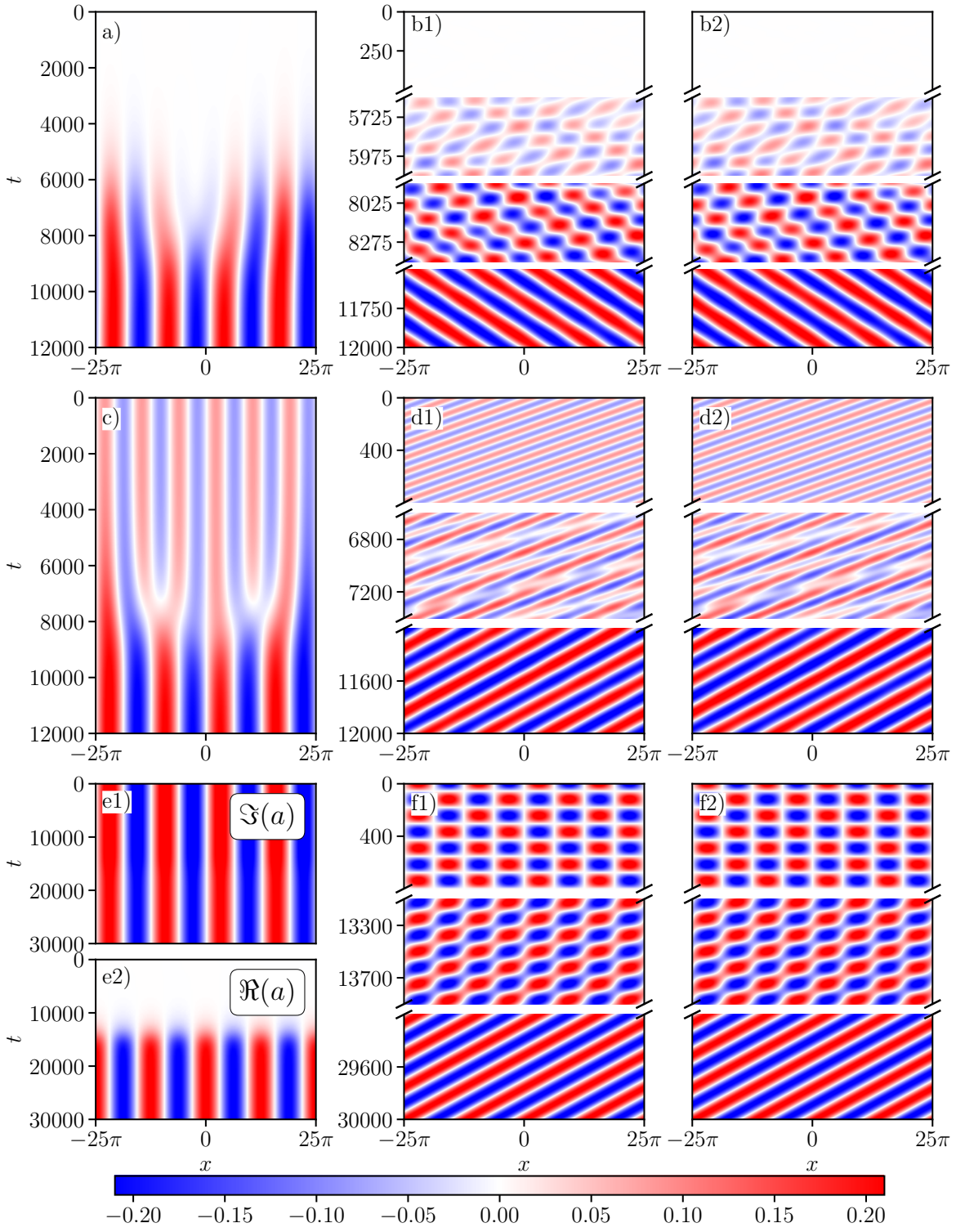

Figure 3.6: Spacetime plots for the amplitude (left column), the approximate full dynamics reconstructed from the amplitude equation (middle column) and the full dynamics obtained with the NRCH model (right colum) with different initial condition, namely white noise (first row), an unstable travelling wave (second row) and a standing wave (third row). (a), (c) and (e1) show the field $\Im(a)$, whereas (e2) shows $\Re(a)$. Panel (b), (d) and (f) display u_1. The parameters are $\mu = 1/16$, $l = 50\pi$, $\alpha = 1$, $\kappa = 1$, $\rho = 0$, the spatial discretisation consists of 512 points.

lower periodicity, leading to the hypothesis that the wavelength selection happens rather in dynamical processes by the largest growing modes and not due to the derived free energy functional.

In the case of the unstable $(n = 6)$-travelling-wave in Fig 3.6 (c) and (d) one observes, that it does not transition to an intermediate $(n = 5)$-state, but after visually staying the same until $t \approx 5000$ directly transitions into the $(n = 4)$-state. This is in contrast to usual, nonoscillatory coarsening processes. The standing wave solution in panels (e) and (f) also seems visually unchanged until at $t \approx 10^4$ it transitions into a travelling wave. As the standing wave initial condition here corresponds to a vanishing real part of the amplitude, real and imaginary part show qualitatively different behaviour, with the imaginary part staying unchanged and the real part growing until it reaches the same magnitude at $t \approx 15,000$. As expected for a single mode, real and imaginary part of the amplitude are phase shifted by $\pi/2$.

To conclude the discussion of the behaviour close to the onset of the instability, we emphasise the observation that time simulations have to be treated with special care when judging the stability of time periodic states. All intermediate states in panels (b), (d) and (f) stay qualitatively unchanged for several periods, here up to 50 periods for the standing wave state, despite being unstable. This is by no means an exclusive property of the conserved Hopf bifurcation (in fact the central idea of every multiscale analysis is to separate a slow transient at the onset of an instability), but here the linear Schrödinger-type relation between fast and slow timescale can lead to complicated oscillations on the fast timescale. In contrast to this, in panels (a), (c), and (e), i.e. on the slow timescale, the dynamics look surprisingly simple.

Next we briefly demonstrate, that further away from the onset of the instability we start to see qualitative differences between the amplitude equation and the full dynamics. Following the previous discussion of the bifurcation analysis, we note in Fig. 3.5 that at $\mu = 0.28$ both predict the $(n = 4)$-travelling wave state to be unstable. At $\mu = 0.32$ though, the amplitude equation predicts it to have stabilised, whereas the full NRCH equation predicts it to be still unstable (see the dotted vertical lines in Fig. 3.5). The results of time simulations at these μ-values with a white noise initial condition are displayed in Fig. 3.7. The observed final states are in all cases in line with the stability results of the respective bifurcation analysis.

Fig. 3.7 (b) retains the qualitative agreement between amplitude and full dynamics. Note that during the formation of the pattern i.e. at $t \approx 350$ there appear intermediate $(n = 4)$-structures, that then settle to the final state of the $(n = 3)$-solution due to their instability. These four-periodic structures appear similarly in panel (c), with the difference that there they are stable and become the permanent final-state of the amplitude equation.

Until $t \approx 500$ panels (d1) and (d2) look qualitatively similar. Then, both settle into an $(n = 4)$-travelling wave solution, where the full dynamics in panel (d2) start to show a modulation, i.e. individual peaks become thinner [wider] and higher [lower] with a higher period than the travelling wave, until at $t \approx$ 1500 two peaks merge and the dynamics settle to a stable three-periodic travelling wave solution.

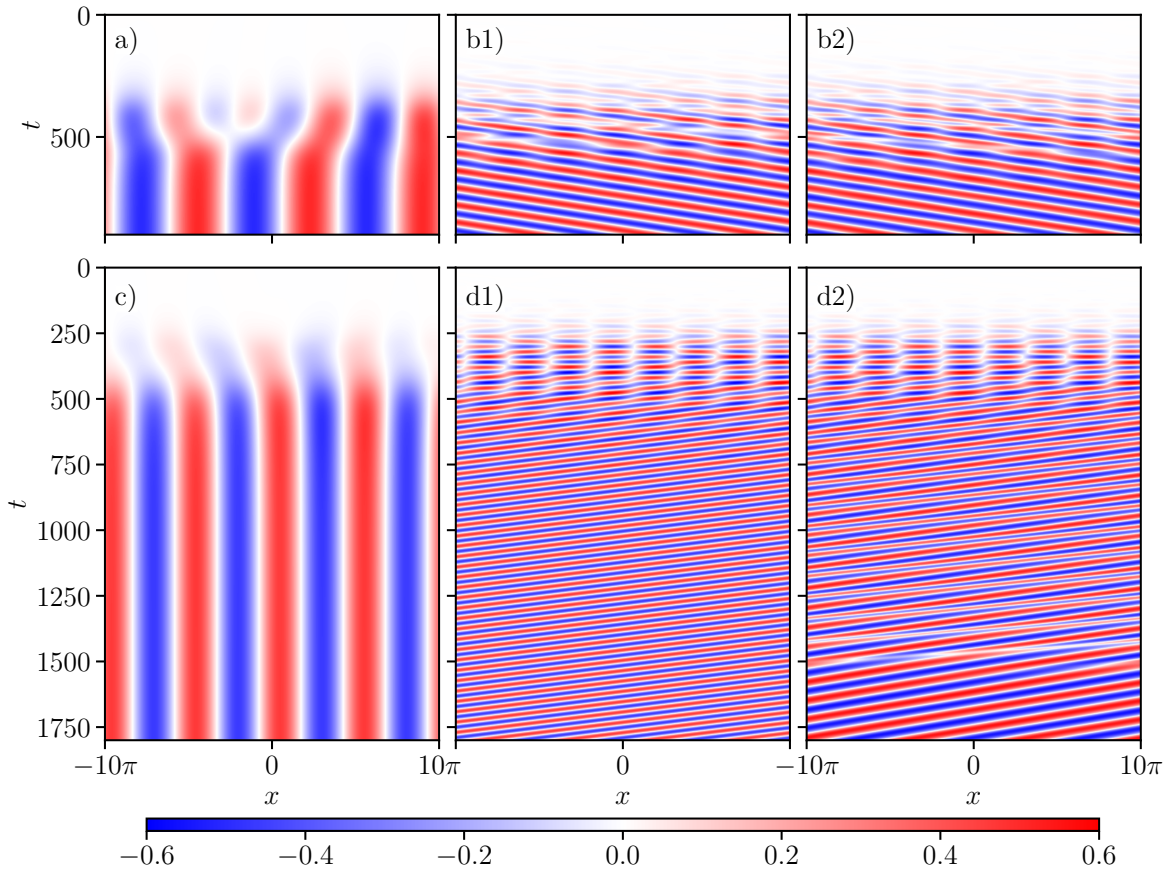

Figure 3.7: Spacetime plots for the amplitude $\Im(a)$ (left column), the approximate dynamics for u_{1a} obtained from the amplitude equation (middle column) and the full dynamics u_1 of the NRCH model (right colum) with white noise initial condition ($\sim 10^{-3}$) at $\mu = -0.28$ (first row) and $\mu = -0.32$ (second row). The parameters are $l = 20\pi$, $\alpha = 1$, $\kappa = 1$, $\rho = 0$, the spatial discretisation consists of 512 points.

3.7. The general case

Having established the scheme for the weakly nonlinear analysis for the minimal system and having shown that it gives analytical and numerical insights for the onset behaviour, we now proceed to discuss several amendments that occur in a more general case, namely the ad-hoc nonreciprocal Cahn-Hilliard model introduced in Eqs. (1.5)[14]. There, as we no longer restrict to vanishing mean concentrations, we introduce new variables $\tilde{\boldsymbol{u}}$ as deviations from the mean field $\bar{\boldsymbol{u}}$, i.e. $\boldsymbol{u}(x,t) = \bar{\boldsymbol{u}} + \tilde{\boldsymbol{u}}(x,t)$ and obtain

$$\begin{aligned} \partial_t \tilde{u}_1 &= \partial_{xx}\left[(\sigma_1 + 3\bar{u}_1^2)\tilde{u}_1 + 3\bar{u}_1\tilde{u}_1^2 + \tilde{u}_1^3 - \partial_{xx}\tilde{u}_1 - (\rho+\alpha)\tilde{u}_2\right] \\ \partial_t \tilde{u}_2 &= \partial_{xx}\left[(\sigma_2 + 3\bar{u}_2^3)\tilde{u}_2 + 3\bar{u}_2\tilde{u}_2^2 + \tilde{u}_2^3 - \kappa\partial_{xx}\tilde{u}_2 - (\rho-\alpha)\tilde{u}_1\right], \end{aligned} \tag{3.54}$$

[14]This is not the most general case, which – in line with the discussion in section 2.4 – one can argue to be the generalised nonreciprocal Cahn-Hilliard model derived by Frohoff-Hülsmann and Thiele [20]. But since it contains 34 parameters, the occurring terms in the derivation would become hard to handle. Nonetheless we do not expect to see new fundamental obstacles arising in the most general case.

where we already dropped constant terms from the bracket, that vanish after applying the derivatives. We then drop the tildes and impose the condition of being close to the onset of the conserved Hopf bifurcation , i.e. the trace of the linear system is of $\mathscr{O}(\varepsilon^2)$ and the determinant is positive. To express this in the expansion, we reparametrise the linear self-interaction contributions as

$$-\mu + c := \sigma_1 + 3\bar{u}_1^2 \qquad \text{and} \qquad -\mu - c := \sigma_2 + 3\bar{u}_2^2. \tag{3.55}$$

Then the system reads

$$\begin{aligned} \partial_t u_1 &= \partial_{xx}\left[(-\mu + c)u_1 + 3\bar{u}_1 u_1^2 + u_1^3 - \partial_{xx}u_1 - (\rho + \alpha)u_2\right] \\ \partial_t u_2 &= \partial_{xx}\left[(-\mu - c)u_2 + 3\bar{u}_2 u_2^2 + u_2^3 - \kappa\partial_{xx}u_2 - (\rho - \alpha)u_1\right]. \end{aligned} \tag{3.56}$$

As before, the expansion parameter ε is then defined via $|\mu| = \varepsilon^2|\tilde{\mu}| \ll 1$. Then, we again formally expand the field in orders of ε and introduce the scalings $\partial_t = \varepsilon^2\partial_\tau + \varepsilon^4 T$ and $\partial_x = \varepsilon\partial_X$. We start solving Eq. (3.56) order by order. The linear equation arising at $\mathscr{O}(\varepsilon^3)$ then reads

$$\partial_\tau \begin{pmatrix} u_1^{(1)} \\ u_2^{(1)} \end{pmatrix} = \partial_{XX} \begin{pmatrix} c & -(\rho + \alpha) \\ -(\rho - \alpha) & -c \end{pmatrix} \begin{pmatrix} u_1^{(1)} \\ u_2^{(1)} \end{pmatrix} \tag{3.57}$$

Using the ansatz $\boldsymbol{u}^{(1)} \sim e^{\mathrm{i}(QX + \omega(Q)\tau))}\boldsymbol{v}$ one can again solve the linear system to obtain $\omega(Q) = \pm\omega Q^2$, such that superposition and introduction of $\hat{\omega} = \omega\partial_{XX}$ yields

$$\begin{aligned} &\boldsymbol{u}^{(1)} = e^{-\mathrm{i}\hat{\omega}\tau}A(X,T)\boldsymbol{v}_+ + c.c. \\ &\text{with} \quad \omega = \pm\sqrt{\alpha^2 - \rho^2 - c^2} \quad \text{and} \quad \boldsymbol{v}_\pm = \sqrt{\frac{\alpha - \rho}{2\alpha}} \begin{pmatrix} \frac{c \mp i\sqrt{\alpha^2 - \rho^2 - c^2}}{\alpha - \rho} \\ 1 \end{pmatrix}. \end{aligned} \tag{3.58}$$

Before continuing, we can already derive important consequences for travelling wave solutions, where $A \sim e^{\mathrm{i}KX}$. If $\rho \neq 0$ the two fields will no longer have equal amplitudes and if $c \neq 0$ the two fields will no longer be phase-shifted by $\pi/2$. Instead the relative amplitude and phase are then given by:

$$\frac{\max(u_1)}{\max(u_2)} = \sqrt{\frac{\alpha + \rho}{\alpha - \rho}} \quad \text{and} \quad \phi_r = \tan^{-1}\left(\frac{\sqrt{\alpha^2 - \rho^2 - c^2}}{c}\right). \tag{3.59}$$

The occuring equation at $\mathscr{O}(\varepsilon^4)$ reads

$$\begin{aligned} &\underline{L}u^{(2)} = \boldsymbol{q}_4 \\ &\text{with} \qquad \underline{L} = \partial_\tau \underline{1} - \partial_{XX} \begin{pmatrix} c & -(\rho + \alpha) \\ -(\rho - \alpha) & -c \end{pmatrix} \qquad \text{and} \qquad \boldsymbol{q}_4 = \partial_{XX} \begin{pmatrix} 3\bar{u}_1 (u_1^{(1)})^2 \\ 3\bar{u}_2 (u_2^{(1)})^2 \end{pmatrix}. \end{aligned} \tag{3.60}$$

To apply the Fredholm alternative at $\mathscr{O}(\varepsilon^4)$ we need the eigenvectors of the adjoint linear operator $\underline{L}^\dagger$, which are given by

$$\boldsymbol{v}_\pm^\dagger = \sqrt{\frac{\alpha+\rho}{2\alpha}} \begin{pmatrix} \frac{-c\mp \mathrm{i}\sqrt{\alpha^2-\rho^2-c^2}}{\alpha+\rho} \\ 1 \end{pmatrix}, \tag{3.61}$$

where we note that $\langle \boldsymbol{v}_+^\dagger; \boldsymbol{v}_- \rangle = 0$. Therefore now we take the elements $e^{-\mathrm{i}\hat{\omega}\tau}\delta(X-X')\boldsymbol{v}_+^\dagger$ from the kernel of $\underline{L}^\dagger$ to apply the Fredholm-alternative.

The Fredholm alternative at $\mathscr{O}(\varepsilon^4)$ is automatically fulfilled. To show that, we pick an arbitrary occurring term that arises after inserting the amplitudes into q_4 and multiplying out the binomial.

$$\begin{aligned} &\left\langle e^{-\mathrm{i}\hat{\omega}\tau}\delta(X-X')\boldsymbol{v}_+^\dagger; \partial_{XX}\left(e^{\mathrm{i}\hat{\omega}\tau}A^*(X,T)\right)\left(e^{-\mathrm{i}\hat{\omega}\tau}A(X,T)\right)\tilde{v}\right\rangle \\ =&\left\langle e^{-\mathrm{i}\hat{\omega}\tau}\sum e^{\mathrm{i}Q(X-X')}\boldsymbol{v}_+^\dagger; \partial_{XX}\left(e^{\mathrm{i}\hat{\omega}\tau}\sum_K \tilde{A}^*(K,T)e^{-\mathrm{i}KX}\right)\left(e^{-\mathrm{i}\hat{\omega}\tau}\sum_K \tilde{A}(K,T)e^{\mathrm{i}KX}\right)\tilde{v}\right\rangle \\ \sim &\sum_{Q,K,K'} e^{\mathrm{i}QX'}\tilde{A}^*(K,T)\tilde{A}(K',T)\left(-(-K+K')^2\right)\int e^{\mathrm{i}\omega\tau(-Q^2-K^2+K'^2)}\mathrm{d}\tau\int e^{\mathrm{i}X(-Q-K+K')}\mathrm{d}X. \end{aligned} \tag{3.62}$$

Hence nonvanishing contributions have to fulfill

$$-Q^2-K^2+K'^2=0 \qquad \text{and} \qquad -Q-K+K'=0, \tag{3.63}$$

which can only hold if either $Q=0$ and $K=K'$ or $K=0$ and $Q=K'$. Both terms do not contribute as the first one vanishes due to $-K+K'=0$ and the second one as $\tilde{A}^*(0,T)=0$. A similar argument holds for all contributions.

Applying the Fredholm alternative at $\mathscr{O}(\varepsilon^5)$, the nonlinearity picks up the prefactor

$$\begin{aligned} \beta &= \frac{2}{\langle \boldsymbol{v}_+^\dagger; \boldsymbol{v}_+\rangle}\left[|(\boldsymbol{v}_+)_1|^2(\boldsymbol{v}_+)_1(\boldsymbol{v}_+^\dagger)_1^* + |(\boldsymbol{v}_+)_2|^2(\boldsymbol{v}_+)_2(\boldsymbol{v}_+^\dagger)_2^*\right] \\ &= \frac{\alpha^2-\rho^2}{\omega^2+\mathrm{i}\omega c}\left[\frac{(\omega-\mathrm{i}c)^2}{2\alpha(\alpha+\rho)}+\frac{\alpha+\rho}{2\alpha}\right]. \end{aligned} \tag{3.64}$$

Further the contribution to the rigidity term in the amplitude equation then evaluates as

$$\begin{aligned} \nu &= \frac{1}{\langle \boldsymbol{v}_+^\dagger; \boldsymbol{v}_+\rangle}\left[|(\boldsymbol{v}_+)_1(\boldsymbol{v}_+^\dagger)_1^* + \kappa(\boldsymbol{v}_+)_2(\boldsymbol{v}_+^\dagger)_2^*\right] \\ &= \frac{\alpha^2-\rho^2}{2(\omega^2+\mathrm{i}\omega c)}\left[\frac{(\omega-\mathrm{i}c)^2}{\alpha^2-\rho^2}+\kappa\right]. \end{aligned} \tag{3.65}$$

Here, we neglect contributions from the quadratic nolinearity at $\mathscr{O}(\varepsilon^5)$, i.e we assume, that the relevant nonlinear contributions arise from the cubic nonlinearity. To fully incorporate the quadratic nonlinearities, one needs to solve the inhomogeneous part of the linear system at $\mathscr{O}(\varepsilon^4)$, using e.g. a Greens-function of the Schrödinger equation and substitute the result at $\mathscr{O}(\varepsilon^5)$. Further we neglect "resonances" that can arise from the cubic nonlinearity, e.g. from terms $\sim \left[e^{-\mathrm{i}\hat{\omega}\tau}A(X,T)\right]^3$, that do not

impact single-mode solutions. For a more detailed discussion of these terms see appendix C.

Finally the envelope equation for the general case is

$$\boxed{\partial_t a = \partial_{xx}\left(-\mu a + \frac{3}{2}\beta(2a\overline{|a|^2} - \mathscr{F}^{-1}[\tilde{a}|\tilde{a}|^2]) - \nu\partial_{xx}a\right)}. \tag{3.66}$$

Here the complex parameters β and ν were introduced, such that the previously discussed minimal case is obtained for $\beta = \nu = 1$. Further for $c = 0$, the amplitude equation has real coefficients. Then $\beta = 1$ and ν becomes the arithmetic mean of the two rigidities. Also, $\kappa = 1$ always yields $\nu = 1$ independently of all other parameters. In the general case β and ν are complex coefficients, such that Eq. (3.66) is nonvariational, possibly allowing for more complex and also oscillatory behaviour to occur on the slow timescale.

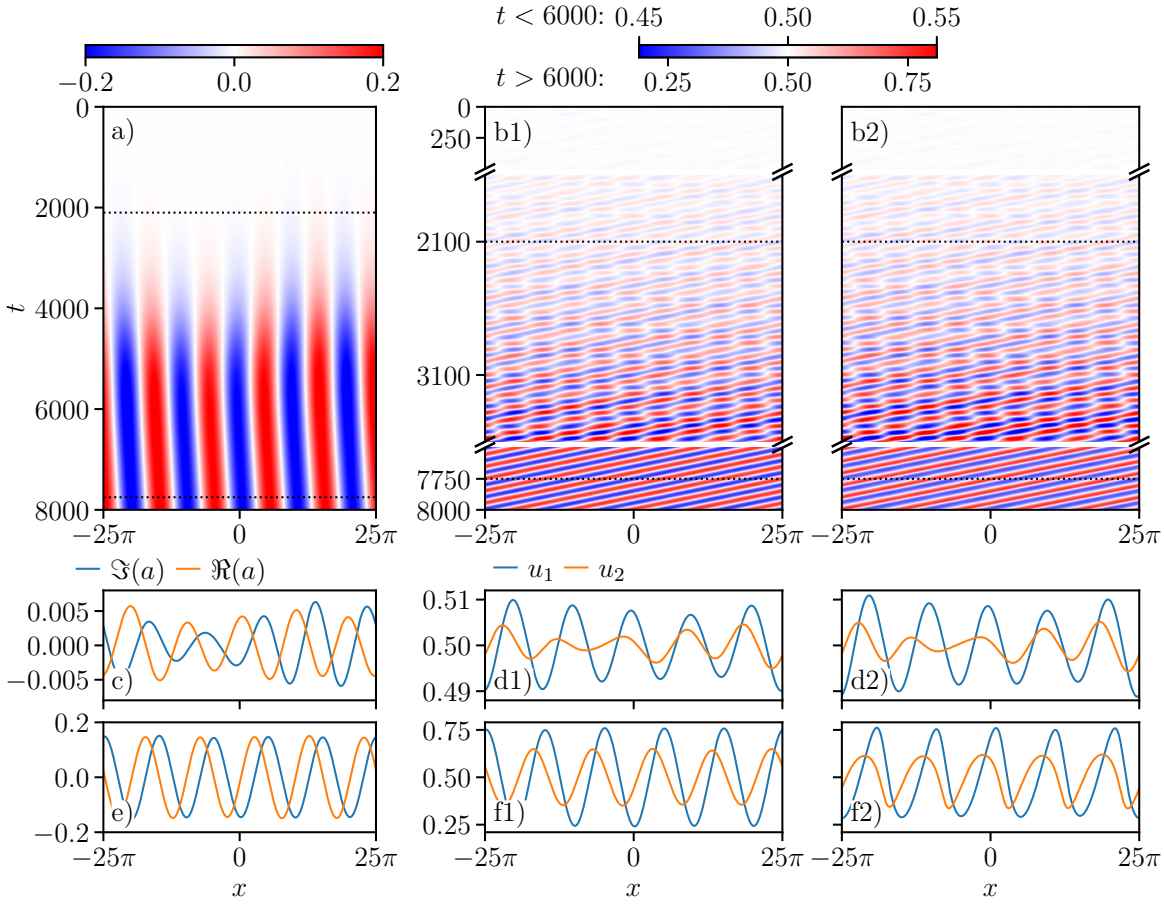

Figure 3.8: Spacetime plots for (a) $\Im(a)$, (b1) the approximate dynamics for u_{1a} obtained from the amplitude equation and (b2) the full dynamics u_1 of the NRCH model with white noise initial condition ($\sim 10^{-3}$). Panels (c)-(f) show profiles of the fields at the times indicated by the dotted horizontal lines in panels (a) and (b). The parameters are $l = 50\pi$, $\alpha = 2$, $\kappa = 0.5$, $\rho = 1$, $\bar{u}_1 = \bar{u}_2 = 0.5$, $\sigma_1 = -5/16$ and $\sigma_2 = -21/16$. The corresponding amplitude parameters are $\mu = 1/16$, $\beta = 1 + 0.151\mathrm{i}$ and $\nu = 0.75 + 0.075\mathrm{i}$. The spatial discretisation consists of 1024 points.

Finally, we briefly demonstrate numerically that the envelope equation predicts the correct onset behaviour. We therefore choose a generic configuration that is close to the onset of the conserved Hopf instability, i.e. here again at $\mu = 1/16$. In the generic case, both β and ν are complex. Fig. 3.8 shows a time simulation with random noise initial condition. The qualitative agreement of the spacetime-plots in panel (b) demonstrates that the envelope equation captures the correct behaviour in this generalised case. Now the amplitude does not settle to a periodic state, but becomes itself a travelling wave, analogously to the travelling wave states in the complex Ginzburg-Landau equation. Panels (c) and (d) show the solution profiles at an early stage. There, as the field values and the amplitudes are still small, the nonlinearities do not have a large impact on the dynamics which is therefore dominated by the linear behaviour, which is exactly handled by the amplitude equation. The stationary states shown in panels (f1) and (f2) match qualitatively, where especially an $(n = 5)$-periodic profile is attained in both panels. Nonetheless one registers that the profiles of the travelling states in the full NRCH dynamics differ from the perfect sinusoidal shape that is predicted from the amplitude equation. Further we notice that at the end of the displayed time interval, the solutions in panels (f1) and (f2) run slightly out of phase.

3.8. Outlook

A detailed analysis of the envelope equation in the general case is beyond the scope of this work, but an interesting avenue for future research. Similarly to the travelling states in the complex Ginzburg-Landau equation, one can analytically investigate the travelling wave state in the new amplitude equation. We expect to be able to generalise the discussion of the linear stability of single modes in section 3.5.1 to the general case, i.e. the criterion derived for the minimalistic version in section 3.3 with real parameters occurring in the amplitude equation is comparable to the Eckhaus criterion and we expect a generalisation to an equivalent of the Benjamin-Feir-Newell criterion.

Then one could obtain a largest stable wavenumber, that might again be the most relevant in the numerical investigation of wavelength selection. The theory could then be applied to the models from Saha et al. [19] and Brauns and Marchetti [17] to compare with their numerically observed wavelengths.

Further one could extend the discussion to different boundary conditions. Using Neumann-boundary conditions breaks the translational symmetry and forbids travelling wave states. As observed by Frohoff-Hülsmann and Thiele [20], the first emerging branch is then only a one-periodic standing wave branch which is stable. Guided by analogies, one would expect that standing waves of higher periodicity stabilise in a similar way as described here for the travelling waves and that these are most likely to be realised in time simulations starting with initial noise.

Finally, parts of the derivation might be reused to investigate the conserved Hopf instability in the NRCH system in a higher spatial dimension using e.g. a Galerkin method. There, as observed by Saha et al. [19], moving pattern-solutions are dominant close to onset and only further away from onset a travelling wave solution is realised.

4. Coexistence in active Mixtures

In this chapter we extend the concept of a Maxwell construction of phase coexistence to specific active mixtures. After reviewing the Maxwell construction for Cahn-Hilliard-type systems, we introduce a class of systems that allow for a Maxwell construction despite having properties of active mixtures. These systems are examples of a "conserved spurious gradient dynamics". Then, two main examples will be discussed, namely one-component systems that arise in motility-induced phase separation and a general conserved linearly coupled two-component system which is a generalisation of the previously used NRCH model.

4.1. Review: The Maxwell construction in Cahn-Hilliard-type systems

Before turning to the general case, we review the Maxwell construction in a Cahn-Hilliard-type system in one spatial dimension, i.e. in a system of the form

$$\partial_t u = \partial_{xx} \frac{\delta \mathscr{F}}{\delta u} \quad \text{with} \quad \mathscr{F}[u] = \int_{-l/2}^{l/2} \left[f(u) + \frac{1}{2}(\partial_x u)^2 \right] \mathrm{d}x. \tag{4.1}$$

Here, $f(u)$ is a local contribution to the free energy density, that we do not need to further specify but think of as some kind of double-well potential, i.e. any analytic function with (at least) two minima. We have also set the rigidity to one. Further, we assume boundary conditions that prevent fluxes across the boundary and preserve the total mass $\bar{u} = \int_{-l/2}^{l/2} u \mathrm{d}x$ in the system. Applying the functional variation the dynamic equation reads

$$\partial_t u = \partial_{xx}(f'(u) - \partial_{xx} u) \qquad \text{with} \qquad f'(u) = \frac{\partial f}{\partial u}. \tag{4.2}$$

The Maxwell-construction is often derived starting from the variational principle, assuming that the free energy $\mathscr{F}[u]$ is minimised under the constraint of mass conservation, where the chemical potential μ[15] then arises as the Lagrange multiplier for mass conservation. Here though, thinking towards a generalisation that does not make use of an extremisation principle, we choose a different derivation. Assuming a steady state in the system, i.e. setting $\partial_t u = 0$ in Eq. (4.2), we integrate twice. The first integration constant vanishes due to the boundary condition that prevents fluxes across the boundary. The chemical potential μ then arises as the second integration constant, i.e. we obtain

$$f'(u) - \partial_{xx} u = \mu. \tag{4.3}$$

We now assume the concentration profile to be approximately constant at two arbitrary positions x_A and x_B with distinct concentrations $u_a = u(x_B)$ and $u_b = u(x_B)$, see Fig. 4.1. As there all derivatives vanish,

[15] Sticking to usual conventions, we employ μ as the symbol for the chemical potential although it was already used as the symbol for the control parameter in section 3. In this section it is exclusively used as a chemical potential.

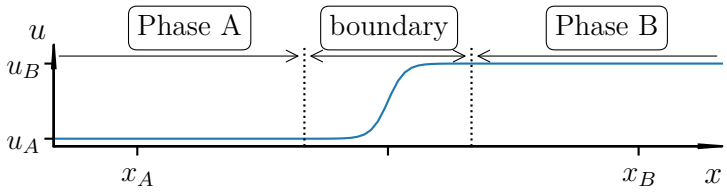

Figure 4.1: Illustration of the assumed situation for the Maxwell construction with homogeneous phases A and B with concentrations u_A and u_B respectively.

we trivially find

$$f'(u_a) = \mu = f'(u_b), \tag{4.4}$$

i.e. the bulk chemical potentials of the homogeneous phases coincide. Then, the pressure relation is obtained via multiplying Eq. (4.3) with $\partial_x u$ and integrating from x_A to x_B

$$\begin{aligned} &\int_{x_A}^{x_B} \left[f'(u) - \partial_{xx}u\right] \partial_x u \,\mathrm{d}x = \int_{x_A}^{x_B} \mu \partial_x u \,\mathrm{d}x \\ \Longrightarrow \quad &\int_{x_A}^{x_B} \frac{\mathrm{d}}{\mathrm{d}x}\left[f(u) - \frac{1}{2}(\partial_x u)^2\right] \mathrm{d}x = \mu(u_B - u_A). \end{aligned} \tag{4.5}$$

Inserting the boundaries, the derivative terms vanish and we obtain the equal pressure relation

$$f(u_A) - \mu u_A = -p = f(u_B) - \mu u_B, \tag{4.6}$$

Taken together, Eqs. (4.4) and Eqs. (4.6) are called the Maxwell construction as they are a necessary condition for coexistence that solely relies on the free energy density of homogeneous phases f.

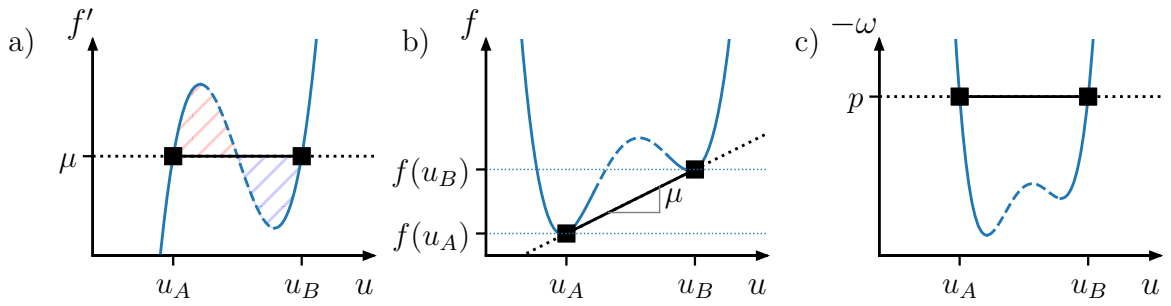

Figure 4.2: Shown are three graphical representations of the Maxwell construction, solid [dashed] lines mark stable [unstable] concentrations of homogneneous states. Panel (a) illustrates the equal area construction, panel (b) the common tangent construction and panel (c) the equal pressure relation.

Common graphical representations of the Maxwell construction are shown in Fig. 4.2. Panel (a) displays the equal-area construction as it was orginally introduced by Clerk-Maxwell [2] in the u, f'-plane. There, u_A and u_B are determined by the condition that the corresponding values of f' have to coincide,

i.e. that the black line is horizontal and that the volume of the red and blue area is equal.
Integrating with respect to u one obtains the common-tangent construction in the u, f-plane shown in panel (b), where a straight line with slope μ is tangential to the curve defined by the free energy density at the coexisting concentrations u_A and u_B. Finally, one can also display the grand potential-density of homogenous phases $\omega = f - f'u$. Then, as displayed in panel (c), the Maxwell construction becomes again a horizontal line, where the coexisting concentrations are determined through the condition that there the second derivatives of the grand potential density ω'' coincide.
Here, we also mention that Eq. (4.5) can be interpreted without assuming homogeneous phases. Then, collecting all terms on one side, we find the quantity

$$\mathscr{H} = f(u) - \frac{1}{2}(\partial_x u)^2 - \mu u \tag{4.7}$$

that is uniform in space, i.e. $\partial_x \mathscr{H} = 0$. Note that the first two terms do not coincide with the free energy density as here the derivative term is negative[16]. This quantity is often called a (spatial) Hamiltonian in analogy to the conserved quantity that can be constructed from the principle of least action in classical mechanics when transforming to the canonical variables. In this picture the grand potential density $f + \frac{1}{2}(\partial_x u)^2 - \mu u$ takes the role of a Lagrangian, from which we then obtain the Hamiltonian given in Eq. (4.7).

4.2. Conserved spurious gradient dynamics

Next, we generalise the previous discussion to a class of systems that we call "conserved spurious gradient dynamics". We consider a multi-component order parameter field $\boldsymbol{u}(\vec{x},t)$ which consists of N conserved components $u_i(x,t)$, $i = 1,\dots,N$. Their dynamics is described by a continuity equation which particularly can be written as

$$\partial_t \boldsymbol{u} = \vec{\nabla} \cdot \left(\underline{Q}(\boldsymbol{u}) \vec{\nabla} \left(\underline{M}(\boldsymbol{u}) \frac{\delta \mathscr{F}[\boldsymbol{u}]}{\delta \boldsymbol{u}} \right) \right), \tag{4.8}$$

with matrices $\underline{Q}(\boldsymbol{u}), \underline{M}(\boldsymbol{u}) \in \mathbb{R}^{N\times N}$ and a local functional $\mathscr{F}[\boldsymbol{u}] = \int_\Omega f(\boldsymbol{u}, \vec{\nabla}\boldsymbol{u}, \vec{\nabla}^2\boldsymbol{u}, ...)\mathrm{d}^n x$. $\underline{Q}(\boldsymbol{u})$ is symmetric and positive definite, and $\underline{M}(\boldsymbol{u})$ is at the moment left arbitrary. We will later see, that a Maxwell construction is possible, when $\underline{M}(\boldsymbol{u})$ can be written as a total derivative of a bijective function. Compared to section 4.1 we employed several generalisations by introducing multiple spatial dimensions, multiple fields, allowing for arbitrary derivative terms to occur in the free energy and incorporating the mobility $\underline{Q}(\boldsymbol{u})$. Despite these generalisations, in the case where $\underline{M}(\boldsymbol{u}) = \underline{1}$ the system is of standard gradient dynamics form for conserved scalar fields, i.e. then $\mathscr{F}[\boldsymbol{u}]$ is a Lyapunov-functional of the system, if it is bounded from below, and the system will approach an equilibrium. The introduction of $\underline{M}$ makes the gradient dynamics "spurious". If $\underline{M}$ is not positive definite $\mathscr{F}[\boldsymbol{u}]$ does not necessarily decrease monotonically in time. Then, the system is no longer forced to approach an equi-

[16] This is analogous to Newtonian systems. There, the interpretation of $f + \frac{1}{2}(\partial_x u)^2 - \mu u$ would be a Lagrangian $\mathscr{L} = T - V$. Then, the corresponding Hamiltonian is $\mathscr{H} = T + V$, i.e. the sign of the "kinetic term" changes.

librium, despite having "almost" a variational form.

Next, we introduce two simple and frequently used models of active mixtures and demonstrate, that they correspond to examples of the proposed structure of Eq. (4.8). Since any continuos function in one field can be written as a gradient of a potential, there arise two minimal ways how nonvariational behaviour can occur. First, keeping a one-field description, one can introduce next-to-leading order derivative terms that break the variational structure. Second, one can consider a two-field system, where the nonvariational character can arise through nonreciprocal coupling.

We start with the former. Examples of one-field active models often arise as mean-field theories in the context of motility-induced phase separation. A typical model reads [33, 34]

$$\partial_t u = \vec{\nabla}\cdot(Q(u)\vec{\nabla}g(u)) \qquad \text{with} \qquad g(u) = g_0(u) + \lambda(u)|\vec{\nabla}u|^2 - \kappa(u)\vec{\nabla}^2 u\,, \tag{4.9}$$

where $Q(u)$, $\lambda(u)$, $g_0(u)$ and $\kappa(u)$ are arbitrary functions depending on the field u. Note that in general, due to the latter two terms $g(u)$ cannot be written as a functional derivative. However, there are variational systems that are contained as special cases. Namely, for $\lambda(u) = -\kappa'(u)/2$, the derivative terms can be written as a functional variation of $\kappa(u)|\vec{\nabla}u|^2/2$.

As shown by Solon et al. [33], Eq. (4.9) can always be brought into the spurious variational form of Eq. (4.8), i.e. $g(u) = m(u)\frac{\delta\mathscr{F}[u]}{\delta u}$, if we define $m(u)$ implicitly via

$$\kappa(u)m'(u) = \big(2\lambda(u) + k'(u)\big)\,m(u), \tag{4.10}$$

where dashes indicate derivatives with respect to u. Note that in the described variational special case the r.h.s. of Eq. (4.10) vanishes. Then, the differential equation is trivially solved by $m = 1$ and the variational structure is recovered.

In the general nonvariational case, the corresponding generalised free energy $\mathscr{F}[u]$ reads

$$\mathscr{F}[u] = \int_\Omega \left[f_h(u) + \frac{\kappa(u)}{2m(u)}|\vec{\nabla}u|^2\right] \mathrm{d}^n x \quad \text{with} \quad f_h(u) = \int^u \frac{g_0(\hat{u})}{m(\hat{u})}\mathrm{d}\hat{u}. \tag{4.11}$$

For a demonstration that Eq. (4.9) is recovered from Eq. (4.8), i.e. for the proof that $m(u)\frac{\delta\mathscr{F}(u)}{\delta u} = g(u)$, see appendix D.1.

Next, we introduce a generalisation of the NRCH equation, i.e. a general model for two linear coupled fields $\boldsymbol{u} = (u_1, u_2)^T$, i.e.

$$\begin{aligned}
\partial_t u_1 &= \vec{\nabla}^2\left(\frac{\delta\mathscr{F}_1[u_1]}{\delta u_1} - (\rho+\alpha)u_2\right)\\
\partial_t u_2 &= \vec{\nabla}^2\left(\frac{\delta\mathscr{F}_2[u_2]}{\delta u_2} - (\rho-\alpha)u_1\right),
\end{aligned} \tag{4.12}$$

where both species u_1 and u_2 are individually conserved. Without coupling they obey gradient dynamics driven by their internal free energies $\mathscr{F}_1[u_1] = \int_\Omega f_1(u_1, \vec{\nabla}u_1, \vec{\nabla}^2u_1, ...)\mathrm{d}^n x$ and $\mathscr{F}_2[u_2] = \int_\Omega f_2(u_2, \vec{\nabla}u_2, \vec{\nabla}^2u_2, ...)\mathrm{d}^n x$, that do not have to be further specified here, i.e. the NRCH system

introduced in Eq. (1.5) arises as a speficic choice of these functionals. Note that we omit the mobility matrix $\underline{Q}(u)$ for a simpler notation as it does not affect the following discussion. The linear interaction is again parameterised through a symmetric term ρ and an antisymmetric term α. For the fully symmetric case where $\alpha = 0$, the coupling terms can be derived from an interaction free energy contribution $\mathscr{F}_\mathrm{c} = -\rho \int_\Omega u_1 u_2 \,\mathrm{d}^n x$ and the reciprocal system is variational. However, in all cases this model fulfils the structure of Eq. (4.8) with

$$\begin{aligned} \partial_t \boldsymbol{u} &= \vec{\nabla}^2 \left(\underline{M} \frac{\delta \mathscr{F}[\boldsymbol{u}]}{\delta \boldsymbol{u}} \right) \quad \text{with} \quad \underline{M} = \begin{pmatrix} \frac{\rho+\alpha}{\rho} & 0 \\ 0 & \frac{\rho-\alpha}{\rho} \end{pmatrix} \\ \text{and} \quad \mathscr{F}[\boldsymbol{u}] &= \frac{\rho}{\rho+\alpha} \mathscr{F}_1[u_1] + \frac{\rho}{\rho-\alpha} \mathscr{F}_2[u_2] - \rho \int_\Omega u_1 u_2 \,\mathrm{d}^n x \,. \end{aligned} \tag{4.13}$$

Here, the freedom of exchanging a multiplicative constant between $\underline{M}$ and $\mathscr{F}[\boldsymbol{u}]$ was used such that for $\alpha = 0$, we obtain $\underline{M} = \underline{1}$ and therefore a "true" variational form. Remarkably, this reformulation of a linearly nonreciprocally interacting system can also be directly applied on a microscopic level and leads to similar coefficients (see [35, 36]).

Note that since here $\underline{M}$ is constant, it commutes with $\vec{\nabla}$, such that we can rewrite the expression as $\partial_t \boldsymbol{u} = \vec{\nabla} \cdot [\underline{M} \vec{\nabla} \frac{\delta \mathscr{F}}{\delta \boldsymbol{u}}]$, where $\underline{M}$ takes the place of a mobility matrix, and the whole system seems to have the form of a gradient dynamics. However, this resemblance is only superficial, as the generalised energy $\mathscr{F}[\boldsymbol{u}]$ and the matrix $\underline{M}$ in Eq. (4.13) do not satisfy the thermodynamic principles, i.e. cannot be obtained via summing free energy contributions and using Onsager relations. This is best seen in the active case where $|\alpha| > |\rho|$. Then, $\underline{M}$ is indefinite and $\mathscr{F}[\boldsymbol{u}]$ is not bounded from below, i.e. $\mathscr{F}[\boldsymbol{u}]$ is not a Lyapunov-functional anymore. This implies that the system does not necessarily follow any extremal principle and does not need to approach an equilibrium, i.e. oscillatory behaviour can occur.

4.3. Maxwell construction for conserved spurious gradient dynamcis

Following section 4.1 we assume coexisting homogeneous states and show that a spurious Maxwell construction arises as a necessary condition for phase coexistence. Setting $\partial_t \boldsymbol{u} = 0$ in Eq. (4.8), we integrate and set the first integration constant to zero to impose the condition of zero net flow across the boundaries (e.g. realised by Neumann- or periodic boundary conditions). We multiply with $\underline{Q}(\boldsymbol{u})^{-1}$ and integrate again to obtain

$$\underline{M}(\boldsymbol{u}) \frac{\delta \mathscr{F}(\boldsymbol{u})}{\delta \boldsymbol{u}} = \boldsymbol{\mu}, \tag{4.14}$$

where the chemical potential $\boldsymbol{\mu}$ arises again as an integration constant. To obtain the generalized pressure relation, we integrate $\frac{\delta \mathscr{F}[\boldsymbol{u}]}{\delta \boldsymbol{u}} \cdot \vec{\nabla} \boldsymbol{u}$ along an arbitrary path $\vec{r}(s)$, $s \in [0,1]$ between two coexisting homogeneous states $\boldsymbol{u}_A = \boldsymbol{u}(\vec{r}_A)$ and $\boldsymbol{u}_B = \boldsymbol{u}(\vec{r}_B)$ at $\vec{r}_A$ and $\vec{r}_B$ respectively. First, a direct evaluation of the integral yields

$$\int_{\vec{r}_A}^{\vec{r}_B} \frac{\delta \mathscr{F}[\boldsymbol{u}]}{\delta \boldsymbol{u}} \vec{\nabla} \boldsymbol{u} \cdot \mathrm{d}\vec{r}(s) = f_h(\boldsymbol{u}_B) - f_h(\boldsymbol{u}_A), \tag{4.15}$$

where we define the free energy density of homogeneous phases as $f_h(\boldsymbol{u}) = f(\boldsymbol{u}, \vec{\nabla}\boldsymbol{u} = 0, \vec{\nabla}^2\boldsymbol{u} = 0, ...)$. We emphasise that this is the result of a nontrivial calculation based on the idea, that the integrand can be written as the gradient of a hamiltonian $\mathscr{H}$, i.e. $\frac{\delta\mathscr{F}[\boldsymbol{u}]}{\delta u}\vec{\nabla}\boldsymbol{u} = \vec{\nabla}(\mathscr{H} + \boldsymbol{\mu}\boldsymbol{\chi}(\boldsymbol{u}))$, for the calculation see appendix D. This generalises the idea from Eq. (4.5), where the diffusive term could be written as a total derivative, i.e. $\partial_{xx}u\partial_x u = \partial_x(\partial_x u)^2$. Further note that this equation is only valid in the case of homogeneous states.

Second, we can also express the integral by making use of the constant chemical potential

$$\begin{aligned}
\int_{\vec{r}_A}^{\vec{r}_B} \frac{\delta\mathscr{F}[\boldsymbol{u}]}{\delta\boldsymbol{u}}\vec{\nabla}\boldsymbol{u}\cdot\mathrm{d}\vec{r}(s) &= \int_{\vec{r}_A}^{\vec{r}_B} \left(\underline{M}^{-1}(\boldsymbol{u})\underline{M}(\boldsymbol{u})\frac{\delta\mathscr{F}[\boldsymbol{u}]}{\delta\boldsymbol{u}}\right)\vec{\nabla}\boldsymbol{u}\cdot\mathrm{d}\vec{r}(s) \\
&= \int_{\vec{r}_A}^{\vec{r}_B} \left(\underline{M}^{-1}(\boldsymbol{u})\boldsymbol{\mu}\right)\vec{\nabla}\boldsymbol{u}\cdot\mathrm{d}\vec{r}(s) \\
&= \boldsymbol{\mu}\int_{\vec{r}_A}^{\vec{r}_B} \left(\left(\underline{M}^{-1}(\boldsymbol{u})\right)^T\vec{\nabla}\boldsymbol{u}\right)\cdot\mathrm{d}\vec{r}(s) \\
&= \boldsymbol{\mu}\int_{\boldsymbol{u}_A}^{\boldsymbol{u}_B} \left(\underline{M}^{-1}(\boldsymbol{u})\right)^T\mathrm{d}\boldsymbol{u}(\vec{r}(s))
\end{aligned} \tag{4.16}$$

In general the remaining integral depends on the integration path that we choose between the homogeneous phases, i.e. on the specific choice of $\vec{r}(s)$. Nevertheless, in the case when $(\underline{M}^{-1})^T$ can be written as a total tensorial derivative, i.e. $(\underline{M}^{-1})^T = \frac{\mathrm{d}\boldsymbol{\chi}}{\mathrm{d}\boldsymbol{u}}$ for bijective vectorial functions $\boldsymbol{\chi}(\boldsymbol{u})$, the integration becomes path independent and finally yields

$$\int_{\vec{r}_A}^{\vec{r}_B} \left(\frac{\delta\mathscr{F}[\boldsymbol{u}]}{\delta\boldsymbol{u}}\vec{\nabla}\boldsymbol{u}\right)\cdot\mathrm{d}\vec{r}(s) = \boldsymbol{\mu}\left(\boldsymbol{\chi}(\boldsymbol{u}_B) - \boldsymbol{\chi}(\boldsymbol{u}_A)\right). \tag{4.17}$$

Using the equality of Eq. (4.15) and Eq. (4.17), we can therefore define a pressure

$$p = f_h(\boldsymbol{u}) - \boldsymbol{\mu}\boldsymbol{\chi}(\boldsymbol{u}), \tag{4.18}$$

that is identical for coexisting homogeneous phases. Note that in general the pressure in Eq. (4.18) differs from a classical thermodynamics Maxwell construction, where $\boldsymbol{u}$ is used instead of $\boldsymbol{\chi}(\boldsymbol{u})$. The two only coincide in the variational case when we can set $\boldsymbol{\chi}(\boldsymbol{u}) = \boldsymbol{u}$.

Comparing our derivation to the notion of "Generalized thermodynamics" from Solon et al. [33], where a Maxwell construction is proposed for single-field systems of the form $\partial_t u = \vec{\nabla}\cdot(Q\vec{\nabla}\frac{\delta\mathscr{F}}{\delta R})$ where $R(u)$ is a bijective function, our derivation represents a generalisation to the multi-field case. Applying the variational chain rule $\frac{\delta\mathscr{F}}{\delta R} = \frac{\delta\mathscr{F}}{\delta u}\frac{du}{dR}$ reveals that $\frac{\mathrm{d}u}{\mathrm{d}R} = (\frac{\mathrm{d}R}{\mathrm{d}u})^{-1}$ coincides with M in Eq. (4.8), and therefore χ coincides with R in the single-field case.

We now proceed to investigate the consequences of this Maxwell construction in the introduced models.

4.4. Maxwell construction for active model B

In the case of motility induced phase separation, i.e. for the case of one-field in Eq. (4.9), $(\underline{M}^{-1}(\boldsymbol{u}))^T$ reduces to $m^{-1}(u)$ and can always be integrated if $m(u)$ is bijective. Then a Maxwell construction is

always possible. To give a simple, nontrivial example for a Maxwell construction, we set $\kappa = \kappa_0$, $\lambda = \lambda_0$ and $g_0(u) = -u + u^3$ in Eq. (4.9), which is often referred to as "active model B" [34]. The coexistence conditions for active model B have already been investigated by Wittkowski et al. [37]. Nevertheless, here we derive them in the formalism of conserved spurious gradient dynamics and compare to the known results.

For active model B Eq. (4.10) reduces to $\kappa_0 m'(u) = 2\lambda_0 m(u)$ and is solved by

$$\begin{aligned} & m(u) = \exp\left(\frac{2\lambda_0}{\kappa_0}u\right), \\ \text{yielding} \quad & \chi(u) = \int^u m(\hat{u})^{-1}\mathrm{d}\hat{u} = -\frac{\kappa_0}{2\lambda_0}\left[\exp\left(-\frac{2\lambda_0}{\kappa_0}u\right) - 1\right] \\ \text{and} \quad & f_h(u) = \int^u \frac{g_0(\hat{u})}{m(\hat{u})}\mathrm{d}\hat{u} \\ = & \left(\frac{\kappa_0}{2\lambda_0}\right)^4 \left[\exp\left(-\frac{2\lambda_0}{\kappa_0}u\right)\left(\left(\frac{2\lambda_0}{\kappa_0}\right)^3 u(1-u^2) + \left(\frac{2\lambda_0}{\kappa_0}\right)^2 (1-3u^2) - 6\frac{2\lambda_0}{\kappa_0}u - 6\right) - \left(\frac{2\lambda_0}{\kappa_0}\right)^2 + 6\right]. \end{aligned} \tag{4.19}$$

Integration constants were chosen to reflect the variational limit, i.e. $\lim_{\lambda_0\to 0}\chi(u) = u$ and $\lim_{\lambda_0\to 0} f_h(u) = -u^2/2 + u^4/4$. Therefore we can construct the generalised pressure $p = f_h(u) - \mu\chi(u)$ according to Eq. (4.18). The possible coexisting densities u_a and u_b are fully determined by the conditions $p(u_a) = p(u_b)$ and $\mu(u_a) = \mu(u_b)$, where μ is the bulk chemical potential $\mu(u_{a,b}) = g_0(u_{a,b})$ as usual. To obtain further insights, for $2\lambda_0/\kappa_0 = \varepsilon \ll 1$ the spurious Maxwell construction can be expanded around the solution of the variational limit case $\lambda_0 = 0$. Applying this expansion to Eq. (4.19) yields

$$\begin{aligned} \chi(u) &= u - \frac{1}{2}\varepsilon u^2 + \mathscr{O}\left(\varepsilon^2\right) \\ f_h(u) &= -\frac{1}{2}u^2 + \frac{1}{4}u^4 + \frac{1}{15}\varepsilon(5u^3 - 3u^5) + \mathscr{O}\left(\varepsilon^2\right). \end{aligned} \tag{4.20}$$

Then, expanding the plateau values about the solution of the variational case where $\lambda_0^v = 0$, $u_{a,b}^v = \pm 1$ and $\mu^v = 0$, i.e. via expanding $u_{a,b} = \pm 1 + \varepsilon u_{a,b}^{(1)} + \mathscr{O}(\varepsilon^2)$, we obtain

$$\mu(u_{a,b}) = -u_{a,b} + u_{a,b}^3 = 0 + 2\varepsilon u_{a,b}^{(1)} + \mathscr{O}(\varepsilon^2), \tag{4.21}$$

and hence

$$p(u_{a,b}) = f_h(u) - \chi(u)\mu = \varepsilon\left(\pm\frac{2}{15} \mp 2u_{a,b}^{(1)}\right) + \mathscr{O}(\varepsilon^2). \tag{4.22}$$

Therefore the equality of the chemical potentials in Eq. (4.21) implies $u_a^{(1)} = u_b^{(1)}$ and then the pressure

equality $p(u_a) = p(u_b)$ in Eq. (4.22) yields $u_{a,b}^{(1)} = \frac{1}{15}$. Resubstituting $\varepsilon = \frac{2\lambda_0}{\kappa_0}$ results in

$$\begin{aligned} u_{a,b} &= \pm 1 + \frac{1}{15}\varepsilon + \mathcal{O}(\varepsilon^2) = \pm 1 + \frac{2\lambda_0}{15\kappa_0} + \mathcal{O}\left(\left(\frac{\lambda_0}{\kappa_0}\right)^2\right) \\ \text{and} \qquad \mu &= \frac{2}{15}\varepsilon + \mathcal{O}(\varepsilon^2) = \frac{4\lambda_0}{15\kappa_0} + \mathcal{O}\left(\left(\frac{\lambda_0}{\kappa_0}\right)^2\right), \end{aligned} \tag{4.23}$$

where the chemical potential μ corresponds to the result derived by Wittkowski et al. [37]. Similarly one can investigate the limit $\lambda_0/\kappa_0 \to \infty$. As the first term in f_h in Eq. (4.19) cancels with the contribution from the chemical potential, the fastest diverging contribution in p reads

$$\lim_{\frac{\lambda_0}{\kappa_0}\to\infty} p \sim \left(\frac{\kappa_0}{2\lambda_0}\right)^2 \exp\left(-\frac{2\lambda_0}{\kappa_0}u\right)(1-3u^2) \tag{4.24}$$

Assuming $u_a < 0$ and $u_b > 0$, the exponential diverges for u_a whereas it goes to zero for u_b. Therefore the terms can only cancel if $(1-3u_a^2) = 0$, i.e. if $u_a = -1/\sqrt{3}$. The corresponding chemical potential is $\mu_\infty = -u_a + u_a^3 = 2/(3\sqrt{3})$, which was also first derived in Ref. [37]. Then, solving $\mu_\infty = -u_b + u_b^3$ yields $u_b = 2/\sqrt{3}$. A similar discussion holds for $\lambda_0/\kappa_0 \to -\infty$ by exchanging the roles of u_a and u_b.

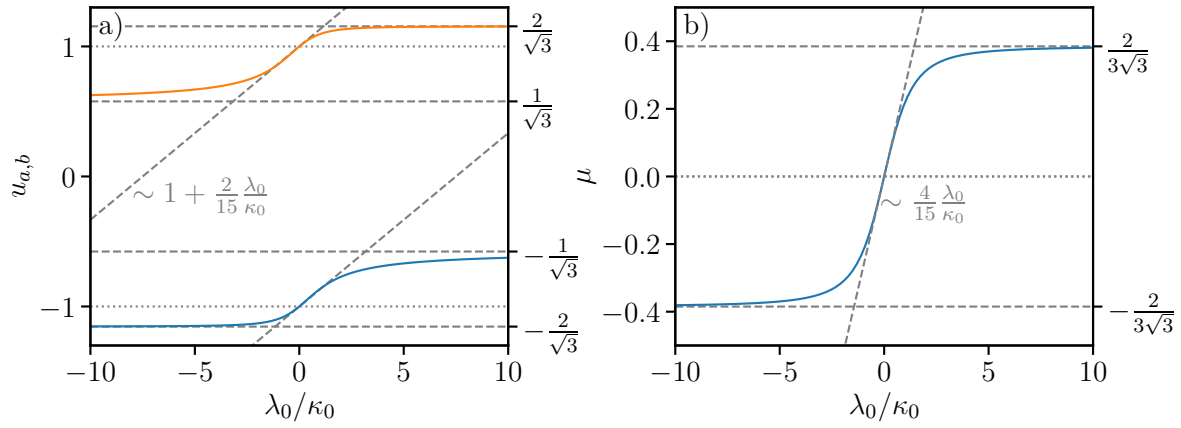

Figure 4.3: The panels show a comparision of the analytically obtained asymptotics (dashed lines) of the Maxwell construction for active model B with a numerical solution of the coexistence conditions (solid lines) depending on λ/κ_0. Panel (a) displays the coexisting concentrations u_a (blue) and u_b (orange). Panel (b) shows the chemical potential μ of phase coexistence. $\lambda/\kappa_0 = 0$ reflects the variational limit of the Cahn-Hilliard equation.

To conclude our discussion of coexistence in active model B, we compare a numerical solution of the derived coexistence conditions to the analytically obtained asymptotic behaviour in Fig. 4.3. Panel (a) shows the coexisting concentrations and panel (b) the chemical potential for phase coexistence in dependence of λ_0/κ_0. In all cases the curves show the derived asymptotic behaviour. Again we emphasise that these results have already been obtained elsewhere, but with different methods. In fact Fig. 4.3 (a) recreates Ref. [34, Fig. 6.3] and (b) recreates Ref. [37, Fig. 4]. Nonetheless, our formalism

allows us to derive these in a systematic way, i.e. once the model is brought into spurious gradient dynamics form, the Maxwell construction can be obtained in a straightforward fashion.

4.5. Phase behaviour of the nonreciprocal Cahn-Hilliard model

Applying the derived formalism we find the chemical potential $\boldsymbol{\mu} = (\mu_1, \mu_2)^T$ of the system Eq. (4.13) to be

$$\begin{aligned} \mu_1 &= \frac{\delta \mathscr{F}_1[u_1]}{\delta u_1} - (\rho + \alpha)u_2, \\ \mu_2 &= \frac{\delta \mathscr{F}_2[u_2]}{\delta u_2} - (\rho - \alpha)u_1. \end{aligned} \tag{4.25}$$

For the specific constant diagonal $\underline{M}$ in Eq. (4.13) we can define $\boldsymbol{\chi}(\boldsymbol{u}) = \left(\frac{\rho}{\rho+\alpha}u_1, \frac{\rho}{\rho-\alpha}u_2\right)^T$, such that $(\underline{M}^{-1})^T = \frac{\mathrm{d}\boldsymbol{\chi}}{\mathrm{d}\boldsymbol{u}}$ is fulfilled and then evaluate the pressure $p = f_h(\boldsymbol{u}) - \boldsymbol{\mu}\boldsymbol{\chi}(\boldsymbol{u})$ to obtain

$$p = \frac{\rho}{\rho+\alpha}(f_{1,h}(u_1) - u_1\mu_1) + \frac{\rho}{\rho-\alpha}(f_{2,h}(u_2) - u_2\mu_2) - \rho u_1 u_2, \tag{4.26}$$

with the single-species free energy densities of homogeneous phases $f_{1,h}$ and $f_{2,h}$. Again note, that for $\alpha = 0$ this reduces to the usual Maxwell construction on the potential density $f = f_{1,h} + f_{2,h} - \rho u_1 u_2$, whereas for $\alpha \neq 0$ the components of the chemical potential and the single-species bulk free energy densities enter with different prefactors, which cannot occur in the variational case.

The consequences of the coexistence conditions Eq. (4.25) and Eq. (4.26) will now be further investigated by employing the example of the NRCH equation. We consider one spatial dimension and set the one-component free-energy densities of the linear coupled system in Eq. (4.13) to

$$\begin{aligned} f_1 &= \frac{1}{2}\sigma_1 u_1^2 + \frac{1}{4}u_1^4 + \frac{1}{2}(\partial_x u_1)^2 \\ f_2 &= \frac{1}{2}\sigma_2 u_2^2 + \frac{1}{4}u_2^4 + \frac{\kappa}{2}(\partial_x u_2)^2 \end{aligned} \tag{4.27}$$

to obtain the NRCH equation that was introduced in Eq. (1.5). We further assume equal critical temperatures, i.e. $\sigma_1 = \sigma_2 = \sigma$. Next, we employ the two mean densities $\bar{u}_1$ and $\bar{u}_2$ as control parameters. Then we first look at the spinodal lines marking the linear stability boundaries and discuss the binodal lines indicating coexisting states. We will then use both to construct the phase diagram for homogeneous steady states.

First we make use of the general discussion of linear stability in the conserved two-component case in section 2 and present the results in dependence of the two mean concentrations.

Fig. 4.4 illustrates the linear stability results. It shows various stability diagrams in the $(\bar{u}_1, \bar{u}_2)$ phase plane for different rigidity ratios κ and nonreciprocity values $\Xi = \rho^2 - \alpha^2$. In all panels the blank [orange] regions mark linear stable [unstable] homogeneous states. The linear ones are bounded by thick colored lines that mark the onset of instability. Thin lines mark instabilities beyond the dominant one or other qualitative changes in the dispersion relations. The top row ($\Xi = 0.5$) shows that for

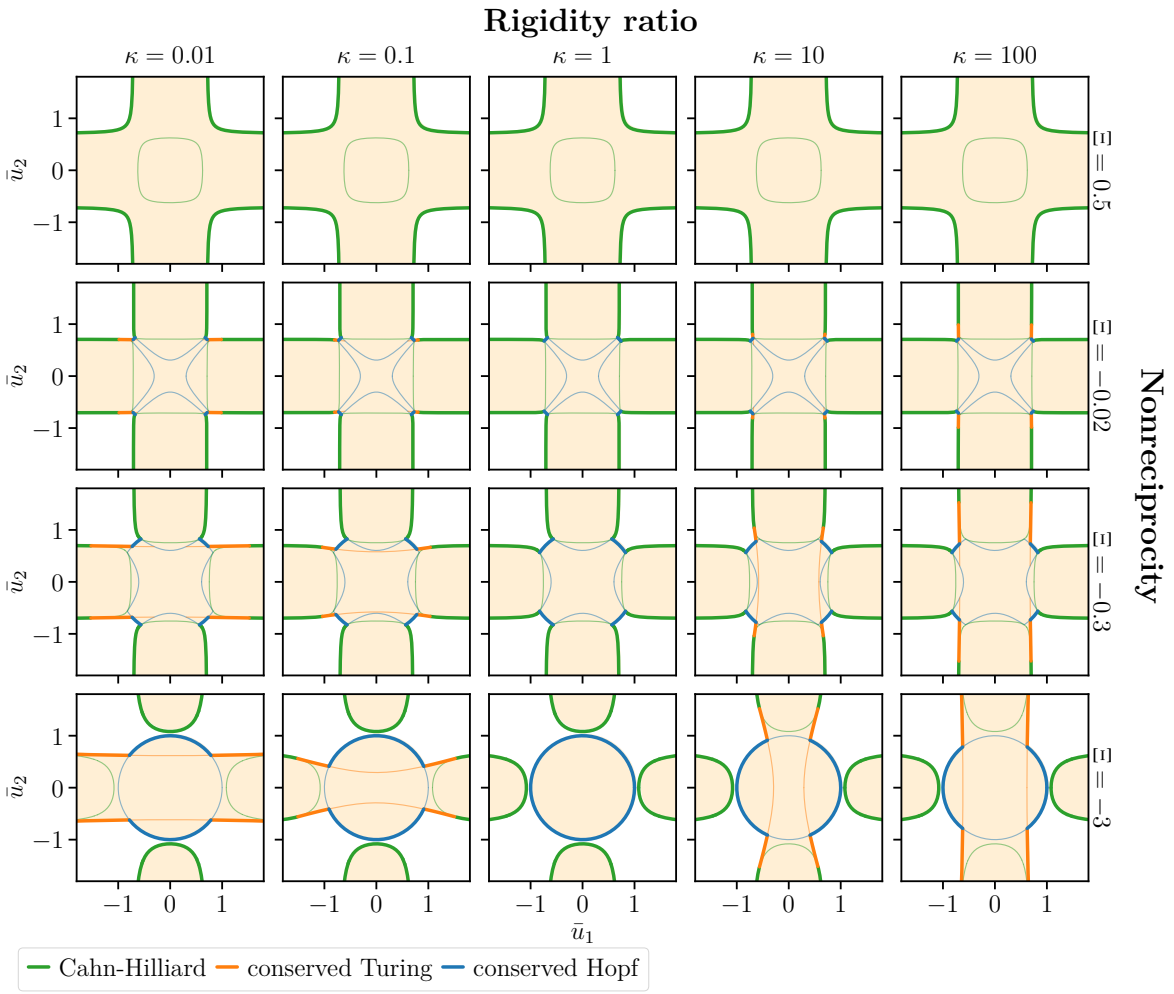

Figure 4.4: Spinodal lines indicate linear stability results of the nonreciprocal CH model for $\sigma = -1.5$ in the $(\bar{u}_1, \bar{u}_2)$-plane. For the different panels the diffusion ratio κ and the nonreciprocity parameter $\Xi = \rho^2 - \alpha^2$ are varied horizontally and vertically, respectively. The linear unstable region is colored. Green, orange and blue lines indicate Cahn-Hilliard, conserved Hopf and conserved Hopf instabilities. Thick lines mark the onset of instabilities where the homogeneous state becomes unstable to the dominant mode. Thin lines mark secondary qualitative changes in the dispersion relation, i.e. an additional eigenvalue at $k = 0$ becoming unstable (green), an additional small scale mode becoming unstable (orange), or two already unstable real eigenvalues at $k = 0$ becoming complex (blue).

passive systems ($\Xi > 0$) the Cahn-Hilliard instability is the only occurring instability type. Rendering the system active ($\Xi = -0.02$, second top row) the conserved Hopf instability (blue line) occurs within the unstable central region and at the four most inner corners of the linear stability boundaries. Furthermore, the conserved Turing instability (orange line) emerges when the system becomes active and if $\kappa \neq 1$. It is the dominant instability between the codimension-two point where conserved Hopf and conserved Turing instabilities occur simultaneously and the point where where the conserved Turing instability transitions into a Cahn-Hilliard instability.

Similar to the common nonconserved two-component reaction-diffusion system the short-scale insta-

bility (conserved Turing) never occurs for equal rigidities ($\kappa = 1$), whereas the lines of primary conserved Turing instabilities the most pronounced for $0 < \kappa \ll 1$ or $\kappa \gg 1$. The third ($\Xi = -0.3$) and fourth ($\Xi = -3$) row in Fig. 4.4 illustrate that (for a given κ) the conserved Turing and conserved Hopf instabilities become the dominant instability modes in larger parameter regions if nonreciprocity is increased. Specifically for very large activity (fourth row) the separated lines of the conserved Hopf instability collide forming two circle segments divided by the conserved Turing instability lines for $\kappa \neq 1$. In particular for $\kappa = 1$ the conserved Turing lines vanish and the conserved Hopf instability line forms a full circle around the center. The Cahn-Hilliard instability is only relevant if one (not both) species has a large mean density in absolute numbers. As a result a gap of linear stable states emerges between conserved Hopf and Cahn-Hilliard lines that connect the stable phases in the corner of the phase diagrams.

Next, we discuss the essential part of the phase diagrams - the binodal lines. They indicate coexisting states according to the spurious Maxwell construction discussed in Section 4.3. Homogeneous states $\boldsymbol{u}^{(A)}$ and $\boldsymbol{u}^{(B)}$ obey the coexistence conditions (cf. Eqs. (4.25) and (4.26))

$$\mu_1(\boldsymbol{u}^{(A)}) = \mu_1(\boldsymbol{u}^{(B)}), \qquad \mu_2(\boldsymbol{u}^{(A)}) = \mu_2(\boldsymbol{u}^{(B)}) \quad \text{and} \quad p(\boldsymbol{u}^{(A)}) = p(\boldsymbol{u}^{(B)}). \tag{4.28}$$

These three equations have four unknowns, namely the two fields (u_1, u_2) in compartments A and B. Since we do not consider any interfaces effects, i.e., assuming an infinitely large system with two phases A and B, Eqs. (4.28) are simple algebraic equations. The resulting binodals are lines in the (u_1, u_2)-phase plane and, here, are obtained using a pseudo-arclength continuation method discussed e.g. by Holl et al. [11]. We start with some initial solution of Eqs. (4.28) as initial state and follow the binodal lines employing μ_1 and μ_2 as control parameters.

Fig. 4.5 displays three typical phase diagrams obtained for increasing nonreciprocity α. We start with a short review of the reciprocal case with $\alpha = 0$ depicted in panel a) that has already been discussed in Frohoff-Hülsmann et al. [14]. In the four corners there are four different phases corresponding to combinations of high and low concentrations of u_1 and u_2, e.g. the $\downarrow\uparrow$-phase of low u_1- and high u_2-concentration in the top left corner. Each combination of phases can pairwise coexist, with the exception of the $\downarrow\uparrow$-phase and $\uparrow\downarrow$-phase. This is due to the positive sign of the reciprocal coupling, i.e. the coupling energy density reads $-\rho u_1 u_2$ and therefore for $\rho > 0$ favours the $\downarrow\downarrow$- and $\uparrow\uparrow$-phases energetically, hence the state with $\bar{u}_1 = \bar{u}_2 = 0$ will dissolve into these.

We further find two triple-points where three phases with the same chemical potential and pressure coexist. The enclosed triangle is a triplepoint region, where all homogeneous initial states separate into domains of these three phases. Figuratively speaking, these appear where two different binodal regions intersect. Numerically they are obtained by solving the coexistence conditions Eqs. (4.28) for three distinct phases $\boldsymbol{u}^{(A)}$, $\boldsymbol{u}^{(B)}$ and $\boldsymbol{u}^{(C)}$.

Further note that the phase diagram reflects the symmetries of the underlying equations, which is in the reciprocal case a symmetry under field inversion $(u_1, u_2) \to (-u_1, -u_2)$ and exchange of the fields $(u_1, u_2) \to (u_2, u_1)$. Graphically this corresponds to symmetry under inflection at the origin and symmetry under reflection along the first bisector respectively.

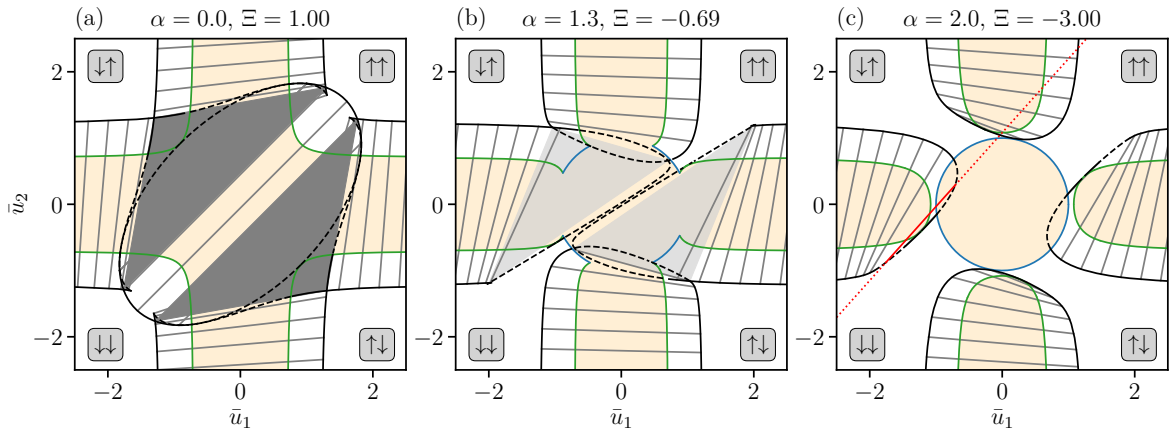

Figure 4.5: Phase diagrams of the nonreciprocal Cahn-Hilliard-model in the average composition-plane for increasing nonreciprocal coupling parameter α. Binodal lines are depicted in solid black and tie lines connecting coexisting stable state in solid grey. Dashed black lines indicate unstable binodal lines, where at least one of the coexisting states is linearly unstable. The dark grey area in panel (a) marks a stable three-phase coexistence region, whereas the lightgrey area in panel (b) marks an unstable one. The corners mark single phase regions, where e.g. in the top left corner only the $\downarrow\uparrow$-phase ($\hat{=}$ low u_1-concentration and high u_2-concentration) is present. The green and solid blue lines mark Cahn-Hillard and conserved Hopf-instabilities as in Fig. 4.4. The remaining parameters are $\kappa = 1$, $\rho = 1$ and $\sigma = -1.5$. The red line in panel (c) indicates a binodal, that connects a stable with an oscillatory unstable state.

We now turn to the active case depicted in panels (b) and (c). Here, due to $\alpha \neq 0$, the equations loose the field exchange symmetry and only retain the symmetry under field inversion, i.e. inflection at the origin (or equivalently 180°-rotations). The outer regions of the phase diagram, where at least one mean concentration is high, remain almost unchanged by the increasing nonreciprocity, as the system is dominated by the nonlinear contributions to the single species free energy (namely the $\sim u_{1,2}^4$-terms). For low average concentrations though, the phase behaviour is heavily influenced by the increasing nonreciprocity.

At the value $\alpha = 1.3$, the three phase contact regions have become unstable as the participating points close to the Hopf instability line have entered the unstable regime and therefore render the whole triple point region unstable. This is accompanied by the disappearance of a stable coexistence between the $\downarrow\downarrow$-phase and the $\uparrow\uparrow$-phase.

Increasing the nonreciprocal coupling further to $\alpha = 2$ in panel (c) separates the binodal lines from each other, the unstable coexistence of the $\downarrow\downarrow$-phase and the $\uparrow\uparrow$-phase fully vanishes and the triplepoints disappear. Two of the possible coexistences ($\downarrow\uparrow$-$\uparrow\uparrow$ and $\downarrow\downarrow$-$\uparrow\downarrow$) are now always stable whereas the other two retain small regions of coexistence between a stable state and a state which is oscillatory unstable. Increasing the nonreciprocity even further fully separates the binodals from the inner region of oscillatory instability. Then all phases become connected in the composition space, i.e. if the average composition is continuously changed, one can transfer one phase to the other without passing a phase separation or an instability.

For the passive case the previous analysis of the phase behaviour gives sufficient information about the longtime-behaviour of an infinite system with given mean concentrations $\bar{u}_1$ and $\bar{u}_2$. For example starting with an average composition in a stable coexistence region, we can tell just from the inspection of the phase-diagram, that it will dissolve into two homogeneous domains with plateau values defined by the tie-line on which we started and that the final domain sizes are determined by the lever rule. Similar arguments work for every initial condition, as the whole composition plane is covered with stable singular phases, stable two-phase coexistence or stable triplepoint regions. With increasing activity though one will eventually pass the point $|\alpha| > |\rho|$, where oscillatory states can occur. For example in Fig. 4.5 (c) one can choose a homogeneous initial state, that is Cahn-Hilliard-unstable, but lies on a tie-line that connects a stable to an oscillatory unstable phase. This does not occur in classical thermodynamic systems and we cannot easily deduce the systems behaviour from the sole inspection of the phase diagram.

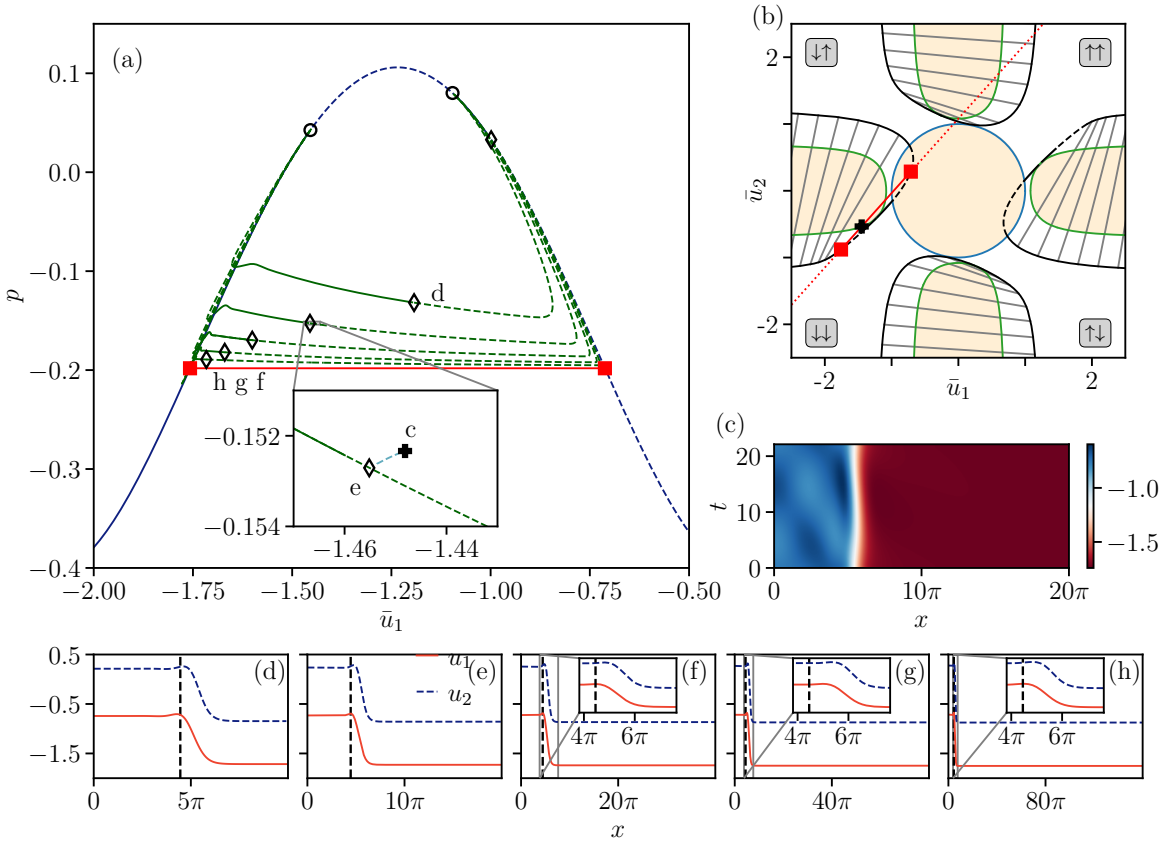

Figure 4.6: Maxwell constructions for various domain sizes ($L = 10\pi, 20\pi, 40\pi, 80\pi, 160\pi$) along the tie line indicated as a red line in (b) given by $\bar{u}_2(\bar{u}_1) = 1.115\,\bar{u}_1 + 1.081$. The inset highlights the region where the steady phase-separated state for $L = 20\pi$ becomes unstable in a Hopf bifurcation at $(\bar{u}_1, \bar{u}_2) \approx (-1.455, -0.542)$. (c) shows $u_1(x,t)$ for the emerging time periodic branch. (d)-(h) show the profiles at the Hopf-bifurcation (diamond symbols in (a)). Remaining parameters are as in Fig. 4.5 (c).

We therefore investigate the case in Fig. 4.5 (c) further. In Fig. 4.6 we follow the binodal given by the

dotted red line in panel (b) to obtain the bifurcation diagram depicted in panel (a). We also consider varying system sizes to deduce reliable information about the limit of an infinite system. We first note that – as expected – the bifurcation diagram approaches the Maxwell line (red) in the limit of an infinite system comparable to the passive case (for the approach to the Maxwell construction in the passive case, see [10]).

Independently of the system size the stable branch of the homogeneous $\downarrow\downarrow$-phase coming from the left destabilises in a subcritical pitchfork bifurcation at $\bar{u}_1 \approx -1.5$ corresponding to the Cahn-Hilliard instability indicated in green in the phase diagram. Then the branches of phase separated states stabilise as they fold back in a saddle-node bifurcation. These saddle nodes converge to the left binodal point upon increasing the system size. The branches of phase separated states then again destabilise in a secondary Hopf-bifurcation. The value of $\bar{u}_1$, where this bifurcation occurs, strongly depends on the system size, ranging from $\bar{u}_1 \approx -1.2$ for $L = 10\pi$ to $\bar{u}_1 \approx -1.8$ for $L = 160\pi$, indicating that in the limit of an infinite system it also coincides with the left binodal point. This is further illustrated by panels (d)-(h), which show the phase-separated branch at the onset of the Hopf instability. Independently of the system size, the phase-separated state becomes unstable, when the domain with the linearly unstable $\downarrow\uparrow$-phase reaches a size of ≈ 14, indicated by the dashed vertical lines in each panel. The unstable phase-separated state then recombines with the homogeneous state, stabilising it in another subcritical pitchfork bifurcation at $\bar{u}_1 \approx -1.1$. Then at $\bar{u}_1 \approx -1.0$ the homogeneous state again becomes unstable in the primary Hopf-bifurcation that is indicated by the solid blue line in the phase diagram.

Finally we take a brief look at the emerging oscillatory branches. First for a system size of $L = 20\pi$ we follow the emerging time-periodic branch at the Hopf-bifurcation indicated at the inset in Fig. 4.6 (a). A space time-plot of one period is given in panel (c). The oscillation only takes place in the domain, where the oscillatory unstable $\downarrow\uparrow$-phase is present. As it is linearly stable, the right domain with the $\downarrow\downarrow$-phase does not take part in the oscillation. In a sense, the classical coexistence of homogeneous stationary phases is replaced with a new stable coexistence of a stationary phase with an oscillatory phase.

4.6. Outlook: Crystalline phases

Finally, we briefly demonstrate, how the Maxwell-constructon on active mixtures can be extended to crystalline phases, i.e. phases with spatially periodic fields. We therefore introduce another linear coupled system in one spatial dimension, where we now employ the single-species free energy densities of a phase field-crystal model, i.e.

$$\begin{aligned} f_1 &= \frac{1}{2}\sigma_1 u_1^2 + \frac{1}{2}[(q_1^2 + \partial_{xx})u_1]^2 + \frac{1}{4}u_1^4 \\ f_2 &= \frac{1}{2}\sigma_2 u_2^2 + \frac{1}{2}[(q_2^2 + \partial_{xx})u_2]^2 + \frac{1}{4}u_2^4. \end{aligned} \tag{4.29}$$

Here, for simplicity, we set the critical wavenumbers to one, i.e. $q_1 = q_2 = 1$, and the critical temperatures to be equal, i.e. $\sigma_1 = \sigma_2 = \sigma$. We then obtain

$$\begin{aligned} \partial_t u_1 &= \partial_{xx}\left[\sigma u_1 - (1+\partial_{xx})^2 u_1 + u_1^3 - (\rho+\alpha)u_2\right] \\ \partial_t u_2 &= \partial_{xx}\left[\sigma u_2 - (1+\partial_{xx})^2 u_2 + u_2^3 - (\rho-\alpha)u_1\right], \end{aligned} \tag{4.30}$$

i.e. we obtain a system of two nonreciprocally interacting phase-field-crystal equations. With similar boundary conditions as in the NRCH case, steady states have to obey

$$\begin{aligned} \mu_1 &= \sigma u_1 - (1+\partial_{xx})^2 u_1 + u_1^3 - (\rho+\alpha)u_2 \\ \mu_2 &= \sigma u_2 - (1+\partial_{xx})^2 u_2 + u_2^3 - (\rho-\alpha)u_1. \end{aligned} \tag{4.31}$$

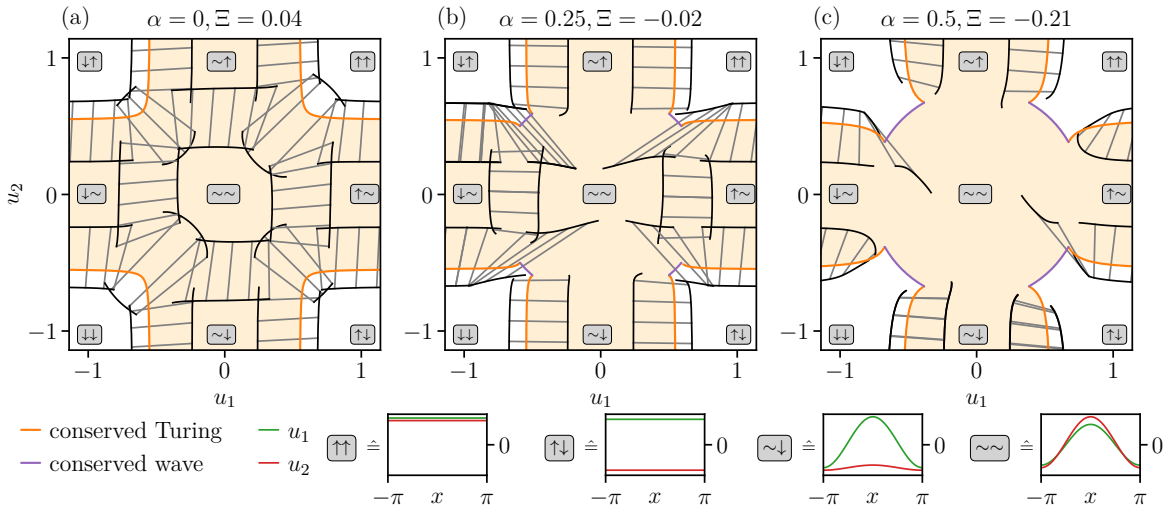

Figure 4.7: Phase diagrams of the nonreciprocal phase-field-crystal model in the average composition-plane for increasing nonreciprocal coupling parameter α. Binodal lines are depicted in solid black and tie lines connecting coexisting stable state in solid grey. The corners mark single phase regions of homogeneous states, where e.g. in the top left corner only the $\downarrow\uparrow$-phase ($\hat{=}$ low u_1-concentration and high u_2-concentration) is present. The symbols used for the phases indicate spatially homogeneous and oscillatory behaviour of u_1 and u_2, e.g. a $\downarrow\sim$-phase means u_1 has a negative concentration and u_2 shows a spatial oscillation. The solid orange and solid purple lines mark conserved Turing and conserved Hopf instabilities respectively. The yellowish region marks the instability of the homogeneous states. The remaining parameters are $\rho = 0.2$ and $\sigma = -0.9$.

Here, the passive case, i.e. $\alpha = 0$ has already been investigated by Holl et al. [11]. There, the Maxwell construction is based on average grand potential densities, i.e. on the concept that if a minimum of the grand potential is realised, then coexisting phases in the thermodynamic limit need to have the same average grand potential densities. Here though we construct the Hamiltonian $\mathscr{H}$ of the steady state

equation, i.e.

$$\begin{aligned} \mathscr{H} &= f - \sum_{i=1}^{k} \boldsymbol{p}_i \partial_x \boldsymbol{q}_i - \boldsymbol{\mu}\boldsymbol{\chi}(\boldsymbol{u}) \\ \text{with} \quad \boldsymbol{q}_i &= \partial_x^{i-1}\boldsymbol{u} \qquad \text{and} \qquad \boldsymbol{p}_i = \sum_{j=i}^{k} (-\partial_x)^{(j-i)} \frac{\partial f}{\partial(\partial_x^j \boldsymbol{u})}, \end{aligned} \tag{4.32}$$

where here $k = 2$ is the highest number of occuring derivatives in f. In appendix D we demonstrate in a very general setting that $\mathscr{H}$ is a spatially uniform quantity for steady states. Using the definition of the spurious gradient dynamics free energy, i.e. Eq. (4.16), then yields

$$\begin{aligned} \mathscr{H} &= \frac{\rho}{\rho+\alpha}(h_1 - u_1\mu_1) + \frac{\rho}{\rho-\alpha}(h_2 - u_2\mu_2) - \rho u_1 u_2 \\ \text{with} \qquad h_{1,2} &= (\partial_x u_{1,2})^2 + (\partial_x u_{1,2})(\partial_{xxx} u_{1,2}) - \frac{1}{2}(\partial_{xx} u_{1,2})^2 + \frac{1}{2}(\sigma+1)u_{1,2}^2 + \frac{1}{4}u_{1,2}^4, \end{aligned} \tag{4.33}$$

where $h_{1,2}$ is the usual Hamiltonian of the steady-state Swift-Hohenberg equation. Note that for homogeneous phases, Eq. (4.33) reduces to $\mathscr{H} = p$ as in Eq. (4.26), and therefore the Maxwell construction is reobtained.

Hence, seen together, Eqs. (4.31) and (4.33) are a generalisation of the Maxwell construction that includes crystalline phases, i.e. we obtain more general coexistence conditions

$$\mu_1^{(A)} = \mu_1^{(B)}, \qquad \mu_2^{(A)} = \mu_2^{(B)} \quad \text{and} \quad \mathscr{H}^{(A)} = \mathscr{H}^{(B)}, \tag{4.34}$$

where $\mu_1^{(A)} = \mu_1(\boldsymbol{u}^{(A)}, \partial_x \boldsymbol{u}^{(A)}, \partial_{xx}\boldsymbol{u}^{(A)}, ...)$ etc.. We then again employ the two-bath continuation method from Holl et al. [11] to obtain phase diagrams, where we additionally average the Hamiltonian and the chemical potentials in each phase to reduce the numerical error. Fig. 4.7 shows phase diagrams that are obtained with this extended Maxwell construction. Panel (a) reproduces the passive, variational case $\alpha = 0$, that has already been discussed by Holl et al. [11]. Since there occur many unstable coexistences with unclear interpretation in the active case, here we only display the – physically more relevant – stable coexistences.

In total we find nine different phases, since each of the concentrations can be high($\uparrow$), low($\downarrow$) or show a spatial oscillation($\sim$). For example, in the $\sim\sim$-phase the two concentrations show a pronounced spatial oscillation.

In the passive case in (a), we find that each adjacent phase can pairwise coexist including the coexistence of the $\sim\sim$-phase with the homogeneous phases, e.g. the $\uparrow\uparrow$-phase. Then, going to the nonreciprocal case, we note that with increasing nonreciprocity the binodal lines recede from the center of the phase diagram. For $\alpha = 0.25$, i.e. in a weakly nonreciprocal case in Fig. 4.7, the stable coexistence between the $\sim\sim$-phase and $\sim\uparrow$ and $\sim\downarrow$-phase has already disappeared. Then, going to a larger nonreciprocal coupling of $\alpha = 0.5$, the only remaining coexistence in the central region are the ones of $\sim\sim$-phase with $\downarrow\uparrow$-phase and $\uparrow\downarrow$-phase. Therefore, the overall effect on the activitity on phase-coexistence seems comparable to the Cahn-Hilliard case. Further studies on the approach of the Maxwell construction

and the occuring oscillatory states present an interesting avenue for future research. Finally, we note that this method could also be applied for the general case of the NRCH equation with $\kappa \neq 1$ that can have a conserved Turing instability and crystalline states. However, its application is numerically more challenging as the occuring wavenumbers strongly depend on $\bar{u}_1$ and $\bar{u}_2$ and the phases can therefore not be approximated by a domain with fixed length of one or a few spatial periods.

5. Conclusion and outlook

The goal of this thesis was to reveal underlying principles of pattern formation in active mixtures. More specifically, we aimed at the development of a general description of active mixtures close to the onset of a conserved large scale oscillatory instability. Further we wanted to generalise conditions of phase coexistence.

First, we reviewed the concepts of linear and weakly nonlinear analysis. In passing, we developed a normal form for linearised conserved and nonconserved two-component systems, that describes a systems linear stability based on the three properties self interaction, rigidity ratio and nonreciprocity. We then introduced a classification of eight different linear instabilities and discussed minimal examples for their occurrence, i.e. examples with a minimal number of fields and a minimal order of the highest occurring derivative. In this context, the NRCH equation can be seen as a minimal example for the conserved Hopf instability. Further, we introduced the amplitude equation for each instability. As the dispersion relations of the Allen-Cahn and Cahn-Hilliard instability do not imply different timescales, the Allen-Cahn and Cahn-Hilliard equation can be seen as their amplitude equation, where the "trivial amplitude" describes the values of the original conserved fields. However, this is not the case for the conserved Hopf instability, where the dispersion relation implies that oscillations occur on a timescale that is fast compared to the timescale of the linear growth of the unstable modes. Pointing out, that the conserved Hopf instability is the paradigmatical instability for active mixtures, we motivated the need for an amplitude equation, i.e. for a universal description of a large-scale conserved oscillatory instability.

Based on the dispersion relation, we then derived a timescale-separating ansatz for the conserved Hopf instability. There, we revealed that the relation between amplitude and original fields is analogous to the linear Schrödinger equation, i.e. that the amplitude reflects a wave packet that is propagated by a linear-Schrödinger-type time-evolution operator. Using the time translation symmetry of the underlying system, we pointed out, that local nonlinearities are forbidden to occur in the amplitude equation. Using a simplified version of the NRCH equation, we then derived the amplitude equation for the conserved Hopf instability. Analysing the amplitude equation then revealed a natural mechanism of coarsening suppression, i.e. that there exist stable travelling-wave solutions in the original equation with spatial periodicity greater than one. Comparing the full NRCH model to the amplitude equation in a bifurcation analysis and in direct time simulations, showed a coherent picture of the relation between the two. Especially, we could analytically derive and numerically prove, that travelling waves with periodicity greater than one are produced in sequences of secondary bifurcations that stabilise the corresponding branch. We then turned to a more general case of the NRCH equation. There we showed, that in general, the amplitude equation will have complex coefficients, which leads to travelling-wave states on the slow timescale.

Extending the discussion of the linear stability analysis for travelling-wave states to the general case is an interesting avenue for future research. Analogous to the complex Ginzburg-Landau equation, one expects to see an equivalent of the Benjamin-Feir-Newell criterion, that yields a finite largest stable wavenumber. Also a further generalisation to a higher spatial dimension might be possible.

We then turned towards phase coexistence. First, reviewing the Maxwell construction for a Cahn-Hilliard-type system, we demonstrated, how the coexistence condition is obtained from the evaluation of an integral along a path that connects homogeneous phases. We derived a Maxwell construction for "conserved spurious gradient dynamics", a class of systems that allow for a Maxwell construction, but that do not necessarily approach an equilibrium. We showed that certain scalar field theories that are used to describe motility-induced phase separation fit the proposed structure. Then, turning to the special case of active model B, we used our formalism to obtain the coexistence conditions and investigated their asymptotics close to and far away from the variational limit case. The results coincide with those already derived by Wittkowski et al. [37], but the formalism allows for a systematic derivation.
A second example for conserved spurious gradient dynamics were linear coupled two-field systems. First, we showed, that the NRCH equation fits the model structure and investigated the resulting phase diagrams. We observed that for increasing nonreciprocal coupling the binodals recede from the center of the phase diagram. For the active case we inspected a binodal, that connects a stable state to a state with an oscillatory instability in more detail. We demonstrated that finite systems still approach the Maxwell line for increasing system sizes, but that the bifurcation point moves, such that the region of stable phase separated states approaches zero. We then tracked the branches emerging at the conserved Hopf-bifurcations, which indicate that here the coexistence of stable stationary phases is replaced with a coexistence between a stable and an oscillatory phase.
Finally we investigated another linear coupled system by replacing the Cahn-Hilliard-type one-component free energy densities with the corresponding free energy densities of a phase-field-crystal model. This shifts the primary instabilities towards a finite wavelength and the system forms crystalline phases for small concentrations. Constructing the Hamiltonian of the steady state equation, we were able to obtain phase diagrams that include crystalline phases. Again, increasing the activity lead to the binodals receding from the center of the phase diagram.
An interesting avenue for future research is the investigation of phase coexistence in the NRCH model for the case of unequal rigidities.Further, one could investigate the nonconserved equivalent of conserved spurious gradient dynamics. There, to realise phase coexistence, one has to introduce external chemical potentials, that lead to the similar steady state equations as in the conserved case. For chemical potentials close to coexistence, one can in special cases analytically derive formulae for the front velocities of one stable state invading the other (see e.g. Alvarez-Socorro et al. [38] and Stegemerten et al. [39]). These could then possibly be also systematically derived using a "nonconserved spurious gradient dynamics".
In conclusion, we shed light onto the behaviour that distinguishes active mixtures from their passive counterparts. Here, the NRCH equation is a paradigmatic example, that can be used to investigate conserved large-scale oscillatory instabilities as well as a Maxwell construction that indicates the coexistences between stationary and oscillatory phases. Although here they were treated separately, their combination might also be an important avenue for future research on a path towards a universal description of oscillatory phases in active mixtures.

Bibliography

[1] I. Newton. *Philosophiae Naturalis Principia Mathematica. Auctore Js. Newton ...* la. Jussu Societatis Regiae ac Typis Josephi Streater., 1687. DOI: 10.3931/E-RARA-440.

[2] J. Clerk-Maxwell. "On the Dynamical Evidence of the Molecular Constitution of Bodies". In: *Nature* 11.279 (1875), pp. 357–359. DOI: 10.1038/011357a0.

[3] A. M. Turing. "The chemical basis of morphogenesis". In: *Philos. Trans. R. Soc. Lond. Ser. B-Biol. Sci.* 237 (1952), pp. 37–72. DOI: 10.1098/rstb.1952.0012.

[4] M. C. Cross and P. C. Hohenberg. "Pattern formation out of equilibrium". In: *Rev. Mod. Phys.* 65 (1993), pp. 851–1112. DOI: 10.1103/RevModPhys.65.851.

[5] R. Hoyle. *Pattern Formation*. Cambridge University Press, 2006. DOI: 10.1017/cbo9780511616051.

[6] A. P. Solon et al. "Pressure and phase equilibria in interacting active Brownian spheres". In: *Phys. Rev. Lett.* 114 (2015), p. 198301. DOI: 10.1103/PhysRevLett.114.198301.

[7] M.J. Bowick et al. "Symmetry, Thermodynamics, and Topology in Active Matter". In: *Physical Review X* 12.1 (2022). DOI: 10.1103/physrevx.12.010501.

[8] M. Fruchart et al. "Non-reciprocal phase transitions". In: *Nature* 592.7854 (2021), pp. 363–369. DOI: 10.1038/s41586-021-03375-9.

[9] U. Thiele. *Lecture "Introduction to Nonequilibrium Thermodynamics - Onsager's variational principle"*. en. 2021. DOI: 10.5281/ZENODO.4545320.

[10] U. Thiele et al. "First order phase transitions and the thermodynamic limit". In: *New J. Phys.* 21 (2019), p. 123021. DOI: 10.1088/1367-2630/ab5caf.

[11] M. P. Holl, A. J. Archer, and U. Thiele. "Efficient calculation of phase coexistence and phase diagrams: Application to a binary phase-field crystal model". In: *J. Phys.: Condens. Matter* 33 (2021), p. 115401. DOI: 10.1088/1361-648X/abce6e.

[12] J. W. Cahn and J. E. Hilliard. "Free energy of a nonuniform system. 1. Interfacial free energy". In: *J. Chem. Phys.* 28 (1958), pp. 258–267. DOI: 10.1063/1.1744102.

[13] J.W. Cahn and J. E. Hilliard. "Free Energy of a Nonuniform System. III. Nucleation in a Two-Component Incompressible Fluid". In: *The Journal of Chemical Physics* 31.3 (1959), pp. 688–699. DOI: 10.1063/1.1730447.

[14] T. Frohoff-Hülsmann, J. Wrembel, and U. Thiele. "Suppression of coarsening and emergence of oscillatory behavior in a Cahn-Hilliard model with nonvariational coupling". In: *Phys. Rev. E* 103 (2021), p. 042602. DOI: 10.1103/PhysRevE.103.042602.

[15] T. Frohoff-Hülsmann et al. "Stationary broken parity states in active matter models". In: *Physical Review E* 107.6 (2023). DOI: 10.1103/physreve.107.064210.

[16] T. Frohoff-Hülsmann and U. Thiele. "Localised states in coupled Cahn-Hilliard equations". In: *IMA J. Appl. Math.* 86 (2021), pp. 924–943. DOI: 10.1093/imamat/hxab026.

[17] F. Brauns and M. C. Marchetti. “Non-reciprocal pattern formation of conserved fields”. In: *arxiv* (2023). arXiv: 2306.08868v2 [nlin.PS].

[18] Z. H. You, A. Baskaran, and M. C. Marchetti. “Nonreciprocity as a generic route to traveling states”. In: *Proc. Natl. Acad. Sci. U. S. A.* 117 (2020), pp. 19767–19772. DOI: 10.1073/pnas.2010318117.

[19] S. Saha, J. Agudo-Canalejo, and R. Golestanian. “Scalar Active Mixtures: The Non-Reciprocal Cahn-Hilliard Model”. In: *Phys. Rev. X* 10 (2020), p. 041009. DOI: 10.1103/PhysRevX.10.041009.

[20] T. Frohoff-Hülsmann and U. Thiele. “Nonreciprocal Cahn-Hilliard Model Emerges as a Universal Amplitude Equation”. In: *Phys. Rev. Lett.* 131 (10 2023), p. 107201. DOI: 10.1103/PhysRevLett.131.107201.

[21] T. Frohoff-Hülsmann, U. Thiele, and L. M. Pismen. “Non-reciprocity induces resonances in a two-field Cahn-Hilliard model”. In: *Philosophical Transactions of the Royal Society A: Mathematical, Physical and Engineering Sciences* 381.2245 (2023). DOI: 10.1098/rsta.2022.0087.

[22] S. H. Strogatz. *Nonlinear Dynamics and Chaos*. CRC Press, 2018. DOI: 10.1201/9780429492563.

[23] A. Pototsky, U. Thiele, and H. Stark. “Mode instabilities and dynamic patterns in a colony of self-propelled surfactant particles covering a thin liquid layer”. In: *Eur. Phys. J. E* 39 (2016), pp. 1–19. DOI: 10.1140/epje/i2016-16051-4.

[24] C. Misbah. *Complex Dynamics and Morphogenesis*. Springer Netherlands, 2017. DOI: 10.1007/978-94-024-1020-4.

[25] F. Bergmann, L. Rapp, and W. Zimmermann. “Active phase separation: a universal approach”. In: *Phys. Rev. E* 98 (2018), p. 020603. DOI: 10.1103/PhysRevE.98.020603.

[26] L. Rapp, F. Bergmann, and W. Zimmermann. “Systematic extension of the Cahn-Hilliard model for motility-induced phase separation”. In: *Eur. Phys. J. E* 42 (2019), p. 57. DOI: 10.1140/epje/i2019-11825-8.

[27] E. Knobloch and J. D. Gibbon. “Coupled NLS equations for counter propagating waves in systems with reflection symmetry”. In: *Phys. Lett. A* 154 (1991), pp. 353–356.

[28] J. D. Crawford and E. Knobloch. “Symmetry and symmetry-breaking bifurcations in fluid-dynamics”. In: *Ann. Rev. Fluid Mech.* 23 (1991), pp. 341–387. DOI: 10.1146/annurev.fl.23.010191.002013.

[29] E. Knobloch and J. De Luca. “Amplitude equations for traveling-wave convection”. In: *Nonlinearity* 3 (1990), pp. 975–980. DOI: 10.1088/0951-7715/3/4/001.

[30] E. Knobloch. “Nonlocal amplitude equations”. In: *Pattern Formation in Complex Dissipative Systems*. Ed. by S. Kai. World Scientific, 1992, pp. 263–274. DOI: 10.1142/9789814538039.

[31] H. Uecker, D. Wetzel, and J. D. M. Rademacher. “pde2path - a Matlab package for continuation and bifurcation in 2D elliptic systems”. In: *Numer. Math.-Theory Methods Appl.* 7 (2014), pp. 58–106. DOI: 10.4208/nmtma.2014.1231nm.

[32] M. Golubitsky and I. Stewart. “Hopf Bifurcation with Symmetry”. In: *The Symmetry Perspective*. Birkhäuser Basel, 2002, pp. 87–122. DOI: 10.1007/978-3-0348-8167-8_4.

[33] A. P. Solon et al. “Generalized thermodynamics of phase equilibria in scalar active matter”. In: *Phys. Rev. E* 97 (2018), p. 020602. DOI: 10.1103/PhysRevE.97.020602.

[34] M. E. Cates. “Active Field Theories”. In: *Active Matter and Nonequilibrium Statistical Physics*. Oxford University PressOxford, 2022, pp. 180–216. DOI: 10.1093/oso/9780192858313.003.0006.

[35] A. V. Ivlev et al. “Statistical mechanics where Newton’s third law is broken”. In: *Phys. Rev. X* 5 (2015), p. 011035. DOI: 10.1103/PhysRevX.5.011035.

[36] N. P. Kryuchkov, A. V. Ivlev, and S. O. Yurchenko. “Dissipative phase transitions in systems with nonreciprocal effective interactions”. In: *Soft Matter* 14 (2018), pp. 9720–9729. DOI: 10.1039/c8sm01836g.

[37] R. Wittkowski et al. “Scalar ϕ^4 field theory for active-particle phase separation”. In: *Nat. Commun.* 5 (2014), p. 4351. DOI: 10.1038/ncomms5351.

[38] A. J. Alvarez-Socorro et al. “Nonvariational mechanism of front propagation: theory and experiments”. In: *Phys. Rev. E* 95 (2017), p. 010202. DOI: 10.1103/PhysRevE.95.010202.

[39] F Stegemerten, S. V. Gurevich, and U. Thiele. “Bifurcations of front motion in passive and active Allen-Cahn-type equations”. In: *Chaos* 30 (2020), p. 053136. DOI: 10.1063/5.0003271.

A. The derivation from Ref. [20] without conservation laws

Here we repeat the derivation from Frohoff-Hülsmann and Thiele [20], adjusted to the nonconserved case, i.e. the Hopf instability in absence of any conservation laws, to show that it does not result in the complex Ginzburg-Landau equation, but in a two-component-reaction-diffusion system. To do so we consider a general reflection-symmetric multi-component system. It is written as coupled kinetic equations for N nonconserved ($\boldsymbol{n} = (n_1, \ldots, n_N)$) scalar field variables with a general right-hand side $\boldsymbol{F}$:

$$\partial_t \boldsymbol{n} = \boldsymbol{F}(\boldsymbol{n}, \partial_{xx}). \tag{A.1}$$

For scalar fields, reflection symmetry implies that Eqs. (A.1) are invariant under the transformation $x \to -x$. Therefore, the individual terms within $\boldsymbol{F}$ do either not include derivatives or an even number of them. We aassume that the bifurcation happens at a uniform steady state $\boldsymbol{n}_0$ with $\boldsymbol{F}(\boldsymbol{n}_0) = 0$.

As we assume to be sufficiently close to the critical point of a Hopf-bifurcation, i.e. a pair of complex conjugate eigenvalues (at $k = 0$) of $\boldsymbol{F}(\boldsymbol{n} = \boldsymbol{n}_0)$ has recently crossed the imaginary axis with nonzero imaginary part of $\mathcal{O}(1)$. Hence we can pick two (linear independent and orthonormalized) eigenvectors $\boldsymbol{n}_\rho$ and $\boldsymbol{n}_\sigma$ of $\frac{\partial \boldsymbol{F}}{\partial \boldsymbol{n}}\big|_{\boldsymbol{n}_0}$, such that we can factorize

$$\left.\frac{\partial \boldsymbol{F}}{\partial \boldsymbol{n}}\right|_{\boldsymbol{n}_0} = \left.\frac{\partial \boldsymbol{F}}{\partial \boldsymbol{n}}\right|_{\boldsymbol{n}_0}^{\parallel} + \left.\frac{\partial \boldsymbol{F}}{\partial \boldsymbol{n}}\right|_{\boldsymbol{n}_0}^{\perp}, \tag{A.2}$$

where "$\parallel$" denotes projection onto the subspace spanned by $\boldsymbol{n}_\rho$ and $\boldsymbol{n}_\sigma$ and "$\perp$" onto its orthogonal complement. From here, we will refer to these subspaces as the parallel and the perpendicular subspace. Note that if we redefined the fields beforehand, such that $\frac{\partial \boldsymbol{F}}{\partial \boldsymbol{n}}\big|_{\boldsymbol{n}_0}$ is diagonal and in the new basis $\boldsymbol{n}_\rho = \boldsymbol{e}_1$ and $\boldsymbol{n}_\sigma = \boldsymbol{e}_2$, this factorization simply correponds to:

$$\left.\frac{\partial \boldsymbol{F}}{\partial \boldsymbol{n}}\right|_{\boldsymbol{n}_0} = \begin{pmatrix} \lambda_\rho & & & & \\ & \lambda_\sigma & & & \\ & & \lambda_3 & & \\ & & & \lambda_4 & \\ & & & & \ldots \end{pmatrix} = \begin{pmatrix} \lambda_\rho & & & & \\ & \lambda_\sigma & & & \\ & & 0 & & \\ & & & 0 & \\ & & & & \ldots \end{pmatrix} + \begin{pmatrix} 0 & & & & \\ & 0 & & & \\ & & \lambda_3 & & \\ & & & \lambda_4 & \\ & & & & \ldots \end{pmatrix}. \tag{A.3}$$

From the dispersion relation we then know, that $\lambda_{\rho,\sigma} = r \pm \mathrm{i}\omega$ with r being of $\mathcal{O}(\varepsilon^2)$ and that all λ_i, $i \geq 3$ have negative real part of $\mathcal{O}(1)$. Here though we do not redefine the fields and stay with the original basis to stay in line with Ref. [20].

To perform the weakly nonlinear analysis valid in the vicinity of instability onset, we expand all fields in the smallness parameter $\varepsilon \ll 1$, i.e.,

$$\boldsymbol{n}(X,t,\tau) = \boldsymbol{n}_0 + \varepsilon \boldsymbol{n}_1(X,t,\tau) + \varepsilon^2 \boldsymbol{n}_2(X,t,\tau) + \boldsymbol{n}_3(X,t,\tau) + \ldots, \tag{A.4}$$

introduce scalings by writing $\partial_x = \varepsilon\partial_X$ and $\partial_t = \partial_t + \varepsilon^2\partial_\tau$, and also expand the right hand side of Eqs. (A.1) as

$$\boldsymbol{F} = \varepsilon\boldsymbol{F}_1 + \varepsilon^2\boldsymbol{F}_2 + \varepsilon^3\boldsymbol{F}_3 + \dots, \tag{A.5}$$

where $\boldsymbol{F}_0 = \boldsymbol{F}(\boldsymbol{n}_0) = \boldsymbol{0}$ was used. The various coefficients are given by corresponding Taylor expansions, e.g.

$$\boldsymbol{F}_2 = \boldsymbol{n}_1 \cdot \frac{1}{2}\frac{\partial^2 \boldsymbol{F}}{\partial \boldsymbol{n}^2}\bigg|_{\boldsymbol{n}_0} \cdot \boldsymbol{n}_1 + \frac{\partial \boldsymbol{F}}{\partial \boldsymbol{n}}\bigg|_{\boldsymbol{n}_0} \cdot \boldsymbol{n}_2 \tag{A.6}$$

All expansions and scalings are inserted into the model equations Eqs. (A.1), that are then considered order by order in ε. Due to the scaling implied by the dispersion relation, one needs to successively consider all orders up to $\mathscr{O}(\varepsilon^3)$ to obtain evolution equations that capture dynamic effects on the slow timescale τ.

Order ε

The N equations become the algebraic system

$$\partial_t \boldsymbol{n}_1(X,t,\tau) = \boldsymbol{F}_1 = \frac{\partial \boldsymbol{F}}{\partial \boldsymbol{n}}\bigg|_{\boldsymbol{n}_0} \cdot \boldsymbol{n}_1(X,t,\tau) \tag{A.7}$$

linear in N unknown quantities $\boldsymbol{n}_1$. Since this problem is fully linear, we can treat the subspace spanned by $\boldsymbol{n}_\rho$ and $\boldsymbol{n}_\sigma$ and its orthogonal complement separately. On the perpendicular subspace, we have that $\frac{\partial \boldsymbol{F}}{\partial \boldsymbol{n}}|^{\perp}_{\boldsymbol{n}_0}$ has full rank and therefore the solvability condition, i.e. avoiding secular growth (or here decay) that destroys the time scale ansatz is, that $\boldsymbol{n}_1(X,t,\tau)$, is part of the subspace spanned by $\boldsymbol{n}_\rho$ and $\boldsymbol{n}_\sigma$. We can therefore conclude, that

$$\boldsymbol{n}_1(X,t,\tau) = \rho_1(X,t,\tau)n_\rho + \sigma_1(X,t,\tau)n_\sigma, \tag{A.8}$$

and hence after scalar multiplying with $\boldsymbol{n}_\rho$ and $\boldsymbol{n}_\sigma$, we obtain the system

$$\partial_t \begin{pmatrix} \rho_1(X,t,\tau) \\ \sigma_1(X,t,\tau) \end{pmatrix} = \begin{pmatrix} F_{\rho\rho} & F_{\sigma\rho} \\ F_{\rho\sigma} & F_{\sigma\sigma} \end{pmatrix} \begin{pmatrix} \rho_1(X,t,\tau) \\ \sigma_1(X,t,\tau) \end{pmatrix}, \tag{A.9}$$

where $F_{ij} = \left(\frac{\partial \boldsymbol{F}}{\partial \boldsymbol{n}}\big|_{\boldsymbol{n}_0} \cdot \boldsymbol{n}_i\right) \cdot \boldsymbol{n}_j$ for $i,j \in \{\rho,\sigma\}$ The eigenvalues read

$$\lambda_\pm = \frac{1}{2}\left(F_{\rho\rho} + F_{\sigma\sigma} \pm \sqrt{(F_{\rho\rho}+F_{\sigma\sigma})^2 - 4(F_{\rho\rho}F_{\sigma\sigma} - F_{\rho\sigma}F_{\sigma\rho})}\right) \tag{A.10}$$

Due to the imposed dispersion relation we have that the trace $F_{\rho\rho} + F_{\sigma\sigma}$ is of $\mathscr{O}(\varepsilon^2)$ and therefore has to vanish at $\mathscr{O}(\varepsilon)$. At this point, we could solve the linear equation, Eq. (A.9), i.e. then we would obtain

that

$$\begin{pmatrix}\rho_1(X,t,\tau)\\ \sigma_1(X,t,\tau)\end{pmatrix} = A(X,\tau)e^{\mathrm{i}\omega t}\boldsymbol{v}_+ + c.c. \quad \text{with} \quad \omega = \sqrt{F_{\rho\rho}F_{\sigma\sigma} - F_{\rho\sigma}F_{\sigma\rho}}, \tag{A.11}$$

with an Amplitude $A(X,\tau)$, a frequency ω and an eigenvector $\boldsymbol{v}_+$. However here we follow the steps from Ref. [20] and stick to ρ_1 and σ_1, i.e. the variables that describe the original fields and not the amplitude.

Order ε^2

Here the occurring equation reads

$$\partial_t \boldsymbol{n}_2 = \boldsymbol{F}_2 = \boldsymbol{n}_1 \cdot \frac{1}{2}\frac{\partial^2 \boldsymbol{F}}{\partial \boldsymbol{n}^2}\bigg|_{\vec{n}_0} \cdot \boldsymbol{n}_1 + \frac{\partial \boldsymbol{F}}{\partial \boldsymbol{n}}\bigg|_{\vec{n}_0} \cdot \boldsymbol{n}_2 \,. \tag{A.12}$$

After plugging in the expression for $\boldsymbol{n}_1$, the inhomogeneous linear differential equation for $\boldsymbol{n}_2$ becomes

$$\partial_t \boldsymbol{n}_2 - \frac{\partial \boldsymbol{F}}{\partial \boldsymbol{n}}\bigg|_{\vec{n}_0} \boldsymbol{n}_2 = \mathscr{N}_2(t,\tau,X) \qquad \text{with} \qquad \mathscr{N}_2(t,\tau,X) = \boldsymbol{n}_{\rho\rho}\rho_1^2 + \boldsymbol{n}_{\sigma\rho}\sigma_1\rho_1 + \boldsymbol{n}_{\sigma\sigma}\sigma_1^2. \tag{A.13}$$

To solve it, we parametrize $\boldsymbol{n}_2$ as:

$$\boldsymbol{n}_2 = \rho_2(X,t,\tau)\boldsymbol{n}_\rho + \sigma_2(X,t,\tau)\boldsymbol{n}_\sigma + \boldsymbol{n}_2^\perp(X,t,\tau) \tag{A.14}$$

Projecting this equation onto the perpendicular subspace yields a differential equation for $\boldsymbol{n}_2^\perp(X,t,\tau)$

$$\partial_t \boldsymbol{n}_2^\perp - \frac{\partial \boldsymbol{F}}{\partial \boldsymbol{n}}\bigg|_{\vec{n}_0} \boldsymbol{n}_2^\perp = \mathscr{N}_2^\perp(t,\tau,X) \qquad \text{with} \qquad \mathscr{N}_2^\perp(t,\tau,X) = \boldsymbol{n}_{\rho\rho}^\perp\rho_1^2 + \boldsymbol{n}_{\sigma\rho}^\perp\sigma_1\rho_1 + \boldsymbol{n}_{\sigma\sigma}^\perp\sigma_1^2 \tag{A.15}$$

The important observation here is that $\frac{\partial \boldsymbol{F}}{\partial \boldsymbol{n}}\big|_{\boldsymbol{n}_0}$ is an endomorphism on both the parallel and the perpendicular subspace, and therefore $\left(\frac{\partial \boldsymbol{F}}{\partial \boldsymbol{n}}\big|_{\boldsymbol{n}_0} \cdot \boldsymbol{n}_2\right)^\perp = \frac{\partial \boldsymbol{F}}{\partial \boldsymbol{n}}\big|_{\boldsymbol{n}_0} \cdot \boldsymbol{n}_2^\perp$.

For the particular solution[17] we use an ansatz with the same nonlinearities as the right hand side, i.e.

$$n_{2,p}^\perp = \tilde{\boldsymbol{n}}_{\rho\rho}^\perp\rho_1^2 + \tilde{\boldsymbol{n}}_{\sigma\rho}^\perp\sigma_1\rho_1 + \tilde{\boldsymbol{n}}_{\sigma\sigma}^\perp\sigma_1^2, \tag{A.16}$$

where $\tilde{\boldsymbol{n}}_{\rho\rho}^\perp, \tilde{\boldsymbol{n}}_{\sigma\rho}^\perp$ and $\tilde{\boldsymbol{n}}_{\sigma\sigma}^\perp$ have to be determined. Then, using Eq. (A.9) the time derivative evaluates

[17] Here this derivation differs slightly from the one for the conserved Hopf-bifurcation in [20]. There, the slowest relevant timescale is of $\mathscr{O}(\varepsilon^2)$, whereas here it is $\mathscr{O}(1)$. Therefore in the former case all modes that remain stable relax instantaneously on the slowest timescale (they are "slaved"), whereas in the latter the Oscillation of the "Hopf-modes" and the relaxation of the stable modes occurs on the same timescale $\mathscr{O}(1)$.

as:

$$\begin{aligned}\partial_t \boldsymbol{n}_{2,p}^{\perp} =& 2\tilde{\boldsymbol{n}}_{\rho\rho}^{\perp}\rho_1\partial_t\rho_1 + \tilde{\boldsymbol{n}}_{\sigma\rho}^{\perp}(\sigma_1\partial_t\rho_1 + \rho_1\partial_t\sigma_1) + 2\tilde{\boldsymbol{n}}_{\sigma\sigma}^{\perp}\sigma_1\partial_t\sigma_1 \\ =& \rho_1^2(2F_{\rho\rho}\tilde{\boldsymbol{n}}_{\rho\rho}^{\perp} + F_{\sigma\rho}\tilde{\boldsymbol{n}}_{\sigma\rho}^{\perp}) + \sigma_1^2(2F_{\sigma\sigma}\tilde{\boldsymbol{n}}_{\sigma\sigma}^{\perp} + F_{\rho\sigma}\tilde{\boldsymbol{n}}_{\sigma\rho}^{\perp}) \\ &+ \rho_1\sigma_1(2F_{\sigma\rho}\tilde{\boldsymbol{n}}_{\rho\rho}^{\perp} + (F_{\sigma\rho} + F_{\rho\sigma})\tilde{\boldsymbol{n}}_{\sigma\rho}^{\perp} + 2F_{\rho\sigma}\tilde{\boldsymbol{n}}_{\sigma\sigma}^{\perp}).\end{aligned} \tag{A.17}$$

This shows that matching the coefficients of $\rho_1^2, \rho_1\sigma_1$ and σ_1^2 in Eq. (A.15) yields a set of $3(N-2)$ linear equations to determine the $3(N-2)$ free coefficients of $\boldsymbol{n}_{2,p}^{\perp}$. Again, to avoid secular growth, the homogeneous solution in the perpendicular subspace has to be set to zero. The behaviour on the perpendicular subspace is therefore fully determined by ρ_1, σ_1 and the Taylor-expansion of $\boldsymbol{F}$.
Summarizing we can denote the solution at $\mathscr{O}(\varepsilon^2)$ as

$$\boldsymbol{n}_2 = \rho_2\boldsymbol{n}_\rho + \sigma_2\boldsymbol{n}_\sigma + \tilde{\boldsymbol{n}}_{\rho\rho}^{\perp}\rho_1^2 + \tilde{\boldsymbol{n}}_{\sigma\rho}^{\perp}\sigma_1\rho_1 + \tilde{\boldsymbol{n}}_{\sigma\sigma}^{\perp}\sigma_1^2, \tag{A.18}$$

were the dynamcis in the parallel subspace are still to be determined.

Order ε^3

The $\mathscr{O}(\varepsilon^3)$-equation reads:

$$\begin{aligned}\partial_\tau\boldsymbol{n}_1 + \partial_t\boldsymbol{n}_3 &= \boldsymbol{F}_3 \\ &= \left.\frac{\partial\boldsymbol{F}}{\partial\boldsymbol{n}}\right|_{\boldsymbol{n}_0}\cdot\boldsymbol{n}_3 + \left.\frac{\partial\boldsymbol{F}}{\partial(\partial_{xx}\boldsymbol{n})}\right|_{\boldsymbol{n}_0}\cdot\partial_{XX}\boldsymbol{n}_1 \\ &+ \sum_{i,j}\left.\frac{\partial^2\boldsymbol{F}}{\partial n_i\partial n_j}\right|_{\boldsymbol{n}_0}(\boldsymbol{n}_1)_i(\boldsymbol{n}_2)_j + \frac{1}{6}\sum_{i,j,k}\left.\frac{\partial^3\boldsymbol{F}}{\partial n_i\partial n_j\partial n_k}\right|_{\boldsymbol{n}_0}(\boldsymbol{n}_1)_i(\boldsymbol{n}_1)_j(\boldsymbol{n}_1)_k\end{aligned} \tag{A.19}$$

Similiar to $\mathscr{O}(\varepsilon^2)$ we parametrize $\boldsymbol{n}_3$ as

$$\boldsymbol{n}_3 = \rho_3(X,t,\tau)\boldsymbol{n}_\rho + \sigma_3(X,t,\tau)\boldsymbol{n}_\sigma + \boldsymbol{n}_3^{\perp}(X,t,\tau). \tag{A.20}$$

Analogously to $\mathscr{O}(\varepsilon^2)$ we could solve the equation in the perpendicular subspace to determine $\boldsymbol{n}_3^{\perp}$ in terms of ρ_1, ρ_2, σ_1 and σ_2. Here we do not proceed at this as it is not necessary for the leading order equation.
After inserting the expressions for $\boldsymbol{n}_1$ and $\boldsymbol{n}_2$, i.e. Eqs. (A.8) and (A.18) this yields an inhomogeneous linear differential equation for $\boldsymbol{n}_3$:

$$\begin{aligned}&\partial_t\boldsymbol{n}_3 + \partial_\tau\boldsymbol{n}_1 - \left.\frac{\partial\boldsymbol{F}}{\partial\boldsymbol{n}}\right|_{\boldsymbol{n}_0}\cdot\boldsymbol{n}_3 = \mathscr{N}_3(X,t,\tau) \\ &\text{with}\quad \mathscr{N}_3(X,t,\tau) = \boldsymbol{n}_{\rho xx}\partial_{XX}\rho_1 + \boldsymbol{n}_{\sigma xx}\partial_{XX}\sigma_1 \\ &\qquad + 2\rho_1\rho_2\boldsymbol{n}_{\rho\rho} + (\sigma_1\rho_2 + \rho_1\sigma_2)\boldsymbol{n}_{\sigma\rho} + 2\sigma_1\sigma_2\boldsymbol{n}_{\sigma\sigma} \\ &\qquad + \rho_1^3\boldsymbol{n}_{\rho\rho\rho} + \rho_1^2\sigma_1\boldsymbol{n}_{\rho\rho\sigma} + \rho_1\sigma_1^2\boldsymbol{n}_{\rho\sigma\sigma} + \sigma_1^3\boldsymbol{n}_{\sigma\sigma\sigma}\end{aligned} \tag{A.21}$$

Note that the vectors $\boldsymbol{n}_{\rho\rho}, \boldsymbol{n}_{\sigma\rho}$ and $\boldsymbol{n}_{\sigma\sigma}$ in the second row are precisely the same as at order ε^2, i.e. in Eq. (A.13), whereas the terms in the third row are defined to collect all terms with the corresponding prefactor, e.g. $\boldsymbol{n}_{\rho\rho\rho}$ collects all terms containing ρ_1^3:

$$\boldsymbol{n}_{\rho\rho\rho} = \sum_{i,j} \frac{\partial^2 \boldsymbol{F}}{\partial n_i \partial n_j}\bigg|_{\boldsymbol{n}_0} (\boldsymbol{n}_\rho)_i \left(\tilde{\boldsymbol{n}}^{\perp}_{\rho\rho}\right)_j + \sum_{i,j,k} \frac{1}{6} \frac{\partial^3 \boldsymbol{F}}{\partial n_i \partial n_j \partial n_k}\bigg|_{\boldsymbol{n}_0} (\boldsymbol{n}_\rho)_i (\boldsymbol{n}_\rho)_j (\boldsymbol{n}_\rho)_k \tag{A.22}$$

Recombining dynamics of all orders

To obtain the final equations we introduce the relevant fields, that recombine the dynamics in the relevant eigenmodes at all orders

$$\rho = \boldsymbol{n}\cdot\boldsymbol{n}_\rho = \varepsilon\rho_1 + \varepsilon^2\rho_2 + \varepsilon^3\rho_3 + ... \quad \text{and} \quad \varsigma = \boldsymbol{n}\cdot\boldsymbol{n}_\sigma = \varepsilon\sigma_1 + \varepsilon^2\sigma_2 + \varepsilon^3\sigma_3 + ... \tag{A.23}$$

We project the equations from all orders, i.e. Eqs. (A.8), (A.13) and (A.21) onto $\boldsymbol{n}_\rho$, which yields

$$\mathscr{O}(\varepsilon): \qquad \partial_t\rho_1 = F_{\rho\rho}\rho_1 + F_{\rho\sigma}\sigma_1 \tag{A.24}$$

$$\mathscr{O}(\varepsilon^2): \qquad \partial_t\rho_2 = F_{\rho\rho}\rho_2 + F_{\rho\sigma}\sigma_2 + r_{\rho\rho}\rho_1^2 + r_{\sigma\rho}\rho_1\sigma_1 + r_{\sigma\sigma}\sigma_1^2 \tag{A.25}$$

$$\begin{aligned}\mathscr{O}(\varepsilon^3): \qquad \partial_\tau\rho_1 + \partial_t\rho_3 =& F_{\rho\rho}\rho_2 + F_{\rho\sigma}\sigma_2 + 2r_{\rho\rho}\rho_1\rho_2 + r_{\sigma\rho}(\rho_1\sigma_2 + \sigma_1\rho_2) + 2r_{\sigma\sigma}\sigma_1^2 \\ &+ r_{\rho xx}\partial_{XX}\rho_1 + r_{\sigma xx}\sigma_1 + r_{\rho\rho\rho}\rho_1^3 + r_{\rho\rho\sigma}\rho_1^2\sigma_1 + r_{\rho\sigma\sigma}\rho_1\sigma_1^2 + r_{\sigma\sigma\sigma}\sigma_1^3,\end{aligned} \tag{A.26}$$

where the coefficients are defined as $r_{\rho\rho} = \boldsymbol{n}_{\rho\rho}\cdot\boldsymbol{n}_\rho$ etc.. Now we collect terms from all orders to recreate the field equations:

$$\begin{aligned}\rho &= \varepsilon\rho_1 + \varepsilon^2\rho_2 + \varepsilon^3\rho_3 + \mathscr{O}(\varepsilon^4) \\ \rho^2 &= \varepsilon^2\rho_1^2 + \varepsilon^3 2\rho_1\rho_2 + \mathscr{O}(\varepsilon^4) \\ \rho\varsigma &= \varepsilon^2\rho_1\sigma_1 + \varepsilon^3(\rho_1\sigma_2 + \rho_2\sigma_1) + \mathscr{O}(\varepsilon^4) \\ \rho^3 &= \varepsilon^3\rho_1^3 + \mathscr{O}(\varepsilon^4).\end{aligned} \tag{A.27}$$

Doing the same for ς and reintroducing the original time and lengthscale we arrive at

$$\begin{aligned}\partial_\tau\rho =& F_{\rho\rho}\rho + F_{\rho\sigma}\varsigma + r_{\rho xx}\partial_{xx}\rho + r_{\sigma xx}\partial_{xx}\varsigma \\ &+ r_{\rho\rho}\rho^2 + r_{\rho\sigma}\varsigma\rho + r_{\sigma\rho}\varsigma^2 + r_{\rho\rho\rho}\rho^3 + r_{\rho\rho\sigma}\rho^2\varsigma + r_{\rho\sigma\sigma}\rho\varsigma^2 + r_{\sigma\sigma\sigma}\varsigma^3 \\ \partial_t\varsigma =& F_{\rho\rho}\rho + F_{\sigma\sigma}\varsigma + s_{\rho xx}\partial_{xx}\rho + s_{\sigma xx}\partial_{xx}\varsigma \\ &+ s_{\rho\rho}\rho^2 + s_{\rho\sigma}\varsigma\rho + s_{\sigma\rho}\varsigma^2 + s_{\rho\rho\rho}\rho^3 + s_{\rho\rho\sigma}\rho^2\varsigma + s_{\rho\sigma\sigma}\rho\varsigma^2 + s_{\sigma\sigma\sigma}\varsigma^3,\end{aligned} \tag{A.28}$$

which is a general 2-component reaction-diffusion system (or two nonreciprocal coupled Allen-Cahn equations), that inherits its linear properties from the orginal system, i.e. it is at the onset of a Hopf-bifurcation.

B. Details of the derivation of the amplitude equation

Here we present some formulae used in section 3 and give some calculations in more detail.

B.1. Normalisation and Fourier identities

In Section 3, we employ a spatial and temporal scalar product as

$$\langle \boldsymbol{f}(X,\tau);\boldsymbol{g}(X,\tau)\rangle = \frac{\Omega_{\min}}{L}\int_{-L/2}^{L/2} \mathrm{d}X \int_{0}^{1/\Omega_{\min}} \mathrm{d}\tau \boldsymbol{f}^{\dagger}(X,\tau)\boldsymbol{g}(X,\tau), \tag{B.1}$$

on the Hilbert-space of (complex) spatially and temporally periodic vector functions on $[-L/2,L/2]\times[0,1/\Omega_{\min}]$. On the subspaces of functions with purely spatial dependency and constant vectorial character, e.g. $\boldsymbol{f}(X,\tau)=f(X)\boldsymbol{v}$, this reduces to

$$\langle \boldsymbol{f}(X,\tau);\boldsymbol{g}(X,\tau)\rangle \sim \frac{1}{L}\int_{-L/2}^{L/2} f^{*}(X)g(X)\mathrm{d}X. \tag{B.2}$$

On these subspaces the functions $e^{\mathrm{i}KX}$ with $K=2\pi z/L$, $z\in\mathbb{Z}$ form an orthonormal basis. Therefore any function $f(X)$ can be expanded in this basis, i.e. in a Fourier series as

$$f(X)=\sum_{K}\tilde{f}(K)e^{\mathrm{i}KX} \qquad \text{with} \qquad \tilde{f}(K)=\langle e^{\mathrm{i}KX};f(X)\rangle = \frac{1}{L}\int_{-L/2}^{L/2} f(X)e^{-\mathrm{i}KX}\mathrm{d}X. \tag{B.3}$$

Further a representation of the δ-Distribution is given by

$$\delta(X-X')=\sum_{K} e^{\mathrm{i}K(X-X')}, \tag{B.4}$$

which can be demonstrated by:

$$\begin{aligned}\langle \delta(X-X');f(X)\rangle &= \langle \sum_{K'} e^{\mathrm{i}K'(X-X')};\sum_{K}\tilde{f}(K)e^{\mathrm{i}KX}\rangle \\ &= \sum_{K,K'}\tilde{f}(K)e^{\mathrm{i}K'X'}\underbrace{\langle e^{\mathrm{i}KX};e^{\mathrm{i}K'X}\rangle}_{=\delta_{KK'}} = \sum_{K}\tilde{f}(K)e^{\mathrm{i}KX'}=f(X')\end{aligned} \tag{B.5}$$

With our choice of the Fourier transformation, we can denote **Parsevals theorem** as:

$$\frac{1}{L}\int_{-L/2}^{L/2}|f(X)|^2\mathrm{d}X = \sum_{K,K'}\tilde{f}^{*}(K)\tilde{f}(K')\underbrace{\frac{1}{L}\int_{-L/2}^{L/2} e^{-\mathrm{i}KX}e^{\mathrm{i}K'X}\mathrm{d}X}_{=\langle e^{\mathrm{i}KX},e^{\mathrm{i}K'X}\rangle=\delta_{K,K'}} = \sum_{K}|\tilde{f}(K)|^2. \tag{B.6}$$

B.2. Nonlinearities in real space

We demonstrate how the nonlinearities derived in Eq. (3.21) in their Fourier-space representation transform into real space

$$\begin{aligned}
&\sum_{Q,K}(-Q^2)e^{\mathrm{i}QX'}\tilde{A}(Q,T)\tilde{A}^*(K,T)\tilde{A}(K,T)\\
&\quad=\partial_{X'X'}\sum_Q\tilde{A}(Q,T)e^{\mathrm{i}QX'}\sum_K\left(\frac{1}{L}\int_{-L/2}^{L/2}A(X,T)e^{-\mathrm{i}KX}\mathrm{d}X\right)^*\left(\frac{1}{L}\int_{-L/2}^{L/2}A(\hat{X},T)e^{-\mathrm{i}K\hat{X}}\mathrm{d}\hat{X}\right)\\
&\quad=\partial_{X'X'}A(X',T)\frac{1}{L}\int_{-L/2}^{L/2}\mathrm{d}X\frac{1}{L}\int_{-L/2}^{L/2}\mathrm{d}\hat{X}A^*(X,T)A(\hat{X},T)\sum_K e^{\mathrm{i}K(X-\hat{X})}\\
&\quad=\partial_{X'X'}A(X',T)\frac{1}{L}\int_{-L/2}^{L/2}|A(X,T)|^2\mathrm{d}X=\partial_{X'X'}A\overline{|A|^2},
\end{aligned}\tag{B.7}$$

where $\overline{|A|^2}$ is the spatial average of the absolute value squared. The second contribution transforms back as:

$$\begin{aligned}
&\sum_Q(-Q^2)e^{\mathrm{i}QX'}\tilde{A}(Q,T)\tilde{A}^*(Q,T)\tilde{A}(Q,T)\\
=&\partial_{X'X'}\frac{1}{L^3}\iiint_{[-L/2,L/2]^3}\mathrm{d}X\mathrm{d}\hat{X}\mathrm{d}\tilde{X}A^*(X,T)A(\hat{X},T)A(\tilde{X},T)\sum_Q e^{\mathrm{i}Q(X'+X-\hat{X}'-\tilde{X})}\\
=&\partial_{X'X'}\frac{1}{L^2}\iint_{[-L/2,L/2]^2}\mathrm{d}X\mathrm{d}\hat{X}A^*(X,T)A(\hat{X},T)A(X'+X-\hat{X})\\
=&\partial_{X'X'}\frac{1}{L^2}\iint_{[-L/2,L/2]^2}\mathrm{d}X\mathrm{d}\hat{X}A^*(-X,T)A(\hat{X},T)A(X'-X-\hat{X})\\
=&\partial_{X'X'}[A(X)\star A(X)\star A^*(-X)](X'),
\end{aligned}\tag{B.8}$$

where the last line indicates the convolution of three functions defined by the expression in the line above.

B.3. Functional variation of the free energy and Fourier space free energy

Here we give more details on the functional variations of the free energy given in Eq. (3.29). We can rewrite the first term as

$$\mathscr{F}_1=\frac{3l}{2}\left(\frac{1}{l}\int_{-l/2}^{l/2}|a|^2\mathrm{d}x\right)^2=\frac{3}{2l}\int_{-l/2}^{l/2}\mathrm{d}x\int_{-l/2}^{l/2}\mathrm{d}x'a^*(x)a^*(x')a(x)a(x')\tag{B.9}$$

Then we obtain the funtional derivative as

$$\begin{aligned}
\int_{-l/2}^{l/2} \frac{\delta \mathscr{F}_1}{\delta a^*} \psi^* \mathrm{d}x &= \lim_{\varepsilon\to 0} \frac{1}{\varepsilon} \left(\mathscr{F}_1[a^* + \varepsilon\psi^*, a] - \mathscr{F}_1[a^*, a] \right) \\
&= \lim_{\varepsilon\to 0} \frac{1}{\varepsilon} \left(\frac{3}{2l} \int_{-l/2}^{l/2} \mathrm{d}x \int_{-l/2}^{l/2} \mathrm{d}x' \left[a^*(x) + \varepsilon\psi^*(x) \right] \left[a^*(x') + \varepsilon\psi^*(x') \right] a(x) a(x') - \mathscr{F}_1[a^*] \right) \\
&= \frac{3}{2l} \int_{-l/2}^{l/2} \left(a^*(x) \int_{-l/2}^{l/2} a^*(x') a(x') \mathrm{d}x' \right) \psi^*(x) \mathrm{d}x + \frac{3}{2l} \int_{-l/2}^{l/2} \left(a^*(x') \int_{-l/2}^{l/2} a^*(x) a(x) \mathrm{d}x \right) \psi^*(x') \mathrm{d}x' \\
&= \int_{-l/2}^{l/2} \underbrace{\left(\frac{3}{l} a^*(x) \int_{-l/2}^{l/2} a^*(x') a(x') \mathrm{d}x' \right)}_{= \frac{\delta \mathscr{F}_1}{\delta a^*}} \psi^*(x) \mathrm{d}x,
\end{aligned} \tag{B.10}$$

where we exchanged the variable names $x \leftrightarrow x'$ in the second term in the last step. We proceed similarly for the second term given by

$$\mathscr{F}_2 = \frac{3}{4l^2} \iiint_{[-\frac{l}{2}, \frac{l}{2}]^3} a^*(x) a^*(-x') a(x'') a(x - x' - x'') \mathrm{d}x \mathrm{d}x' \mathrm{d}x''. \tag{B.11}$$

Then we obtain the functional derivative as

$$\begin{aligned}
&\int_{-l/2}^{l/2} \frac{\delta \mathscr{F}_2}{\delta a^*} \psi^* \mathrm{d}x = \lim_{\varepsilon\to 0} \frac{1}{\varepsilon} \left(\mathscr{F}_2[a^* + \varepsilon\psi^*, a] - \mathscr{F}_2[a^*, a] \right) \\
&= \lim_{\varepsilon\to 0} \frac{1}{\varepsilon} \left(\frac{3}{4l^2} \iiint_{[-\frac{l}{2}, \frac{l}{2}]^3} \left[a^*(x) + \varepsilon\psi^*(x) \right] \left[a^*(-x') + \varepsilon\psi^*(-x') \right] a(x'') a(x - x' - x'') \mathrm{d}x \mathrm{d}x' \mathrm{d}x'' - \mathscr{F}_2[a^*, a] \right) \\
&= \int_{-l/2}^{l/2} \left(\frac{3}{4l^2} \iint_{[-\frac{l}{2}, \frac{l}{2}]^2} a^*(-x') a(x'') a(x - x' - x'') \mathrm{d}x' \mathrm{d}x'' \right) \psi^*(x) \mathrm{d}x \\
&\quad + \int_{-l/2}^{l/2} \left(\frac{3}{4l^2} \iint_{[-\frac{l}{2}, \frac{l}{2}]^2} a^*(x) a(x'') a(x - x' - x'') \mathrm{d}x \mathrm{d}x'' \right) \psi^*(-x') \mathrm{d}x' \\
&= \int_{-l/2}^{l/2} \underbrace{\left(\frac{3}{2l^2} \iint_{[-\frac{l}{2}, \frac{l}{2}]^2} a^*(-x') a(x'') a(x - x' - x'') \mathrm{d}x' \mathrm{d}x'' \right)}_{= \frac{\delta \mathscr{F}_2}{\delta a^*}} \psi^*(x) \mathrm{d}x,
\end{aligned} \tag{B.12}$$

where in the last step, we transformed the second term using the substitution $x' \to -x'$ and then again exchanged $x \leftrightarrow x'$. Next, we show how the functional reads in Fourier space (for $\mathscr{F}_1$ this directly follows from Parsevals theorem). Therefore we substitute the Fourier transformations $a(x) = \sum_k \tilde{a}(k) e^{ikx}$ and $a^*(x) = \sum_k \tilde{a}^*(k) e^{-ikx}$ into Eq. (B.11):

$$\begin{aligned}
\mathscr{F}_2 &= \frac{3}{4l^2} \iiint\limits_{[-\frac{l}{2},\frac{l}{2}]^3} a^*(x) a^*(-x') a(x'') a(x - x' - x'') \mathrm{d}x \mathrm{d}x' \mathrm{d}x''. \\
&= \frac{3}{4l^2} \sum_{k_1,k_2,k_3,k_4} \tilde{a}^*(k_1)\tilde{a}^*(k_2)\tilde{a}(k_3)\tilde{a}(k_4) \underbrace{\int\limits_{-l/2}^{l/2} e^{i(-k_1+k_4)x} \mathrm{d}x}_{=l\delta_{k_1,k_4}} \underbrace{\int\limits_{-l/2}^{l/2} e^{i(k_2-k_4)x'} \mathrm{d}x'}_{=l\delta_{k_2,k_4}} \underbrace{\int\limits_{-l/2}^{l/2} e^{i(k_3-k_4)x''} \mathrm{d}x''}_{=l\delta_{k_3,k_4}} \\
&= \frac{3l}{4} \sum_{k_4} \tilde{a}^*(k_4)\tilde{a}^*(k_4)\tilde{a}(k_4)\tilde{a}(k_4) = \frac{3l}{4} \sum_k |\tilde{a}(k)|^4
\end{aligned} \tag{B.13}$$

C. Further nonlinearities in the general case

In the general case, we have to investigate further contributions from the cubic nonlinearity, i.e. here the full contribution in terms of the fields read

$$\begin{aligned}
&\partial_{XX} \begin{pmatrix} {u_1^{(1)}}^3 \\ {u_2^{(1)}}^3 \end{pmatrix} \\
&= \partial_{XX} \Bigg[\left(e^{-\mathrm{i}\hat{\omega}\tau} A(X,T) \right)^3 \begin{pmatrix} (\boldsymbol{v}_+)_1^3 \\ (\boldsymbol{v}_+)_2^3 \end{pmatrix} + 3 \left(e^{\mathrm{i}\hat{\omega}\tau} A^*(X,T) \right) \left(e^{-\mathrm{i}\hat{\omega}\tau} A(X,T) \right)^2 \begin{pmatrix} (\boldsymbol{v}_+)_1^2 (\boldsymbol{v}_-)_1 \\ (\boldsymbol{v}_+)_2^2 (\boldsymbol{v}_-)_2 \end{pmatrix} \\
&\qquad + 3 \left(e^{\mathrm{i}\hat{\omega}\tau} A^*(X,T) \right)^2 \left(e^{-\mathrm{i}\hat{\omega}\tau} A(X,T) \right) \begin{pmatrix} (\boldsymbol{v}_+)_1 (\boldsymbol{v}_-)_1^2 \\ (\boldsymbol{v}_+)_2 (\boldsymbol{v}_-)_2^2 \end{pmatrix} + \left(e^{\mathrm{i}\hat{\omega}\tau} A^*(X,T) \right)^3 \begin{pmatrix} (\boldsymbol{v}_-)_1^3 \\ (\boldsymbol{v}_-)_2^3 \end{pmatrix} \Bigg] \\
&= \partial_{XX} \Bigg[\frac{1}{2} \left(e^{-\mathrm{i}\hat{\omega}\tau} A(X,T) \right)^3 \boldsymbol{v}_1 + \frac{3}{2} \left(e^{\mathrm{i}\hat{\omega}\tau} A^*(X,T) \right) \left(e^{-\mathrm{i}\hat{\omega}\tau} A(X,T) \right)^2 \boldsymbol{v}_2 \\
&\qquad + \frac{3}{2} \left(e^{\mathrm{i}\hat{\omega}\tau} A^*(X,T) \right)^2 \left(e^{-\mathrm{i}\hat{\omega}\tau} A(X,T) \right) \boldsymbol{v}_3 + \frac{1}{2} \left(e^{\mathrm{i}\hat{\omega}\tau} A^*(X,T) \right)^3 \boldsymbol{v}_4 \Bigg],
\end{aligned} \tag{C.1}$$

where $\boldsymbol{v}_1, \boldsymbol{v}_2, \boldsymbol{v}_3$ and $\boldsymbol{v}_4$ are defined by the vectorial expressions in the line above. Unlike in the simplistic example, here the first and third contribution do in general not vanish from the vectorial scalar product, when applying the Fredholm alternative with $e^{-\mathrm{i}\hat{\omega}\tau} \delta(X - X') \boldsymbol{v}_+^\dagger$. Applying the procedure from section 3.3 for the first term yields

$$\begin{aligned}
&\left\langle e^{-\mathrm{i}\hat{\omega}\tau} \delta(X - X') \boldsymbol{v}_+^\dagger ; \partial_{XX} \left(e^{-\mathrm{i}\hat{\omega}\tau} A(X,T) \right)^3 \boldsymbol{v}_1 \right\rangle \\
&= \left\langle e^{-\mathrm{i}\hat{\omega}\tau} \sum_Q e^{\mathrm{i}Q(X-X')} \boldsymbol{v}_+^\dagger ; \partial_{XX} \left(e^{-\mathrm{i}\hat{\omega}\tau} \sum_K \tilde{A}(K,T) e^{\mathrm{i}KX} \right)^3 \boldsymbol{v}_1 \right\rangle
\end{aligned}$$

$$\sim \sum_{Q,K,K',K''} e^{\mathrm{i}QX'} \tilde{A}(K,T)\tilde{A}(K',T)\tilde{A}(K'',T)\left(-(K+K'+K'')^2\right) \times$$
$$\times \int e^{\mathrm{i}\omega\tau(-Q^2+K^2+K'^2+K''^2)}\mathrm{d}\tau \int e^{\mathrm{i}X(-Q+K+K'+K'')}\mathrm{d}X. \tag{C.2}$$

Again, the two integrals vanish whenever one of the integrands has a nonzero phase. Therefore only terms with

$$-Q^2+K^2+K'^2+K''^2=0 \quad \text{and} \quad -Q+K+K'+K''=0 \tag{C.3}$$

contribute. Inserting the second equation into the first yields

$$KK'+KK''+K'K''=0. \tag{C.4}$$

If then $A(X,T)$ is close to a single mode solution, i.e. if $\tilde{A}(K,T)$ has a sharp peak in K space, all contributions vanish as the expression is strictly positive for $K \approx K' \approx K''$. A similar argument holds for the third term in Eq. (C.1).

D. Functional variations and Hamiltonian

Here we briefly derive the general functional variation of a local functional as defined in section 4, i.e. $\mathscr{F}[\boldsymbol{u}] = \int_\Omega f(\boldsymbol{u}, \vec{\nabla}\boldsymbol{u}, \vec{\nabla}^2\boldsymbol{u}, ...)\mathrm{d}^n x$

$$\begin{aligned}
&\int_\Omega \frac{\delta\mathscr{F}[\boldsymbol{u}]}{\delta\boldsymbol{u}}\psi\mathrm{d}^n x = \lim_{\varepsilon\to 0}\frac{\mathscr{F}[\boldsymbol{u}+\varepsilon\psi]-\mathscr{F}[u]}{\varepsilon} \\
&= \lim_{\varepsilon\to 0}\frac{1}{\varepsilon}\left[\int_\Omega f(\boldsymbol{u}+\varepsilon\psi, \vec{\nabla}\boldsymbol{u}+\vec{\nabla}\varepsilon\psi, \vec{\nabla}^2\boldsymbol{u}+\varepsilon\vec{\nabla}^2\psi, ...)\mathrm{d}^n x - \mathscr{F}[\boldsymbol{u}]\right] \\
&= \int_\Omega \left[\frac{\partial f}{\partial \boldsymbol{u}}\psi + \frac{\partial f}{\partial(\vec{\nabla}\boldsymbol{u})}\cdot\vec{\nabla}\psi + \frac{\partial f}{\partial(\vec{\nabla}^2\boldsymbol{u})}\vec{\nabla}^2\psi + ...\right]\mathrm{d}^n x \\
&= \int_\Omega \underbrace{\left[\frac{\partial f}{\partial \boldsymbol{u}} - \vec{\nabla}\cdot\frac{\partial f}{\partial(\vec{\nabla}\boldsymbol{u})} + \vec{\nabla}^2\frac{\partial f}{\partial(\vec{\nabla}^2\boldsymbol{u})} + ...\right]}_{=\frac{\delta\mathscr{F}[\boldsymbol{u}]}{\delta\boldsymbol{u}}}\psi\mathrm{d}^n x,
\end{aligned} \tag{D.1}$$

Next, we show the identity used in Eq. (4.15) in one dimension, i.e. $\vec{x}\to x$, as the notation becomes quite messy in n dimensions. This is equivalent to assuming the phase boundary to have a planar geometry. Then we state that

$$\begin{aligned}
&\frac{\delta\mathscr{F}[\boldsymbol{u}]}{\delta u}\partial_x u = \partial_x(\mathscr{H}+\boldsymbol{\mu}\boldsymbol{\chi}(u)) \quad \text{with} \quad \mathscr{H}+\boldsymbol{\mu}\boldsymbol{\chi}(u) = f - \sum_{i=1}^{k}\boldsymbol{p}_i\partial_x\boldsymbol{q}_i \\
&\text{with} \quad \boldsymbol{q}_i = \partial_x^{i-1}\boldsymbol{u} \qquad \text{and} \qquad \boldsymbol{p}_i = \sum_{j=i}^{k}(-\partial_x)^{(j-i)}\frac{\partial f}{\partial(\partial_x^j\boldsymbol{u})}.
\end{aligned} \tag{D.2}$$

where k is the highest order of occuring derivatives. This is a standard procedure from classical mechanics, where we switch to canonical coordinates and construct a Hamiltonian, where here f takes the role of the Lagrangian. We then proof that

$$\begin{aligned}
\partial_x(\mathscr{H}+\boldsymbol{\mu}\boldsymbol{\chi}(u)) =& \partial_x\left[f-\sum_{i=1}^{k}\left(\partial_x^i\boldsymbol{u}\right)\left(\sum_{j=i}^{k}(-\partial_x)^{(j-i)}\frac{\partial f}{\partial(\partial_x^j\boldsymbol{u})}\right)\right] \\
=& \sum_{i=0}^{k}(\partial_x^{i+1}\boldsymbol{u})\frac{\partial f}{\partial(\partial_x^i\boldsymbol{u})}-\sum_{i=1}^{k}\left(\partial_x^{i+1}\boldsymbol{u}\right)\left(\sum_{j=i}^{k}(-\partial_x)^{(j-i)}\frac{\partial f}{\partial(\partial_x^j\boldsymbol{u})}\right) \\
&+\sum_{i=1}^{k}\left(\partial_x^i\boldsymbol{u}\right)\left(\sum_{j=i}^{k}(-\partial_x)^{(j-i+1)}\frac{\partial f}{\partial(\partial_x^j\boldsymbol{u})}\right) \\
=& \sum_{i=1}^{k}\left(\partial_x^{i+1}\boldsymbol{u}\right)\underbrace{\left(-\sum_{j=i}^{k}(-\partial_x)^{(j-i)}\frac{\partial f}{\partial(\partial_x^j\boldsymbol{u})}+\sum_{j=i+1}^{k}(-\partial_x)^{(j-i+1)}\frac{\partial f}{\partial(\partial_x^j\boldsymbol{u})}+\frac{\partial f}{\partial(\partial_x^i\boldsymbol{u})}\right)}_{=0} \\
&(\partial_x\boldsymbol{u})\sum_{j=1}^{k}(-\partial_x)^j\frac{\partial f}{\partial(\partial_x^j\boldsymbol{u})}+(\partial_x\boldsymbol{u})\frac{\partial f}{\partial u}=\frac{\delta\mathscr{F}[\boldsymbol{u}]}{\delta\boldsymbol{u}}(\partial_x\boldsymbol{u}).
\end{aligned} \tag{D.3}$$

where the crucial step is to shift the index $i \to i+1$ in the second term in the second row. Then the evaluation of the integral in Eq. (4.15) is trivial, i.e. going back to full dimensions we obtain

$$\int_{\vec{r}_A}^{\vec{r}_B}\frac{\delta\mathscr{F}[\boldsymbol{u}]}{\delta\boldsymbol{u}}\vec{\nabla}\boldsymbol{u}\cdot\mathrm{d}\vec{r}(s)=\int_{\vec{r}_A}^{\vec{r}_B}\vec{\nabla}(\mathscr{H}+\boldsymbol{\mu}\boldsymbol{\chi}(u))\cdot\mathrm{d}\vec{r}(s)=[\mathscr{H}+\boldsymbol{\mu}\boldsymbol{\chi}(u)]_{\vec{r}_A}^{\vec{r}_B}=f_h(\boldsymbol{u}_B)-f_h(\boldsymbol{u}_A), \tag{D.4}$$

where we used in the last step that the only contribution to $\mathscr{H}+\boldsymbol{\mu}\boldsymbol{\chi}(u)$ in homogeneous phases is the free energy density f_h, which can be seen in Eq. (D.2). Then, it is also simple to show that $\mathscr{H}$ is constant, i.e. we find

$$\vec{\nabla}\mathscr{H}=\frac{\delta\mathscr{F}[\boldsymbol{u}]}{\delta\boldsymbol{u}}\vec{\nabla}\boldsymbol{u}-\vec{\nabla}(\boldsymbol{\mu}\boldsymbol{\chi}(\boldsymbol{u}))=\left[\frac{\delta\mathscr{F}[\boldsymbol{u}]}{\delta\boldsymbol{u}}-\boldsymbol{\mu}\frac{\partial\boldsymbol{\chi}(\boldsymbol{u})}{\partial\boldsymbol{u}}\right]\vec{\nabla}\boldsymbol{u}=\left[\underline{M}(\boldsymbol{u})\frac{\delta\mathscr{F}[\boldsymbol{u}]}{\delta\boldsymbol{u}}-\mu\right]\left(\underline{M}(\boldsymbol{u})^{-1}\right)^T\vec{\nabla}\boldsymbol{u}=0. \tag{D.5}$$

D.1. Calculations for MIPS

We briefly demonstrate, that the definitions of $m(u)$ in Eq. (4.10) and $\mathscr{F}[u]$ in Eq. (4.11) yield a spurious-gradient dynamics description of the MIPS-system in Eq. (4.9). To do so, we show that the part containing derivatives $\mathscr{F}_d[u] := \int_\Omega \frac{\kappa(u)}{2m(u)}|\vec{\nabla}(u)|\mathrm{d}^n x$ yields $m(u)\frac{\delta\mathscr{F}_d}{\delta u}=\lambda(u)|\vec{\nabla}u|^2-\kappa(u)\vec{\nabla}^2u$ as

desired:

$$
\begin{aligned}
\int_\Omega \left[\frac{\delta F_d}{\delta u}\psi\right] \mathrm{d}^n x &= \lim_{\varepsilon\to 0} \frac{\mathscr{F}_d[u+\varepsilon\psi]-\mathscr{F}_d[u]}{\varepsilon} \\
&= \lim_{\varepsilon\to 0} \frac{1}{\varepsilon}\int_\Omega \left[\frac{\kappa(u+\varepsilon\psi)}{2m(u+\varepsilon\psi)}|\vec{\nabla}u+\varepsilon\vec{\nabla}\psi|^2 - \frac{\kappa(u)}{2m(u)}|\vec{\nabla}u|^2\right]\mathrm{d}^n x \\
&= \int_\Omega \frac{1}{2}\left[(\frac{\kappa'}{m}-\frac{\kappa m'}{m^2})|\vec{\nabla}u|^2\psi + 2\frac{\kappa}{m}\vec{\nabla}u\vec{\nabla}\psi\right]\mathrm{d}^n x \\
&\overset{\text{p.I.}}{=} \int_\Omega \left[-\frac{1}{2}(\frac{\kappa'}{m}-\frac{\kappa m'}{m^2})|\vec{\nabla}u|^2 - \frac{\kappa}{m}\vec{\nabla}^2 u\right]\psi\,\mathrm{d}^n x \\
\implies \quad \frac{\delta F_d}{\delta u} &= -\frac{1}{2}(\frac{\kappa'}{m}-\frac{\kappa m'}{m^2})|\vec{\nabla}u|^2 - \frac{\kappa}{m}\vec{\nabla}^2 u
\end{aligned}
\tag{D.6}
$$

Then, using equation Eq. (4.10), one obtains

$$
\begin{aligned}
m\frac{\delta F_d}{\delta u} &= m\left[-\frac{1}{2}(\frac{\kappa'}{m}-\frac{\kappa m'}{m^2})|\vec{\nabla}u|^2 - \frac{\kappa}{m}\vec{\nabla}^2 u\right] \\
&= -\frac{1}{2}(\kappa' - (2\lambda+\kappa'))|\vec{\nabla}u|^2 - \kappa\vec{\nabla}^2 u \\
&= \lambda|\vec{\nabla}u|^2 - \kappa\vec{\nabla}^2 u.
\end{aligned}
\tag{D.7}
$$

Declaration of Academic Integrity

I hereby confirm that this thesis, entitled _____

From Instabilities to Coexistence in Active Mixtures _____ is solely my own work and that I have used no sources or aids other than the ones stated. All passages in my thesis for which other sources, including electronic media, have been used, be it direct quotes or content references, have been acknowledged as such and the sources cited. I am aware that plagiarism is considered an act of deception which can result in sanction in accordance with the examination regulations.

Münster, 13.09.2023 D. Jae
_____
(date, signature of student)

I consent to having my thesis cross-checked with other texts to identify possible similarities and to having it stored in a database for this purpose.

I confirm that I have not submitted the following thesis in part or whole as an examination paper before.

Münster, 13.09.2023 D. Jae
_____
(date, signature of student)